Mathematical Texture Analysis

Helmut Schaeben

Freiberg University of Mining and Technology, Germany

AGH Krakow, Jun 2-10, 2008

Outline

Texture analysis is a method to quantify the pattern of crystallographic preferred orientation in polycrystalline materials like metals, rocks or ceramics.
The course will give

- an introduction into the basic mathematics of practical texture analysis from the point of view of computerized tomography including
  - rotations,
  - special functions on spheres and SO(3),
  - Radon transforms on SO(3),
  - probability distributions on spheres and SO(3),
  - visualization of probability distributions on spheres and SO(3),
  - resolution of the inversion problem of texture analysis,
  - density estimation for individual orientation measurements;
- an extensive introduction into our new state-of-the-art public domain software MTEX to compute an orientation density function (odf) from experimental pole figures or individual orientation measurements, and evaluate it.

Mathematical Texture Analysis – An Easy Introduction

Texture Analysis

Texture Analysis (1)

The subject of texture analysis is the analyis of crystallographic preferred orientation in polycrystalline materials be it steel or rocks.

Texture Analysis (2)

Many crystals are anisotropic with respect to their physical properties, e.g. heat conductivity or thermal expansion.
A well known example is quartz, for which thermal expansion is positive or negative with respect to different crystallographic directions.

Whether a polycrystalline specimen is isotropic or not depends on the statistical distribution of orientations.
In case of a well developed preferred orientation the specimen approximately behaves as anisotropic as a single crystal, in case of a uniform orientation distribution it is isotropic since anisotropies cancel out.

Crystallographic Orientation (1)

The crystallographic orientation g of an individual crystal is the rotation $g \in G \subset \mathbf{SO}(3)$ which brings a right–handed orthogonal coordinate system K_S fixed to the specimen into coincidence with a right–handed orthogonal coordinate system K_C fixed to the crystal,

$$g \in \mathbf{SO}(3): \; K_S \mapsto K_C.$$

Texture analysis is the analysis of the crystallographic orientation distribution of a polycrystalline specimen.

Orientation imaging refers to the *spatial* analysis of the crystallographic orientation distribution of a polycrystalline specimen.

Crystallographic Orientation (2)

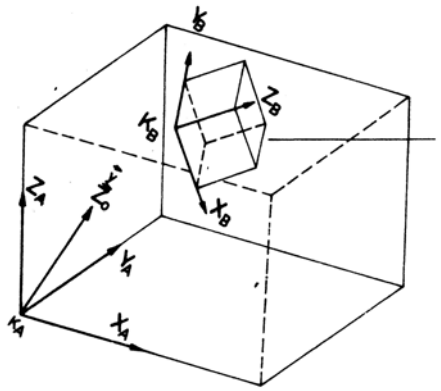

$$K_{\mathcal{C}} = \boldsymbol{g}\, K_{\mathcal{S}}$$

(Figure from Matthies, 1982, p. 16)

Crystallographic Preferred Orientation

Texture analysis is the analysis of the statistical distribution of crystallographic orientations within a polycrystalline specimen by volume.

The volume portion $\Delta V_{\boldsymbol{g}}/V = f(\boldsymbol{g})\Delta\boldsymbol{g}$ of the polycrystalline specimen of total volume V carrying crystals with crystallographic orientations $\boldsymbol{g} \in \Delta G \subset G \subset \mathbf{SO}(3)$ is modeled for $\Delta\boldsymbol{g} \to 0$ by

$$\text{prob}(\boldsymbol{g} \in \Delta G) = \int_{\Delta G} f(\boldsymbol{g})\, d\boldsymbol{g}$$

where f is referred to as orientation probability density function (odf).

Considering crystal symmetry, G is actually a coset of $\mathbf{SO}(3)$.

Origin of Crystallographic Preferred Orientation

A non–uniform distribution, i.e. crystallographic preferred orientation, or texture, originates in various kinds of solid state processes such as primary crystallization, plastic deformation, recrystallization, or phase transformation.

Thus, texture controls all kinds of anisotropic physical properties.

Applications of Texture Analysis: Materials Sciences

In materials sciences, texture analysis typically addresses problems like what pattern of crystallographic preferred orientation is caused by a given process, and refers to process control in the laboratory or quality control in production to guarantee a required crystallographic preferred orientation and corresponding macroscopic physical properties.

- isotropic steel – almost perfect uniform distribution, no crystallographic preferred orientation
- high–temperature semi–conductors – almost perfect "single crystal" crystallographic preferred orientation

Materials Sciences – Isotropic Steel

Materials Sciences – Isotropic Steel

Applications of Texture Analysis: Geosciences

In geosciences, texture analysis is typically applied to the much more difficult problem of which process(es) caused an observed pattern of crystallographic preferred orientation in rocks and aims at an interpretation of the kinematics and dynamics of geological processes contributing to a consistent reconstruction of the geological deformation history.

- differences in the velocity of seismic waves along or across ocean ridges have recently been explained with textures changes during mantle convection
- varying texture may result in a seismic reflector
- texture of marble slabs employed as building facades or tombstone decoration is thought to significantly influence the spectacular phenomena of bending, fracturing, spalling and shattering of the initially intact slab

Applications of Texture Analysis: Geosciences

Paris Cimetiere Montparnasse

Die beiden aus porösen Tertiärkalkstein Calciere grossier gefertigten Stelen in der Bildmitte sind deutlich verbogen und weisen Rissphänomene auf.

Courtesy Prof. S. Siegesmund, Göttingen

Applications of Texture Analysis: Geosciences

Helsinki, Finnlandia Halle

Riesige Fassadenflächen aus Carrara–Marmor zeigen deutliche "Einschüsselungen" (Verbiegungen).

Courtesy Prof. S. Siegesmund, Göttingen

Experimental Techniques

Integral measurements of texture in diffraction experiments with X–ray, neutron, synchrotron radiation.

Its essential mathematics is spherical tomography.

Individual crystallographic orientation measurements with electron back scatter diffraction (EBSD). Texture analyis with EBSD data is the spatial analysis of the orientations, their spatial correlation, and their distribution.

Its essential mathematics is spatial statistics of localized rotations.

Crystallographic Orientation (3)

Let a unique direction $\mathbf{v}$ be represented by $\mathbf{v}_{K_\mathcal{C}}$ with respect to the crystal coordinate system $K_\mathcal{C}$, and by $\mathbf{v}_{K_\mathcal{S}}$ with respect to the specimen coordinate system $K_\mathcal{S}$, where $\boldsymbol{g}\, K_\mathcal{S} = K_\mathcal{C}$.

Then the coordinates of the unique direction $\mathbf{v} \in \mathbb{S}^2$ transform according to

$$\boldsymbol{g}\, \mathbf{v}_{K_\mathcal{C}} \quad = \quad \mathbf{v}_{K_\mathcal{S}}$$

Furtheron, the crystallographic direction $\mathbf{v}_{K_\mathcal{C}}$ will be denoted by the coordinate vector $\mathbf{h}$, and the specimen direction $\mathbf{v}_{K_\mathcal{S}}$ will be denoted by the coordinate vector $\mathbf{r}$. Then

$$\boldsymbol{g}\, \mathbf{h} \quad = \quad \mathbf{r}$$

Crystallographic Orientation (4)

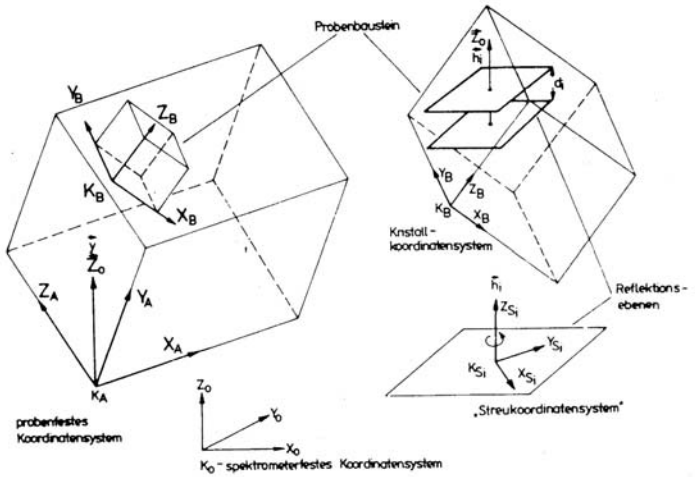

$$K_\mathcal{C} = \boldsymbol{g}\, K_\mathcal{S} : \quad \boldsymbol{g}\, \mathbf{h}_{K_\mathcal{C}} = \mathbf{r}_{K_\mathcal{S}}$$

(Figure from Matthies, 1982, p. 16)

Spherical Tomography

Origins of Spherical Tomography

The papers by **Paul Funk**
Über Flächen mit lauter geschlossenen geodätischen Linien: Math. Ann. 74 **(1913)**, *278–300*
Über eine geometrische Anwendung der Abel'schen Integralgleichung: Math. Ann. 77 **(1916)**, *129–135*
deal with it.

They appeared earlier than
Johann Radon, *Über die Bestimmung von Funktionen durch ihre Integralwerte längs gewisser Mannigfaltigkeiten: Berichte über die Verhandlungen der Königlich Sächsischen Gesellschaft der Wissenschaften zu Leipzig, Math.-Phys. Klasse 69* **(1917)**, *262–277*

Totally geodesic Radon transform for $\mathbf{SO}(3)$

Let $f : \mathbf{SO}(3) \mapsto [0, \infty)$ be a orientation probability density function of a random rotation $\boldsymbol{g} \in \mathbf{SO}(3)$.

For any given direction $\mathbf{h} \in \mathbb{S}^2$ the probability density function of coincidence of the random direction $\boldsymbol{g}\mathbf{h} \in \mathbb{S}^2$ with a given direction $\mathbf{r} \in \mathbb{S}^2$ is provided by the 1d totally geodesic spherical Radon transform

$$\mathcal{R}f(\mathbf{h}, \mathbf{r}) = \frac{1}{2\pi} \int_{G(\mathbf{h},\mathbf{r})} f(\boldsymbol{g}) d\boldsymbol{g} \qquad (1)$$

with fibres

$$G(\mathbf{h}, \mathbf{r}) = \{\boldsymbol{g} \in \mathbf{SO}(3) \,|\, \boldsymbol{g}\mathbf{h} = \mathbf{r}\}$$

The spherical Radon transform is a function on $\mathbb{S}^2 \times \mathbb{S}^2$, where a pair $(\mathbf{h}, \mathbf{r})$ parametrizes a 1d geodesic of $\mathbf{SO}(3)$.

Totally geodesic Radon transform for $\mathbb{S}^3$

Let $f : \mathbb{S}^3 \mapsto [0, \infty)$ be an even probability density function of a random unit quaternion representing a random rotation $\boldsymbol{g} \in \mathbf{SO}(3)$.

For any given direction $\mathbf{h} \in \mathbb{S}^2$ the probability density function of coincidence of the random direction $\boldsymbol{g}\mathbf{h} \in \mathbb{S}^2$ with a given direction $\mathbf{r} \in \mathbb{S}^2$ is provided by the 1d spherical Radon transform

$$\mathcal{R}f(\mathbf{h}, \mathbf{r}) = \frac{1}{2\pi} \int_{G(\mathbf{h},\mathbf{r})} f(\boldsymbol{g}) d\boldsymbol{g} \qquad (2)$$

with fibres

$$G(\mathbf{h}, \mathbf{r}) = \{\boldsymbol{g} \in \mathbf{SO}(3) \,|\, \boldsymbol{g}\mathbf{h} = \mathbf{r}\}$$

The spherical Radon transform is a function on $\mathbb{S}^2 \times \mathbb{S}^2$, where a pair $(\mathbf{h}, \mathbf{r})$ parametrizes a 1d great circle of $\mathbb{S}^3 \subset \mathbb{H}$.

Pole Figure Projection

The *basic crystallographic* X–ray transform associated with an orientation probability density function f is defined as

$$\mathcal{X}f(\mathbf{h},\mathbf{r}) = \frac{1}{2}\Big(\mathcal{R}f(\mathbf{h},\mathbf{r}) + \mathcal{R}f(-\mathbf{h},\mathbf{r})\Big)$$

The crystallographic X–ray transform or the pole probability density function (pole figure) associated with the crystal form H of an orientation probability density function f is defined as

$$\mathcal{X}f(\mathbf{h},\mathbf{r}) = \frac{1}{\mathrm{card}(H)}\sum_{\mathbf{h}\in H}\mathcal{R}f(\mathbf{h},\mathbf{r}) = P(\mathbf{h},\mathbf{r}) = P_{\mathbf{h}}(\mathbf{r}),$$

where the notation $P_{\mathbf{h}}(\mathbf{r})$ emphasizes the practical point of view of $\mathbf{h}$ as a parameter rather than a variable.

These *pole figures* are experimentally accessible by diffraction with X–, neutron– or synchrotron–radiation.

Inverse Spherical Radon Transform – Problem

To which extent and for which assumptions is it possible to determine f globally or locally in a neighbourhood $\mathcal{U}(\mathbb{g}_0)$ numerically from data sampled from $\mathcal{R}f$, more specifically from

$$I_{ij_i} = I(\mathbf{h}_i,\mathbf{r}_{j_i}) = a(\mathbf{h}_i)\,\mathcal{R}f(\mathbf{h}_i,\mathbf{r}_{j_i}) + I^b_{ij_i}$$

Corresponding mathematical problems are

- existence and uniqueness of an inverse $\mathcal{R}^{-1}$ with respect to function spaces
- condition of the problem – ill posed problem
- localization
- data
- numerical methods

Pole Figure Inversion – Problem

To which extent and for which appropriate additional modeling assumptions is it possible to determine f globally on $\mathbf{SO}(3)$ or locally in a neighbourhood $\mathcal{U}(\mathbb{g}_0) \subset \mathbf{SO}(3)$ numerically from data sampled from $\mathcal{X}f$, more specifically from

$$I_{ij_i} = I(\mathbf{h}_i,\mathbf{r}_{j_i}) = a(\mathbf{h}_i)\,\mathcal{X}f(\mathbf{h}_i,\mathbf{r}_{j_i}) + I^b_{ij_i}$$

Ill–posedness (1)

A classic example (Tikhonov) is

$$\begin{aligned} 10x + y &= 11 \\ 100x + 11y &= 111 \end{aligned}$$

with the unique and exact solution $x = 1, y = 1$, and

$$\begin{aligned} 10x + y &= 11,1 \\ 100x + 11y &= 111 \end{aligned}$$

with the unique and exact solution $x = 1,11,\ \ y = 0$

Tikhonov, A.N. and Arsenin, V.Y., 1977, *Solutions of Ill - Posed Problems*: J. Wiley & Sons, New York

Ill–posedness (2)

Slight modifications result in an even worse conditioned system

$$\begin{aligned} x + 10y &= 11 \\ 10x + 101y &= 111 \end{aligned}$$

with the unique and exact solution $x = 1, y = 1$, and

$$\begin{aligned} x + 10y &= 11,1 \\ 10x + 101y &= 111 \end{aligned}$$

with the unique and exact solution $x = 11,1, \;\; y = 0$

Ill–posedness (3)

Another very simple yet instructive example of ill-posedness may be provided by the following two systems of linear equations

$$\begin{aligned} x + 0.999y &= 1 \\ x + y &= 0 \end{aligned}$$

with the unique and exact solution $x = 1000, \;\; y = -1000$, and

$$\begin{aligned} x + 1.001y &= 1 \\ x + y &= 0 \end{aligned}$$

with the unique and exact solution $x = -1000, y = +1000$. Though the matrices of the two systems differ in only one entry, and these two entries differ only by .002, the solutions differ drastically.

Example (1)

Ideal–Lagen

$$f_1(\mathbf{g}; \mathbf{g}_{11}^o, \mathbf{g}_{12}^o, \mathbf{g}_{13}^o) := \sum_{j=1}^{3} \mathbb{1}_{\mathbf{g}_{1i}^o}(\mathbf{g}), \quad f_2(\mathbf{g}; \mathbf{g}_{21}^o, \mathbf{g}_{22}^o, \mathbf{g}_{23}^o) := \sum_{j=1}^{3} \mathbb{1}_{\mathbf{g}_{2i}^o}(\mathbf{g})$$

with

$$\mathbb{1}_{\mathbf{g}_{ij}^o}(\mathbf{g}) = \begin{cases} 1 & \text{if } \mathbf{g} = \mathbf{g}_{ij}^o \\ 0 & \text{otherwise} \end{cases}, \; i = 1,2, \; j = 1,2,3$$

with

$$\begin{aligned} \mathbf{g}_{11}^o &:= (\pi/2, 0, 0), & \mathbf{g}_{21}^o &:= (0,0,0), \quad \text{(blue)} \\ \mathbf{g}_{12}^o &:= (\pi/2, \pi/2, \pi/2), & \mathbf{g}_{22}^o &:= (0, \pi/2, \pi/2), \quad \text{(green)} \\ \mathbf{g}_{13}^o &:= (0, \pi/2, 0), & \mathbf{g}_{23}^o &:= (\pi/2, \pi/2, 0) \quad \text{(red)} \end{aligned}$$

in terms of Euler angles (α, β, γ) according to the "**y**–convention".

The two sets of Ideal–Lagen and their corresponding orientation probability density functions differ by a rotation about **z** by $\pi/2$.

Example (2)

$$\begin{aligned} \mathbf{g}_{11}^o &:= (\pi/2, 0, 0), & \mathbf{g}_{21}^o &:= (0,0,0), \quad \text{blue} & (3) \\ \mathbf{g}_{12}^o &:= (\pi/2, \pi/2, \pi/2), & \mathbf{g}_{22}^o &:= (0, \pi/2, \pi/2), \quad \text{green} & (4) \\ \mathbf{g}_{13}^o &:= (0, \pi/2, 0), & \mathbf{g}_{23}^o &:= (\pi/2, \pi/2, 0) \quad \text{red} & (5) \end{aligned}$$

in terms of Euler angles (α, β, γ) according to the "**y**–convention". Then

$$M(\mathbf{g}_{11}^o) = \begin{pmatrix} 0 & -1 & 0 \\ 1 & 0 & 0 \\ 0 & 0 & 1 \end{pmatrix} \quad \text{and} \quad M(\mathbf{g}_{21}^o) = \begin{pmatrix} 1 & 0 & 0 \\ 0 & 1 & 0 \\ 0 & 0 & 1 \end{pmatrix}$$

$$M(\mathbf{g}_{12}^o) = \begin{pmatrix} -1 & 0 & 0 \\ 0 & 0 & 1 \\ 0 & 1 & 0 \end{pmatrix} \quad \text{and} \quad M(\mathbf{g}_{22}^o) = \begin{pmatrix} 0 & 0 & 1 \\ 1 & 0 & 0 \\ 0 & 1 & 0 \end{pmatrix}$$

$$M(\mathbf{g}_{13}^o) = \begin{pmatrix} 0 & 0 & 1 \\ 0 & 1 & 0 \\ -1 & 0 & 0 \end{pmatrix} \quad \text{and} \quad M(\mathbf{g}_{23}^o) = \begin{pmatrix} 0 & -1 & 0 \\ 0 & 0 & 1 \\ -1 & 0 & 0 \end{pmatrix}$$

Example (3)

and

$$M(\boldsymbol{g})^{o}_{1i} = M(\boldsymbol{g}(\pi/2;\mathbf{z}))\; M(\boldsymbol{g}^{o}_{2i}) = \begin{pmatrix} 0 & -1 & 0 \\ 1 & 0 & 0 \\ 0 & 0 & 1 \end{pmatrix}\; M(\boldsymbol{g}^{o}_{2i}), \quad i = 1,2,3.$$

with

$$M(\boldsymbol{g}^{o}_{11}) = \begin{pmatrix} 0 & -1 & 0 \\ 1 & 0 & 0 \\ 0 & 0 & 1 \end{pmatrix} \quad \text{and} \quad M(\boldsymbol{g}^{o}_{21}) = \begin{pmatrix} 1 & 0 & 0 \\ 0 & 1 & 0 \\ 0 & 0 & 1 \end{pmatrix}$$

$$M(\boldsymbol{g}^{o}_{12}) = \begin{pmatrix} -1 & 0 & 0 \\ 0 & 0 & 1 \\ 0 & 1 & 0 \end{pmatrix} \quad \text{and} \quad M(\boldsymbol{g}^{o}_{22}) = \begin{pmatrix} 0 & 0 & 1 \\ 1 & 0 & 0 \\ 0 & 1 & 0 \end{pmatrix}$$

$$M(\boldsymbol{g}^{o}_{13}) = \begin{pmatrix} 0 & 0 & 1 \\ 0 & 1 & 0 \\ -1 & 0 & 0 \end{pmatrix} \quad \text{and} \quad M(\boldsymbol{g}^{o}_{23}) = \begin{pmatrix} 0 & -1 & 0 \\ 0 & 0 & 1 \\ -1 & 0 & 0 \end{pmatrix}$$

Example (3)

Calculating all crystallographic pole points $\boldsymbol{g}^{o}\mathbf{h}$, i.e. the specimen directions $\mathbf{r} = \boldsymbol{g}^{o}\mathbf{h}$, according to the δ–distributions composing f_1, f_2 yields the correspnding pole figures composed of "Ideal–Lagen"

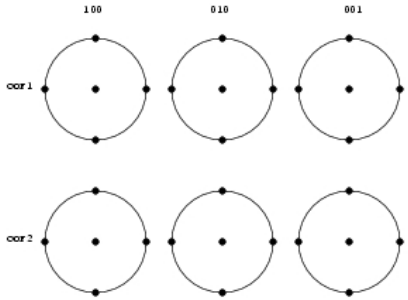

Top row: Pole figures corresponding to f_1
Bottom row: Pole figures corresponding to f_2

Example (4)

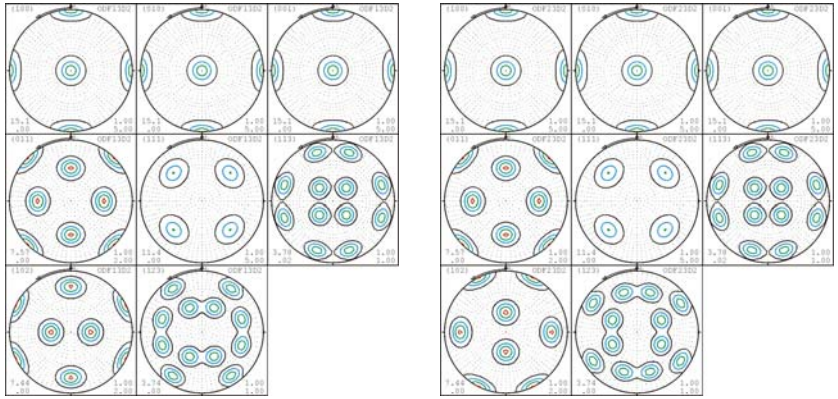

Pole figures $\mathcal{X}f_1(\mathbf{h},\mathbf{r})$ of $f_1(\boldsymbol{g};\boldsymbol{g}^{o}_{11},\boldsymbol{g}^{o}_{12},\boldsymbol{g}^{o}_{13})$ and pole figures $\mathcal{X}f_2(\mathbf{h},\mathbf{r})$ of $f_2(\boldsymbol{g};\boldsymbol{g}^{o}_{21},\boldsymbol{g}^{o}_{22},\boldsymbol{g}^{o}_{23})$, respectively, for several crystal forms with orthorhombic crystal symmetry imposed.

Example – EBSD

Ideal–Lagen

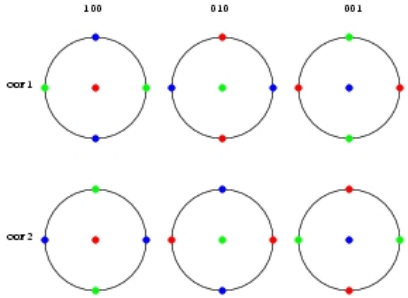

Top row: Pole point plots corresponding to $f_1(\boldsymbol{g};\boldsymbol{g}^{o}_{11},\boldsymbol{g}^{o}_{12},\boldsymbol{g}^{o}_{13})$ where $\boldsymbol{g}^{o}_{11},\boldsymbol{g}^{o}_{12},\boldsymbol{g}^{o}_{13}$ are colour coded blue, green, red, respectively;
Bottom row: Pole point plots corresponding to $f_2(\boldsymbol{g};\boldsymbol{g}^{o}_{21},\boldsymbol{g}^{o}_{22},\boldsymbol{g}^{o}_{23})$ where $\boldsymbol{g}^{o}_{21},\boldsymbol{g}^{o}_{22},\boldsymbol{g}^{o}_{23}$ are colour coded blue, green, red, respectively.

Additional Modeling Assumptions for Pole Figure Inversion (1)

A natural modeling assumption to compensate for the lack of information is

$$f(g) \geq 0$$

Despite its apparent simplicity, this constraint is often hard to realize for many algorithms.

This difficulty may be avoided by explicitly prescribing the form of the ODF, e.g. as superposition of zonal ansatz–functions.

Additional Modeling Assumptions for Pole Figure Inversion (2)

Other additional modeling assumptions may address the smoothness of the function to be reconstructed. The objectives may be to minimize the norm or to maximize the entropy of the solution to be favoured.

The advantage of the entropy criterion is that it guarantees non–negativity without additional efforts.

Conclusions

Pole figures of texture analysis are identified with (means of) the 1d *totally geodesic (spherical) Radon transform* of a function defined on the the 3d sphere in 4d Euclidean space or the group of rotations $\mathbf{SO}(3)$.

Texture analysis in engineering and integral geometry in mathematics can largely benefit of each other ...
... by development of improved numerical inversion methods,
... by exemplifying the practical usefulness of mathematics,

confirming that

"The (Gödel's incompleteness) theorem assures that mathematics is inexhaustible. Our experience assures us that mathematics is inexhaustibly interesting", Arthur Sard, A View of Mathematics

The End

Representation of Crystallographic Orientation

Contents

Rotations in $\mathbb{R}^3$

A (proper) rotation $\boldsymbol{g} : \mathbb{R}^3 \mapsto \mathbb{R}^3$ is a linear mapping preserving handedness of a set of vectors (later: det $M(\boldsymbol{g}) = 1$), and the scalar product of vectors, i.e. the angle of vectors, which is the canonical measure of distance of unit vectors, i.e. on the sphere $\mathbb{S}^2 \subset \mathbb{R}^3$.

Issues

- parametrization of a rotation – mathematical "quantitative" description of a rotation
- representation of a rotation – to perform a rotation
- visualization of a set of rotations – exploratory data analysis

The linear map provided by a matrix (1)

Let $\mathcal{B}_S =< \mathbf{x}, \mathbf{y}, \mathbf{z} >$ and $\mathcal{B}_C =< \mathbf{a}, \mathbf{b}, \mathbf{c} >$ denote two orthonormal bases of the vector space $\mathbb{R}^3$, and let B_S and B_C denote the matrices constituted of the column vectors $\mathbf{x}, \mathbf{y}, \mathbf{z}$ and $\mathbf{a}, \mathbf{b}, \mathbf{c}$, resspectively. Let A denote a (3×3) matrix with rows A_1, A_2, A_3. Let $\mathbf{v} \in \mathbb{R}^3$ and let $\mathbf{v}_S = (v_x, v_y, v_z)^t$ denote the column vector of its coordinates with respect to $\mathcal{B}_S$, i.e.

$$\mathbf{v} = v_x\,\mathbf{x} + v_y\,\mathbf{y} + v_z\,\mathbf{z} = B_S\mathbf{v}_S.$$

The **linear mapping provided by the matrix** A is defined by

$$L_A(\mathbf{v}) = (A_1\mathbf{v}_S)\,\mathbf{a} + (A_2\mathbf{v}_S)\,\mathbf{b} + (A_3\mathbf{v}_S)\,\mathbf{c}$$

The ith–coordinate of $L_A(\mathbf{v})$ with respect to $\mathcal{B}_C$ is $A_i\mathbf{v}_S$.

The linear map provided by a matrix (2)

If the two bases are identical and the usual unit vectors, then

$$L_A\mathbf{v}_{\mathcal{B}} = A\mathbf{v}_{\mathcal{B}} = \mathbf{w}_{\mathcal{B}}$$

where $\mathbf{w}_{\mathcal{B}}$ is the column vector of coordinates of $L_A\mathbf{v}_{\mathcal{B}}$ with respect to $\mathcal{B} = \mathcal{B}_S = \mathcal{B}_C$.

The matrix associated with a linear map (1)

Let $F : \mathbb{R}^3 \mapsto \mathbb{R}^3$ be a linear map, hence

$$\begin{aligned} F(\mathbf{x}) &= a_{11}\,\mathbf{a} + a_{21}\,\mathbf{b} + a_{31}\,\mathbf{c} \\ F(\mathbf{y}) &= a_{12}\,\mathbf{a} + a_{22}\,\mathbf{b} + a_{32}\,\mathbf{c} \\ F(\mathbf{z}) &= a_{13}\,\mathbf{a} + a_{23}\,\mathbf{b} + a_{33}\,\mathbf{c} \end{aligned}$$

The matrix

$$A = \begin{pmatrix} a_{11} & a_{21} & a_{31} \\ a_{12} & a_{22} & a_{32} \\ a_{13} & a_{23} & a_{33} \end{pmatrix}^t = \begin{pmatrix} a_{11} & a_{12} & a_{13} \\ a_{21} & a_{22} & a_{23} \\ a_{31} & a_{32} & a_{33} \end{pmatrix}$$

is called the **matrix associated with the linear mapping** F (cf. Lang, 1969; p. 81) .

The reasons for taking the transpose will become clear in a moment.

The matrix associated with a linear map (2)

Generally, let

$$\mathbf{v} = v_x\,\mathbf{x} + v_y\,\mathbf{y} + v_z\,\mathbf{z}.$$

Then

$$\begin{aligned} F(\mathbf{v}) &= v_x\,F(\mathbf{x}) + v_y\,F(\mathbf{y}) + v_z\,F(\mathbf{z}) \\ &= v_x(a_{11}\mathbf{a} + a_{21}\mathbf{b} + a_{31}\mathbf{c}) + v_y(a_{12}\mathbf{a} + a_{22}\mathbf{b} + a_{32}\mathbf{c}) + v_z(a_{13}\mathbf{a} + a_{23}\mathbf{b} + a_{33}\mathbf{c}) \\ &= (a_{11}v_x + a_{12}v_y + a_{13}v_z)\mathbf{a} + (a_{21}v_x + a_{22}v_y + a_{23}v_z)\mathbf{b} + (a_{31}v_x + a_{32}v_y + a_{33}v_z)\mathbf{a} \\ &= L_A(\mathbf{v}) \end{aligned}$$

thus $F = L_A$.

The matrix associated with a linear mapping $F : \mathbb{R}^3 \mapsto \mathbb{R}^3$ with respect to $\mathcal{B}_S$ and $\mathcal{B}_C$ will be denoted by $M_{\mathcal{B}_C}^{\mathcal{B}_S}(F)$; if the bases are fixed, then the matrix is denoted $M(F)$.

Linear maps and matrices (1)

Summarizingly, let $F : \mathbb{R}^3 \mapsto \mathbb{R}^3$ denote a linear mapping. Let $\mathcal{B}_S$ and $\mathcal{B}_C$ be two bases of $\mathbb{R}^3$, and let K_S and K_C be their corresponding coordinate systems, respectively. For $\mathbf{v} \in \mathbb{R}^3$, denote by $M_{\mathcal{B}}(\mathbf{v})$ the column vector of coordinates of $\mathbf{v}$ with respect to $\mathcal{B}$. Then

$$M_{\mathcal{B}_C}\Big(F(\mathbf{v})\Big) = M_{\mathcal{B}_C}^{\mathcal{B}_S}(F) M_{\mathcal{B}_S}(\mathbf{v})$$

(cf. Lang, 1969; p. 87) .

Linear maps and matrices (2)

It includes the two special

$$M_{\mathcal{B}}\Big(F(\mathbf{v})\Big) = M_{\mathcal{B}}^{\mathcal{B}}(F) M_{\mathcal{B}}(\mathbf{v})$$

and

$$M_{\mathcal{B}_C}(\mathbf{v}) = M_{\mathcal{B}_C}^{\mathcal{B}_S}(id) M_{\mathcal{B}_S}(\mathbf{v})$$

where $M_{\mathcal{B}_C}^{\mathcal{B}_S}(F)$ denotes the matrix associated with the linear mapping F with respect to the bases $\mathcal{B}_S$ and $\mathcal{B}_C$.

It should be noted that the matrix $M_{\mathcal{B}_C}^{\mathcal{B}_S}(id)$ associated with the identity mapping leaving a given vector unchanged is not the unit matrix.

Rotation in $\mathbb{R}^2$ (1)

The only reasonable linear mapping $\mathbb{S}^2 \mapsto \mathbb{S}^2$, $\mathbb{S}^2 \subset \mathbb{R}^3$, is a rotation.

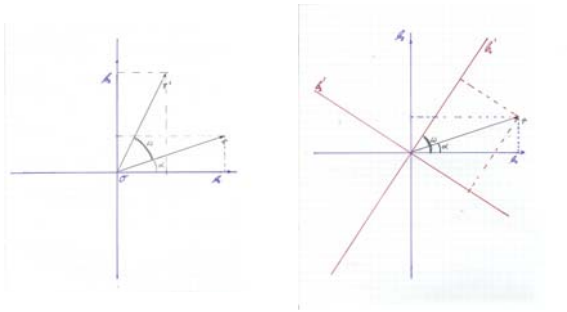

Active and passive rotation in $\mathbb{R}^2, \mathbb{R}^3$.
Left: Active, point rotation with respect to a unique fixed coordinate system;
Right: Passive, frame rotation, transformation of coordinates of a unique fixed point with respect to change of basis.

Rotation in $\mathbb{R}^2$ (2)

Let $\mathcal{B}_S =< \mathbf{x}, \mathbf{y} >$, $\mathcal{B}_C =< \mathbf{a}, \mathbf{b} >$ be two different orthornormal bases, and let B_S, B_C be the associated matrices constituted of the column vectors of $\mathcal{B}_S, \mathcal{B}_C$, respectively, i.e.

$$B_S = \begin{pmatrix} x_1 & y_1 \\ x_2 & y_2 \end{pmatrix} \text{ and } B_C = \begin{pmatrix} a_1 & b_1 \\ a_2 & b_2 \end{pmatrix}$$

Moreover, let K_S and K_C be the two corresponding right–handed coordinate systems with a common origin $\mathcal{O}$.

Active rotation in $\mathbb{R}^2$ (1)

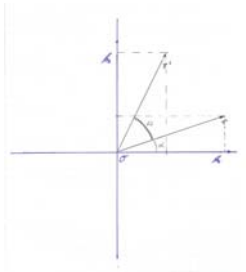

Active rotation maps vectors according to

$$\begin{aligned} \mathfrak{g}(\mathbf{x}) &= \mathbf{a} = \cos\omega\,\mathbf{x} + \sin\omega\,\mathbf{y} \\ \mathfrak{g}(\mathbf{y}) &= \mathbf{b} = -\sin\omega\,\mathbf{x} + \cos\omega\,\mathbf{y} \end{aligned}$$

Hence the matrix associated with the active rotation $\mathfrak{g}$ with respect to the unique basis $\mathcal{B} = \mathcal{B}_S$ is

$$M_{\mathcal{B}}^{\mathcal{B}}(\mathfrak{g}) = \begin{pmatrix} \cos\omega & -\sin\omega \\ \sin\omega & \cos\omega \end{pmatrix}$$

Active rotation in $\mathbb{R}^2$ (2)

Then

$$\mathbf{v} = \begin{pmatrix} \cos\alpha \\ \sin\alpha \end{pmatrix} \mapsto \mathbf{w} = \begin{pmatrix} \cos(\alpha+\omega) \\ \sin(\alpha+\omega) \end{pmatrix}$$

by a rotation about $\mathbf{z}$ by $+\omega$

$$\mathfrak{g}(\omega, \mathbf{z})\,(\mathbf{v}) = \begin{pmatrix} \cos\omega & -\sin\omega \\ \sin\omega & \cos\omega \end{pmatrix} \begin{pmatrix} \cos\alpha \\ \sin\alpha \end{pmatrix} = \begin{pmatrix} \cos(\alpha+\omega) \\ \sin(\alpha+\omega) \end{pmatrix} = \mathbf{w}$$

Active rotation in $\mathbb{R}^2$ (3)

Rewriting the active rotation with a little trigonometry

$$\begin{aligned} \mathfrak{g}(\mathbf{x}) &= \mathbf{a} = \cos\omega\,\mathbf{x} + \sin\omega\,\mathbf{y} = \cos\omega\,\mathbf{x} + \cos(\frac{\pi}{2} - \omega)\,\mathbf{y} \\ \mathfrak{g}(\mathbf{y}) &= \mathbf{b} = -\sin\omega\,\mathbf{x} + \cos\omega\,\mathbf{y} = \cos(\frac{\pi}{2} + \omega)\,\mathbf{x} + \cos\omega\,\mathbf{y} \end{aligned}$$

it is

$$\begin{aligned} M_{\mathcal{B}}^{\mathcal{B}}(\mathfrak{g}) &= \begin{pmatrix} \cos\omega & \cos(\frac{\pi}{2}+\omega) \\ \cos(\frac{\pi}{2}-\omega) & \cos\omega \end{pmatrix} \\ &= \begin{pmatrix} \mathbf{a}^t\mathbf{x} & \mathbf{b}^t\mathbf{x} \\ \mathbf{a}^t\mathbf{y} & \mathbf{b}^t\mathbf{y} \end{pmatrix} = \begin{pmatrix} x_1 & x_2 \\ y_1 & y_2 \end{pmatrix} \begin{pmatrix} a_1 & b_1 \\ a_2 & b_2 \end{pmatrix} = B_S^t\,B_C \end{aligned}$$

Passive rotation in $\mathbb{R}^2$ (1)

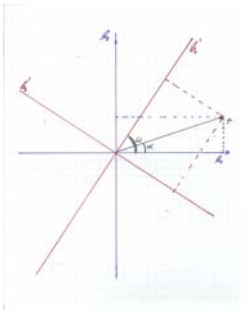

Passive rotation relates coordinates of an unique vector $\mathbf{v}$ with respect to coordinates system K_S to coordinates with resepct to coordinate system K_C, where K_C is the image of K_S under an active rotation by ω, i.e. when the active rotation by ω is applied to both axes of the coordinate system K_C

$$\begin{aligned} \mathbf{a} &= \cos\omega\,\mathbf{x} + \sin\omega\,\mathbf{y} \\ \mathbf{b} &= -\sin\omega\,\mathbf{x} + \cos\omega\,\mathbf{y} \end{aligned}$$

Passive rotation in $\mathbb{R}^2$ (2)

Then

$$\begin{aligned} \mathbf{x} &= \cos\omega\,\mathbf{a} - \sin\omega\,\mathbf{b} \\ \mathbf{y} &= \sin\omega\,\mathbf{a} + \cos\omega\,\mathbf{b} \end{aligned}$$

Let $id : \mathbb{S}^1 \mapsto \mathbb{S}^1$ be the identity mapping relative to the bases $\mathcal{B}_S =< \mathbf{x}, \mathbf{y} >$ and $\mathcal{B}_C =< \mathbf{a}, \mathbf{b} >$. Then

$$\begin{aligned} id(\mathbf{x}) &= \mathbf{x} = \cos\omega\,\mathbf{a} - \sin\omega\,\mathbf{b} \\ id(\mathbf{y}) &= \mathbf{y} = \sin\omega\,\mathbf{a} + \cos\omega\,\mathbf{b} \end{aligned}$$

and the matrix associated with the identity mapping with respect to $\mathcal{B}_S$ and $\mathcal{B}_C$ is

$$M_{\mathcal{B}_C}^{\mathcal{B}_S}(id) = \begin{pmatrix} \cos\omega & \sin\omega \\ -\sin\omega & \cos\omega \end{pmatrix}.$$

Passive rotation in $\mathbb{R}^2$ (3)

It should be noted that $\boldsymbol{g}(\omega, \mathbf{z})$ is represented by

$$M(\boldsymbol{g}(\omega, \mathbf{z})) = \begin{pmatrix} \cos\omega & -\sin\omega \\ \sin\omega & \cos\omega \end{pmatrix}$$

and that $\boldsymbol{g}(-\omega, \mathbf{z})$ is represented by

$$M(\boldsymbol{g}(-\omega, \mathbf{z})) = \begin{pmatrix} \cos\omega & \sin\omega \\ -\sin\omega & \cos\omega \end{pmatrix} = M^t(\boldsymbol{g}(\omega, \mathbf{z})) = M^{-1}(\boldsymbol{g}(\omega, \mathbf{z}))$$

Passive rotation in $\mathbb{R}^2$ (4)

Therefore

$$M_{\mathcal{B}_C}(\mathbf{v}) = \begin{pmatrix} \cos\omega & \sin\omega \\ -\sin\omega & \cos\omega \end{pmatrix} M_{\mathcal{B}_S}(\mathbf{v})$$

formally resembles

$$\mathbf{v}_{K_C} = M(\boldsymbol{g}(-\omega, \mathbf{z}))\,\mathbf{v}_{K_S} \text{ if } K_C = \boldsymbol{g}(\omega, \mathbf{z})\,K_S$$

or, equivalently,

$$M(\boldsymbol{g}(\omega, \mathbf{z}))\,\mathbf{v}_{\boldsymbol{g}\,K_S} = \mathbf{v}_{K_S}$$

Rotation in $\mathbb{R}^3$

Applying the embedding of $\mathbb{R}^2$ in $\mathbb{R}^3$, Eq.(60) may be rewritten as

$$\begin{pmatrix} w_x \\ w_y \\ 0 \end{pmatrix} = \begin{pmatrix} \cos\omega & -\sin\omega & 0 \\ \sin\omega & \cos\omega & 0 \\ 0 & 0 & 1 \end{pmatrix} \begin{pmatrix} v_x \\ v_y \\ 0 \end{pmatrix}$$

with the augmented matrix

$$M(\boldsymbol{g}(\omega, \mathbf{z})) := \begin{pmatrix} \cos\omega & -\sin\omega & 0 \\ \sin\omega & \cos\omega & 0 \\ 0 & 0 & 1 \end{pmatrix}$$

and the rotation in the plane is actually seen as a rotation about $\mathbf{z} \in \mathbb{S}^2$ by the angle ω in $\mathbb{R}^3$.

Rotation in $\mathbb{R}^3$ – Elementary matrix representation (1)

Let $\mathcal{B}_S =< \mathbf{x}, \mathbf{y}, \mathbf{z} >$, $\mathcal{B}_C =< \mathbf{a}, \mathbf{b}, \mathbf{c} >$ be two different orthornormal bases, and let B_S, B_C be the associated matrices constituted of the column vectors of $\mathcal{B}_S, \mathcal{B}_C$, respectively, i.e.

$$B_S = \begin{pmatrix} x_1 & y_1 & z_1 \\ x_2 & y_2 & z_2 \\ x_3 & y_3 & z_3 \end{pmatrix} \text{ and } B_C = \begin{pmatrix} a_1 & b_1 & c_1 \\ a_2 & b_2 & c_2 \\ a_3 & b_3 & c_3 \end{pmatrix}$$

Moreover, let K_S and K_C be the two corresponding right–handed coordinate systems with a common origin $\mathcal{O}$.

Rotation in $\mathbb{R}^3$ – Elementary matrix representation (2)

A unique unit vector $\mathbf{v}$ is then represented by virtue of directions cosines by

$$\begin{aligned} \mathbf{v} &= (\mathbf{v}^t\mathbf{x})\,\mathbf{x} + (\mathbf{v}^t\mathbf{y})\,\mathbf{y} + (\mathbf{v}^t\mathbf{z})\,\mathbf{z} = v_x\,\mathbf{x} + v_y\,\mathbf{y} + v_z\,\mathbf{z} = B_S\; M_{\mathcal{B}_S}(\mathbf{v}) \\ &= (\mathbf{v}^t\mathbf{a})\,\mathbf{a} + (\mathbf{v}^t\mathbf{b})\,\mathbf{b} + (\mathbf{v}^t\mathbf{c})\,\mathbf{c} = v_a\,\mathbf{a} + v_b\,\mathbf{b} + v_c\,\mathbf{c} = B_C\; M_{\mathcal{B}_C}(\mathbf{v})\,, \end{aligned}$$

i.e.

$$M_{\mathcal{B}_S}(\mathbf{v}) = (v_x, v_y, v_z)^t \text{ and } M_{\mathcal{B}_C} = (v_a, v_b, v_c)^t$$

with respect to $\mathcal{B}_S, \mathcal{B}_C$, respectively.

How do the coordinates of $\mathbf{v}$ with respect to $\mathcal{B}_S$ relate to the coordinates of $\mathbf{w}$ with respect to $\mathcal{B}_C$ under rotation?

Rotation in $\mathbb{R}^3$ – Elementary matrix representation (3)

Analogously to the active rotation in the plane, now in terms of direction cosines

$$\begin{aligned} \boldsymbol{g}(\mathbf{x}) &= \mathbf{a} = (\mathbf{a}^t\mathbf{x})\,\mathbf{x} + (\mathbf{a}^t\mathbf{y})\,\mathbf{y} + (\mathbf{a}^t\mathbf{z})\,\mathbf{z} \\ \boldsymbol{g}(\mathbf{y}) &= \mathbf{b} = (\mathbf{b}^t\mathbf{x})\,\mathbf{x} + (\mathbf{b}^t\mathbf{y})\,\mathbf{y} + (\mathbf{b}^t\mathbf{z})\,\mathbf{z} \\ \boldsymbol{g}(\mathbf{z}) &= \mathbf{c} = (\mathbf{c}^t\mathbf{x})\,\mathbf{x} + (\mathbf{c}^t\mathbf{y})\,\mathbf{y} + (\mathbf{c}^t\mathbf{z})\,\mathbf{z} \end{aligned}$$

Hence, the matrix associated with the active rotation $\boldsymbol{g}$ relative to the unique basis $\mathcal{B} = \mathcal{B}_S$ is

$$M^{\mathcal{B}}_{\mathcal{B}}(\boldsymbol{g}) = \begin{pmatrix} \mathbf{a}^t\mathbf{x} & \mathbf{a}^t\mathbf{y} & \mathbf{a}^t\mathbf{z} \\ \mathbf{b}^t\mathbf{x} & \mathbf{b}^t\mathbf{y} & \mathbf{b}^t\mathbf{z} \\ \mathbf{c}^t\mathbf{x} & \mathbf{c}^t\mathbf{y} & \mathbf{c}^t\mathbf{z} \end{pmatrix}^t = \begin{pmatrix} \mathbf{a}^t\mathbf{x} & \mathbf{b}^t\mathbf{x} & \mathbf{c}^t\mathbf{x} \\ \mathbf{a}^t\mathbf{y} & \mathbf{b}^t\mathbf{y} & \mathbf{c}^t\mathbf{y} \\ \mathbf{a}^t\mathbf{z} & \mathbf{b}^t\mathbf{z} & \mathbf{c}^t\mathbf{z} \end{pmatrix} = B_S^t\, B_C$$

and therefore

$$\mathbf{w} = M^{\mathcal{B}}_{\mathcal{B}}(\boldsymbol{g})\mathbf{v}$$

Rotation in $\mathbb{R}^3$ – Elementary matrix representation (4)

Analogously to the passive rotation in the plane

$$\begin{aligned} id(\mathbf{x}) = \mathbf{x} &= (\mathbf{x}^t\mathbf{a})\,\mathbf{a} + (\mathbf{x}^t\mathbf{b})\,\mathbf{b} + (\mathbf{x}^t\mathbf{c})\,\mathbf{c} \\ id(\mathbf{y}) = \mathbf{y} &= (\mathbf{y}^t\mathbf{a})\,\mathbf{a} + (\mathbf{y}^t\mathbf{b})\,\mathbf{b} + (\mathbf{y}^t\mathbf{c})\,\mathbf{c} \\ id(\mathbf{z}) = \mathbf{z} &= (\mathbf{z}^t\mathbf{a})\,\mathbf{a} + (\mathbf{z}^t\mathbf{b})\,\mathbf{b} + (\mathbf{z}^t\mathbf{c})\,\mathbf{c} \end{aligned}$$

and the matrix associated with the identity mapping relative to $\mathcal{B}_S$ and $\mathcal{B}_C$ is

$$M^{\mathcal{B}_S}_{\mathcal{B}_C}(id) = \begin{pmatrix} \mathbf{x}^t\mathbf{a} & \mathbf{y}^t\mathbf{a} & \mathbf{z}^t\mathbf{a} \\ \mathbf{x}^t\mathbf{b} & \mathbf{y}^t\mathbf{b} & \mathbf{z}^t\mathbf{b} \\ \mathbf{x}^t\mathbf{c} & \mathbf{y}^t\mathbf{c} & \mathbf{z}^t\mathbf{c} \end{pmatrix} = B_C^t\, B_S$$

and

$$M_{\mathcal{B}_C}(\mathbf{v}) = M^{\mathcal{B}_S}_{\mathcal{B}_C}(id)\, M_{\mathcal{B}_S}(\mathbf{v})$$

Rotation in $\mathbb{R}^3$ – Elementary matrix representation (5)

There is no way avoiding that

$$M_{\mathcal{B}_C}^{\mathcal{B}_S}(id) = \left(M_{\mathcal{B}}^{\mathcal{B}}(\boldsymbol{g})\right)^t$$

Thus, formally

$$M_{\boldsymbol{g}\mathcal{B}_S}(\mathbf{v}) = \left(M_{\mathcal{B}}^{\mathcal{B}}(\boldsymbol{g})\right)^t M_{\mathcal{B}_S}(\mathbf{v})$$

or

$$\left(M_{\mathcal{B}}^{\mathcal{B}}(\boldsymbol{g})\right) M_{\boldsymbol{g}\mathcal{B}_S}(\mathbf{v}) = M_{\mathcal{B}_S}(\mathbf{v})$$

Rotation in $\mathbb{R}^3$ – Elementary matrix representation (6)

Ruining the notation and denoting the unique vector $\mathbf{v}$ by $\mathbf{r}$ with respect to $K_{\mathcal{S}}$, i.e. $\mathbf{r}$ denotes the column vector of coordinates of $\mathbf{v}$ with respect to $K_{\mathcal{S}}$, and denoting it by $\mathbf{h}$ with respect to $K_{\mathcal{C}}$, i.e. $\mathbf{h}$ denotes the column vector of coordinates of $\mathbf{v}$ with respect to $K_{\mathcal{C}}$,

$$M(\boldsymbol{g})\,\mathbf{v}_{K_{\mathcal{C}}} = \mathbf{v}_{K_{\mathcal{S}}}$$

is turned into

$$\boldsymbol{g}\,\mathbf{h} = \mathbf{r}$$

and carries the interpretation: If the crystallographic coordinate system $K_{\mathcal{C}}$ coincides with the specimen coordinate system $K_{\mathcal{S}}$ when $K_{\mathcal{S}}$ is (actively) rotated by $\boldsymbol{g}$, then the crystallographic direction $\mathbf{h}$ and the specimen direction $\mathbf{r}$ relate to one another by $\boldsymbol{g}\,\mathbf{h} = \mathbf{r}$:

$$\boldsymbol{g}\,\mathbf{h} = \mathbf{r} \text{ if } K_{\mathcal{C}} = \boldsymbol{g}K_{\mathcal{S}}$$

Parametrizations and Representations of Rotations

Parametrizations of a rotation

Basic parametrizations to quantitatively describe a rotation are

- angle $\omega \in [0, \pi]$ and axis $\mathbf{n} \in \mathbb{S}^2$ of rotation *(why not $\omega \in [0, 2\pi)$)*,
- three Euler angles (α, β, γ), $\alpha, \gamma \in [0, 2\pi)$, $\beta \in [0, \pi]$ with respect to three orthogonal axes of three successive rotations
- ...

Representations of a rotation

Basic representations to perform a rotation are

- matrix representation
- quaternion representation
- Rodrigues' representation
- harmonic representation
- ...

Parametrizations and representations of a rotation (1)

- angle $\omega \in [0, \pi]$ and axis $\mathbf{n} \in \mathbb{S}^2 \subset \mathbb{R}^3$ of rotation:

$$\mathbf{g} = \mathbf{g}(\omega, \mathbf{n}), \quad M(\mathbf{g}) = M_{ij}(\omega, \mathbf{n}))_{i,j=1,2,3}$$

  which may be rewritten as

$$\mathbf{g} = \mathbf{g}(\omega \mathbf{n}), \quad M(\mathbf{g}) = M_{ij}(\omega \mathbf{n}))_{i,j=1,2,3}$$

  What is the difference?
- quaternions $\mathbf{q} \in S^3_+ \subset \mathbb{R}^4$:

$$q(\mathbf{g}) = \cos \omega/2 + \mathbf{n} \sin \omega/2$$

  Note: Quaternion multiplication applies.
- Rodrigues' representation $\mathbf{R} \in \mathbb{R}^3$:

$$\mathbf{R}(\mathbf{g}) = \mathbf{n} \tan \omega/2$$

Parametrizations and representations of a rotation (2)

- Euler angles $(\alpha, \beta, \gamma) \in [0, 2\pi] \times [0, \pi] \times [0, 2\pi]$ of 3 successive rotations around (conventionally) fixed axes of rotations:

$$\mathbf{g} = \mathbf{g}(\alpha, \beta, \gamma), \quad M(\mathbf{g}) = M_{ij}(\alpha, \beta, \gamma))_{i,j=1,2,3}$$

  There exist 12 essentially different ways to define Euler angles, and they are all in use, somewhere (Kuipers, 1999).

Parametrization of the inverse rotation in terms of angle and axis of a rotation

If a rotation $\mathbf{g}$ is parametrized in terms of its angle ω and its axis $\mathbf{n} \in \mathbb{S}^2$, then the inverse rotation $\mathbf{g}^{-1}$ is parametrized by $(\omega, -\mathbf{n})$. *Why is it not parametrized by* $(2\pi - \omega, \mathbf{n})$*?*

If a rotation $\mathbf{g}$ is represented by a (3×3) matrix $M \in \mathbf{SO}(3)$, then the inverse rotation $\mathbf{g}^{-1}$ is represented by $M^{-1} = M^t$.

Conjugation of a rotation

Let $\boldsymbol{g}_0$ be an arbitrary rotation, and let $\boldsymbol{g}$ be a rotation parametrized by its angle ω and axis $\mathbf{n}$. The the sequence $\boldsymbol{g}_0\boldsymbol{g}\boldsymbol{g}_0^{-1}$ of three successive rotations is called conjugation of $\boldsymbol{g}$ by $\boldsymbol{g}_0$, and is parametrized by its angle ω and axis $\boldsymbol{g}_0\,\mathbf{n}$, i.e.

$$\boldsymbol{g}_0\boldsymbol{g}(\omega,\mathbf{n})\boldsymbol{g}_0^{-1} = \boldsymbol{g}(\omega,\boldsymbol{g}_0\,\mathbf{n})$$

In particular, a rotation and any of its conjugate have the same angle of rotation.

Matrix representation in terms of angle and axis of a rotation

In terms of the (angle, axis) – parametrization, the rotation $\boldsymbol{g}(\omega,\mathbf{n})$ has the matrix representation

$$M(\boldsymbol{g}(\omega,\mathbf{n})) = \begin{pmatrix} n_1^2(1-\cos\omega)+\cos\omega & n_1n_2(1-\cos\omega)-n_3\sin\omega & n_1n_3(1-\cos\omega)+n_2\sin\omega \\ n_1n_2(1-\cos\omega)+n_3\sin\omega & n_2^2(1-\cos\omega)+\cos\omega & n_2n_3(1-\cos\omega)-n_1\sin\omega \\ n_1n_3(1-\cos\omega)-n_2\sin\omega & n_2n_3(1-\cos\omega)+n_1\sin\omega & n_3^2(1-\cos\omega)+\cos\omega \end{pmatrix}$$

$$= \begin{pmatrix} 1-2(n_2^2+n_3^2)\sin^2\frac{\omega}{2} & -n_3\sin\omega+2n_1n_2\sin^2\frac{\omega}{2} & n_2\sin\omega+2n_1n_3\sin^2\frac{\omega}{2} \\ n_3\sin\omega+2n_1n_2\sin^2\frac{\omega}{2} & 1-2(n_1^2+n_3^2)\sin^2\frac{\omega}{2} & -n_1\sin\omega+2n_2n_3\sin^2\frac{\omega}{2} \\ -n_2\sin\omega 2+2n_1n_3\sin^2\frac{\omega}{2} & n_1\sin\omega+2n_2n_3\sin^2\frac{\omega}{2} & 1-2(n_1^2+n_2^2)\sin^2\frac{\omega}{2} \end{pmatrix}$$

Euler angles (1)

Euler's Theorem states that any two orthonormal coordinate systems can be related by a sequence of rotations (not more than three) about coordinate axes, where two successive rotations must not be about the same axis.

Any rotation $\boldsymbol{g}$ can be represented as a sequence of three successive rotations about conventionally specified coordinate axes by three corresponding "Euler" angles.

There exist twelve choices of sets of axes of rotations (in terms of the coordinate axes of the initial coordinate system) to define correponding Euler angles, and they are all in use, somewhere.

Euler angles (2)

Bunge's Euler angles $(\varphi_1,\phi,\varphi_2)$ of 3 successive rotations around (conventionally) fixed axes of rotations:

- the first rotation by $\varphi_1 \in [0,2\pi)$ about the $\mathbf{z}$–axis,
- the second by $\phi \in [0,\pi]$ about the *new* $\mathbf{x}$–axis,
- the third by $\varphi_2 \in [0,2\pi)$ about the *new* $\mathbf{z}$–axis.

$$\boldsymbol{g}_{\mathrm{HJB}}(\varphi_1,\phi,\varphi_2) := \boldsymbol{g}(\varphi_2,\mathbf{z}'')\boldsymbol{g}(\phi,\mathbf{x}')\boldsymbol{g}(\varphi_1,\mathbf{z})$$

Euler angles (3)

Roe's, Matthies' Euler angles (α, β, γ) of 3 successive rotations around (conventionally) fixed axes of rotations:

- the first rotation by $\alpha \in [0, 2\pi)$ about the **z**–axis,
- the second by $\beta \in [0, \pi]$ about the *new* **y**–axis,
- the third by $\gamma \in [0, 2\pi)$ about the *new* **z**–axis.

$$\boldsymbol{g}_{\mathrm{SM}}(\alpha, \beta, \gamma) := \boldsymbol{g}(\gamma, \mathbf{z}'')\boldsymbol{g}(\beta, \mathbf{y}')\boldsymbol{g}(\alpha; \mathbf{z})$$

Then (α, β) are the spherical coordinates of the crystal direction $\mathbf{z}_{K_C} = \mathbf{c}$ with respect to K_S.

Euler angles (4)

Outside the texture universe, Euler angles (α, β, γ) usually define a rotation $\boldsymbol{g}$ in terms of a sequence $\boldsymbol{g}(\alpha,\ \beta,\ \gamma)$ of 3 successive rotations $\boldsymbol{g}(\alpha,\ \mathbf{z})\,\boldsymbol{g}(\beta,\ \mathbf{y})\,\boldsymbol{g}(\gamma,\ \mathbf{z})$ around (conventionally) fixed axes of rotations:

- the first rotation by $\gamma \in [0, 2\pi)$ about the **z**–axis,
- the second by $\beta \in [0, \pi]$ about the (initial) **y**–axis,
- the third by $\alpha \in [0, 2\pi)$ about the (initial) **z**–axis

of the specimen coordinate system K_S,

$$\boldsymbol{g}(\alpha,\ \beta,\ \gamma) := \boldsymbol{g}(\alpha, \mathbf{z})\boldsymbol{g}(\beta, \mathbf{y})\boldsymbol{g}(\gamma, \mathbf{z})$$

Euler angles (5)

The differently defined Euler angles are related by

$$\begin{aligned}
\boldsymbol{g}(\alpha, \beta, \gamma) &= \boldsymbol{g}(\alpha, \mathbf{z})\boldsymbol{g}(\beta, \mathbf{y})\boldsymbol{g}(\gamma, \mathbf{z}) \\
&= \underbrace{\boldsymbol{g}(\alpha, \mathbf{z})\boldsymbol{g}(\beta, \mathbf{y})\boldsymbol{g}^{-1}(\alpha, \mathbf{z})}_{\boldsymbol{g}(\beta, [\boldsymbol{g}(\alpha, \mathbf{z})\mathbf{y}]) = \boldsymbol{g}(\beta, \mathbf{y}')}\ \underbrace{\boldsymbol{g}(\alpha, \mathbf{z})\boldsymbol{g}(\gamma, \mathbf{z})\boldsymbol{g}^{-1}(\alpha, \mathbf{z})}_{\boldsymbol{g}(\gamma, \mathbf{z})}\ \boldsymbol{g}(\alpha, \mathbf{z}) \\
&= \underbrace{\boldsymbol{g}(\beta, \mathbf{y}')\boldsymbol{g}(\gamma, \mathbf{z})\boldsymbol{g}^{-1}(\beta, \mathbf{y}')}_{\boldsymbol{g}(\gamma, [\boldsymbol{g}(\beta, \mathbf{y}')\mathbf{z}])}\ \boldsymbol{g}(\beta, \mathbf{y}')\boldsymbol{g}(\alpha, \mathbf{z}) \\
&= \boldsymbol{g}(\gamma, \mathbf{z}'')\boldsymbol{g}(\beta, \mathbf{y}')\boldsymbol{g}(\alpha, \mathbf{z}) = \boldsymbol{g}_{\mathrm{SM}}(\alpha, \beta, \gamma)
\end{aligned}$$

Euler angles (6)

Let $\mathbf{a}, \mathbf{b}, \mathbf{c}$ denote the right–handed coordinate axes of the rotated coordinate system K_C. When considering $\mathbf{x}, \mathbf{y}, \mathbf{z}$ in terms of (rotated) $\mathbf{a}, \mathbf{b}, \mathbf{c}$, then of course

$$\begin{aligned}
\boldsymbol{g}(\alpha, \mathbf{z})\boldsymbol{g}(\beta, \mathbf{y})\boldsymbol{g}(\gamma, \mathbf{z}) &= \boldsymbol{g}(\gamma, \mathbf{z}'')\boldsymbol{g}(\beta, \mathbf{y}')\boldsymbol{g}(\alpha, \mathbf{z}) \\
&= \boldsymbol{g}(\gamma, \mathbf{c})\boldsymbol{g}(\beta, \mathbf{b}')\boldsymbol{g}(\alpha, \mathbf{c}'') \\
&= \boldsymbol{g}(\alpha, \mathbf{c})\boldsymbol{g}(\beta, \mathbf{b})\boldsymbol{g}(\gamma, \mathbf{c})
\end{aligned}$$

and

$$\boldsymbol{g}(-\alpha, \mathbf{c}'')\boldsymbol{g}(-\beta, \mathbf{b}')\boldsymbol{g}(-\gamma, \mathbf{c}) = \boldsymbol{g}(-\gamma, \mathbf{c})\boldsymbol{g}(-\beta, \mathbf{b})\boldsymbol{g}(-\alpha, \mathbf{c})$$

Matrix representation in terms of Euler angles (1)

$$M(\boldsymbol{g}(\gamma, \mathbf{z})) = \begin{pmatrix} \cos\gamma & -\sin\gamma & 0 \\ \sin\gamma & \cos\gamma & 0 \\ 0 & 0 & 1 \end{pmatrix}$$

$$M(\boldsymbol{g}(\beta, \mathbf{y})) = \begin{pmatrix} \cos\beta & 0 & \sin\beta \\ 0 & 1 & 0 \\ -\sin\beta & 0 & \cos\beta \end{pmatrix}$$

$$M(\boldsymbol{g}(\alpha, \mathbf{z})) = \begin{pmatrix} \cos\alpha & -\sin\alpha & 0 \\ \sin\alpha & \cos\alpha & 0 \\ 0 & 0 & 1 \end{pmatrix}$$

Matrix representation in terms of Euler angles (2)

$$M(\boldsymbol{g}(\alpha,\beta,\gamma)) = \begin{pmatrix} \cos\alpha & -\sin\alpha & 0 \\ \sin\alpha & \cos\alpha & 0 \\ 0 & 0 & 1 \end{pmatrix} \begin{pmatrix} \cos\beta & 0 & \sin\beta \\ 0 & 1 & 0 \\ -\sin\beta & 0 & \cos\beta \end{pmatrix} \begin{pmatrix} \cos\gamma & -\sin\gamma & 0 \\ \sin\gamma & \cos\gamma & 0 \\ 0 & 0 & 1 \end{pmatrix}$$

$$= \begin{pmatrix} \cos\alpha\cos\beta\cos\gamma - \sin\alpha\sin\gamma & -\cos\alpha\cos\beta\sin\gamma - \sin\alpha\cos\gamma & \cos\alpha\sin\beta \\ \sin\alpha\cos\beta\cos\gamma + \cos\alpha\sin\gamma & -\sin\alpha\cos\beta\sin\gamma + \cos\alpha\cos\gamma & \sin\alpha\sin\beta \\ -\sin\beta\cos\gamma & \sin\beta\sin\gamma & \cos\beta \end{pmatrix}$$

Parametrization ot the inverse rotation in terms of Euler angles

If $\boldsymbol{g} = \boldsymbol{g}(\alpha, \beta, \gamma)$, then the inverse rotation in terms of Matthies'/Bunge's Euler angles is formally parametrized by

$$\boldsymbol{g}^{-1} = \boldsymbol{g}(-\gamma, -\beta, -\alpha) = \boldsymbol{g}(\pi - \gamma, \beta, \pi - \alpha)$$

or

$$\boldsymbol{g}^{-1} = \boldsymbol{g}(-\varphi_2, -\phi, -\varphi_1),$$

resp.

Of course, the matrix representation of the inverse rotation $\boldsymbol{g}^{-1}$ is the transposed matrix of the initial rotation $\boldsymbol{g}$, i.e.

$$M(\boldsymbol{g}^{-1}) = M^{-1}(\boldsymbol{g}) = M^t(\boldsymbol{g})$$

Skew–field of real quaternions (1)

An arbitrary quaternion $q \in \mathbb{H}$ is composed of its scalar and vector part

$$q = q_0 + \mathbf{q} = \mathrm{Sc}q + \mathrm{Vec}q$$

with $\mathbf{q} = \sum_{i=1}^{3} q^i e_i = \mathrm{Vec}q$ and $q_0 = \mathrm{Sc}q$, where $\mathrm{Vec}q$ denotes the vector part of q, and $\mathrm{Sc}q$ denotes the scalar part of q.

Skew–field of real quaternions (2)

The basis elements e_i, $i = 1, 2, 3$, of $\mathbb{H}$ fulfil the algebraic relations

(i) $e_i^2 = -1$, $i = 1, 2, 3$;
(ii) $e_1 e_2 = e_3$, $e_2 e_3 = e_1$, $e_3 e_1 = e_2$;
(iii) $e_i e_j + e_j e_i = 0$, $i, j = 1, 2, 3$; $i \neq j$.

If $\mathrm{Sc}q = 0$, then q is called a pure quaternion, the subset of all pure quaternions is denoted $\mathrm{Vec}\mathbb{H}$. For $q \in \mathrm{Vec}\mathbb{H}$, q and $\mathbf{q}$ are identified, i.e. $q = \mathbf{q}$.

The subset of all scalars may be denoted $\mathrm{Sc}\mathbb{H}$.

In this way $\mathbb{R}$ and $\mathbb{R}^3$ are embedded in $\mathbb{H}$.

Skew–field of real quaternions (3)

Given two quaternions, p, $q \in \mathbb{H}$, their product according to the algebraic rules above is given by

$$pq = p_0 q_0 - \mathbf{p} \cdot \mathbf{q} + p_0 \mathbf{q} + q_0 \mathbf{p} + \mathbf{p} \times \mathbf{q} \ ,$$

where $\mathbf{p} \cdot \mathbf{q}$ and $\mathbf{p} \times \mathbf{q}$ represent the standard inner and wedge product in $\mathbb{R}^3$; thus

$$\begin{aligned} \mathrm{Sc}(pq) &= p_0 q_0 - \mathbf{p} \cdot \mathbf{q} \ , \\ \mathrm{Vec}(pq) &= p_0 \mathbf{q} + q_0 \mathbf{p} + \mathbf{p} \times \mathbf{q} \ . \end{aligned} \qquad (6)$$

Conjugation of a real quaternion

The quaternion

$$q^* = \mathrm{Sc}q - \mathrm{Vec}q$$

is called the conjugate of q.

With conjugated quaternions it is possible to represent the scalar and vector part in an algebraic fashion as

$$\begin{aligned} q_0 &= \mathrm{Sc}q = \frac{1}{2}(q + q^*) \ , \\ \mathbf{q} &= \mathrm{Vec}q = \frac{1}{2}(q - q^*) \ . \end{aligned} \qquad (7)$$

Norm of a real quaternion (1)

It holds that

$$qq^* = q^* q = \|q\|^2 = q_0^2 + (q^1)^2 + (q^2)^2 + (q^3)^2,$$

and the number $\| q \|$ is called the norm of q.

The norm of quaternions coincides with the Euclidean norm of q regarded as an element of the vector space $\mathbb{R}^4$.

The usual Euclidean inner product in the space $\mathbb{R}^4$ corresponds to the scalar part of pq^*, i.e. considering quaternions as vectors in $\mathbb{R}^4$, one gets

$$p \cdot q = \mathrm{Sc}(pq^*),$$

It holds that $(pq)^* = q^* p^*$, and therefore $\| pq \| = \| p \| \, \| q \|$.

Norm of a real quaternion (2)

A quaternion q with $\|q\| = 1$ is called a unit quaternion.

Furthermore, let $\mathbb{S}^2$ denote the unit sphere in $\mathrm{Vec}\,\mathbb{H} \simeq \mathbb{R}^3$ of all unit vectors, and $\mathbb{S}^3$ the sphere in $\mathbb{H} \simeq \mathbb{R}^4$ of all unit quaternions.

In complete analogy to $\mathbb{S}^3 \subset \mathbb{R}^4$, $\mathrm{Sc}(pq^*)$ provides a canonical measure for the spherical distance of unit quaternions $p, q \in \mathbb{S}^3$.

Inverse of a real quaternion

Moreover, each non-zero quaternion q has a unique inverse

$$q^{-1} = q^*/\|q\|^2.$$

with $\|q^{-1}\| = \|q\|^{-1}$.

For unit quaternions it is $q^{-1} = q^*$; for pure unit quaternions it is $q^{-1} = -q$, implying $qq = -1$.

Orthogonality of real quaternions (1)

Definition

. Two quaternions $p, q \in \mathbb{H}$ are said to be orthogonal if pq^* is a pure quaternion. If p, q are orthogonal unit quaternions, they are called orthonormal quaternions.

The condition of orthogonality means that $pq^* \in \mathrm{Vec}\mathbb{H}$, or according to Eq. (7)

$$2\,\mathrm{Sc}(pq^*) = pq^* + qp^* = 0.$$

It is emphasized that pure quaternions with orthogonal vector parts are orthogonal, but that the inverse is not generally true. Orthogonality of two quaternions does not imply orthogonality of their vector parts unless they are pure quaternions.

Proof.

Proposition

. *Two unit quaternions $p, q \in \mathbb{S}^3$ are orthogonal, if and only if $p = vq$, where v is a pure unit quaternion.*

If p and q are orthogonal, then pq^* is a pure quaternion, say v, for some $\mathbf{v} \in \mathbb{S}^2$. Hence, $p = vq \in \mathbb{S}^2 q$. The inverse is evident. □

Representation of real quaternions

An arbitrary quaternion permits the representation

$$q = \| q \| \left(\frac{q_0}{\|q\|} + \frac{\mathbf{q}}{\| \mathbf{q} \|} \frac{\| \mathbf{q} \|}{\|q\|} \right) = \| q \| \left(\cos \frac{\omega}{2} + \frac{\mathbf{q}}{\| \mathbf{q} \|} \sin \frac{\omega}{2} \right)$$

with $\omega = 2 \arccos(q_0/\|q\|)$, and $\| \mathbf{q} \|^2 = \mathbf{q}\mathbf{q}^*$ considering $\mathbf{q}$ as a pure quaternion.

For an arbitrary unit quaternion the representation

$$q = \cos \frac{\omega}{2} + \mathbf{n} \sin \frac{\omega}{2} \tag{8}$$

with the normalized vector part $\mathbf{n} = \mathbf{q}/\|\mathbf{q}\| \in \mathbb{S}^2$ will often be applied in the context of rotations, where $\mathbf{n} \in \mathbb{S}^2$ denotes the axis and ω the angle of a counter–clockwise rotation about $\mathbf{n}$.

Real quaternions and Euler angles

To represent a rotation $\mathbf{g}$ by its corresponding quaternion q in terms of Euler angles $(\alpha, \beta, \gamma)_{\mathrm{SM}}$ or $(\varphi_1, \Phi, \varphi_2)_{\mathrm{HJB}}$, respectively, we use

$$\begin{aligned}
q_1 &= \cos \frac{\alpha+\gamma}{2} \cos \frac{\beta}{2} = \cos \frac{\varphi_1+\varphi_2}{2} \cos \frac{\Phi}{2} \\
q_2 &= \sin \frac{\alpha-\gamma}{2} \sin \frac{\beta}{2} = \cos \frac{\varphi_1-\varphi_2}{2} \sin \frac{\Phi}{2} \\
q_3 &= \cos \frac{\alpha-\gamma}{2} \sin \frac{\beta}{2} = \sin \frac{\varphi_1-\varphi_2}{2} \sin \frac{\Phi}{2} \\
q_4 &= \sin \frac{\alpha+\gamma}{2} \cos \frac{\beta}{2} = \sin \frac{\varphi_1+\varphi_2}{2} \cos \frac{\Phi}{2}
\end{aligned}$$

and check that $q_1 = \cos \frac{\omega}{2} \geq 0$. If this constraint is not affirmed, then we represent $\mathbf{g}$ by $-q$ such that the constraint is now satisfied.

Quaternion representation of rotations in $\mathbb{R}^3$ (1)

Any active rotation $\mathbf{g} \in \mathbf{SO}(3)$ mapping the unit vector $\mathbf{h} \in \mathbb{S}^2$ onto the unit vector $\mathbf{r} \in \mathbb{S}^2$ according to

$$M(\mathbf{g})\, \mathbf{h} = \mathbf{r}$$

can be written in terms of its quaternion representation $q \in \mathbb{H}$ as

$$q(\mathbf{g})\, \mathbf{h}\, q^{-1}(\mathbf{g}) = \mathbf{r} \tag{9}$$

where quaternion multiplication applies.

To perform quaternion multiplication, $\mathbf{h}$ and $\mathbf{r}$ must be read as pure quaternions, i.e. they must be augmented with a zero scalar quaternion part; then Eq. (100) reads

$$q\, h\, q^{-1} = r \tag{10}$$

Quaternion representation of rotations in $\mathbb{R}^3$ (2)

Moreover, for $q \in \mathbb{S}^3$ the previous expression becomes

$$q\, h\, q^* = r$$

which explicitly reads then

$$\mathbf{r} = \mathbf{h} \cos\omega + (\mathbf{n} \times \mathbf{h}) \sin\omega + (\mathbf{n} \cdot \mathbf{h})\, \mathbf{n}\, (1 - \cos\omega) \tag{11}$$

where the representation of Eq. (8) has been applied. Nice proofs that Eq. (100) actually performs a rotation can be found, for instance, at
http://www.cs.berkeley.edu/ laura/cs184/quat/quatproof.html .

Quaternion representation of rotations in $\mathbb{R}^3$ (3)

The unit quaternion $q \in \mathbb{S}^3$ represents the rotation about the axis $\mathbf{q}$ by the angle $\omega = 2\arccos(q_0)$. Therefore, each unit quaternion $q \in \mathbb{S}^3$ can be seen as a representation of a rotation in $\mathbb{R}^3$, i.e. $\mathbb{S}^3$ stands for a double covering of the group $\mathbf{SO}(3)$.

It is emphasized that $\mathbb{S}^2 \subset \mathrm{Vec}\mathbb{H}$ consists of all quaternions representing rotations by the angle π about arbitrary axes, as every unit vector $\mathbf{q}$ can be considered as the pure quaternion $q = \cos(\pi/2) + \mathbf{q}\sin(\pi/2)$.

The unit quaternion q^* represents the inverse rotation $\boldsymbol{g}^{-1}\,\mathbf{r} = \mathbf{h}$.

Proof.

Proposition

. *Let $p, q \in \mathbb{S}^3$ be arbitrary unit quaternions, where q represents the rotation about the axis $\mathbf{n}$ by the angle ω according to Eq. (8). Then the quaternion $pqp^* \in \mathbb{S}^3$ represents the rotation about the rotated axes $p\,\mathbf{n}\,p^* \in \mathbb{S}^2$ by the same angle ω.*

It simply holds that

$$pqp^* = p\Big(\cos\frac{\omega}{2} + \mathbf{n}\sin\frac{\omega}{2}\Big)p^* = \cos\frac{\omega}{2} + p\mathbf{n}p^*\sin\frac{\omega}{2}\ . \qquad (12)$$

□

The left–hand side of Eq. (12) is referred to as representing the conjugation of rotations.

Geometry of Rotations

Quaternion representation of rotations in $\mathbb{R}^3$ (1)

Any rotation $\boldsymbol{g}$ mapping the unit vector $\mathbf{h} \in \mathbb{S}^2$ onto the unit vector $\mathbf{r} \in \mathbb{S}^2$ according to

$$\boldsymbol{g}\,\mathbf{h} = \mathbf{r}$$

can be written in terms of its unit quaternion representation $q \in \mathbb{S}^3 \subset \mathbb{H}$ as

$$q(\boldsymbol{g})\,\mathbf{h}\,q^*(\boldsymbol{g}) = \mathbf{r}$$

where quaternion multiplication applies.

To perform quaternion multiplication, $\mathbf{h}$ and $\mathbf{r}$ must be read as pure quaternions, i.e. they must be augmented with a zero scalar quaternion part; then

$$q\,h\,q^* = r$$

It explicitly reads then

$$\mathbf{r} = \mathbf{h}\cos\omega + (\mathbf{n}\times\mathbf{h})\sin\omega + (\mathbf{n}\cdot\mathbf{h})\,\mathbf{n}\,(1-\cos\omega) \qquad (13)$$

where the representation of Eq. (8) has been applied.

Quaternion representation of rotations in $\mathbb{R}^3$ (2)

The unit quaternion $q \in \mathbb{S}^3$ represents the rotation about the axis $\mathbf{q}$ by the angle $\omega = 2\arccos(q_0)$. Therefore, each unit quaternion $q \in \mathbb{S}^3$ can be seen as a representation of a rotation in $\mathbb{R}^3$, i.e. $\mathbb{S}^3$ stands for a double covering of the group $\mathbf{SO}(3)$.

It is emphasized that $\mathbb{S}^2 \subset \mathrm{Vec}\mathbb{H}$ consists of all quaternions representing rotations by the angle π about arbitrary axes, as every unit vector $\mathbf{q}$ can be considered as the pure quaternion $q = \cos(\pi/2) + \mathbf{q}\sin(\pi/2)$.

The unit quaternion q^* represents the inverse rotation $\boldsymbol{g}^{-1}\,\mathbf{r} = \mathbf{h}$.

Geometrical objects of $\mathbb{S}^3 \subset \mathbb{H}$ and of $\mathbb{S}^2 \subset \mathbb{R}^3$

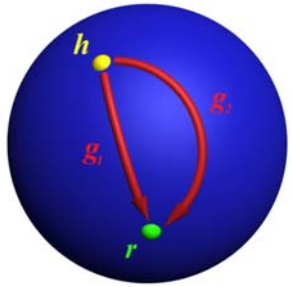

What is the geometrical characterization of the set of all rotations mapping $\mathbf{h} \in \mathbb{S}^2 \subset \mathbb{R}^3$ on $\mathbf{r} \in \mathbb{S}^2$.

Distance of rotations

The distance between two rotations $\boldsymbol{g}_1, \boldsymbol{g}_2$ is defined as

$$d(\boldsymbol{g}_1, \boldsymbol{g}_2) = \omega(\boldsymbol{g}_2\boldsymbol{g}_1^{-1})$$

the rotation angle of the composition $\widetilde{\boldsymbol{g}} = \boldsymbol{g}_2\boldsymbol{g}_1^{-1}$

With respect to their quaternion representation, this distance seems canonical as

$$\begin{aligned} d(\boldsymbol{g}_1, \boldsymbol{g}_2) &= \omega(\boldsymbol{g}_2\boldsymbol{g}_1^{-1}) = 2\arccos\Big(\mathrm{Sc}(q_2 q_1^*)\Big) \\ &= 2\arccos\Big(\mathrm{Sc}(q_2)\mathrm{Sc}(q_1) + \mathbf{q}_2 \cdot \mathbf{q}_1\Big) \\ &= 2\arccos\Big(\frac{1}{2}(q_2 q_1^* + q_1 q_2^*)\Big) \end{aligned}$$

Obviously

$$d(\boldsymbol{g}_1, \boldsymbol{g}_2) = d(\boldsymbol{g}_2, \boldsymbol{g}_1) = d(\boldsymbol{g}_1^{-1}, \boldsymbol{g}_2^{-1}) = d(\boldsymbol{g}_2^{-1}, \boldsymbol{g}_1^{-1})$$

Circle of quaternions

Definition

Let $q_1, q_2 \in \mathbb{S}^3$ be two orthogonal unit quaternions. The set of quaternions

$$q(t) = q_1 \cos t + q_2 \sin t, \quad t \in [0, 2\pi),$$

parametrizes the great–circle denoted $C(q_1, q_2) \subset \mathbb{S}^3$.

For example

$$q_1 = \frac{1 - rh}{\|1 - rh\|} \text{ and } q_2 = \frac{h + r}{\|h + r\|} \tag{14}$$

for $\mathbf{h}, \mathbf{r} \in \mathbb{S}^2$ with $\mathbf{r} \neq -\mathbf{h}$.

Obviously, $(\mathbf{h}, \mathbf{r})$ and $(-\mathbf{h}, -\mathbf{r})$ define the same great circle $C(q_1, q_2) \subset \mathbb{S}^3$.

Torus of quaternions (1)

Definition

Let $q_1, q_2, q_3, q_4 \in \mathbb{S}^3$ be four mutually orthonormal quaternions; let $C(q_1, q_2)$ denote the circle spanned by quaternions q_1, q_2, and $C(q_3, q_4)$ the orthogonal circle spanned by q_3, q_4. The set of quaternions

$$q(s,t;\Theta) = \Big(q_1 \cos s + q_2 \sin s\Big)\cos\Theta + \Big(q_3 \cos t + q_4 \sin t\Big)\sin\Theta\,, \quad s,t \in [0,2\pi),\ \ \Theta \in [0,\pi/2] \tag{15}$$

parametrizes the spherical torus denoted $T(C(q_1,q_2);\Theta) \subset \mathbb{S}^3$ with core $C(q_1,q_2)$.

It is actually known as **Clifford** torus, too.

Torus of quaternions (2)

Proposition

The representation of the torus $T(C_{\mathbf{h},\mathbf{r}};\frac{\rho}{2})$ can be factorized in terms of $C_{\mathbf{h},\mathbf{u}}$ and $C_{\mathbf{r},\mathbf{v}}$ as

$$T(C_{\mathbf{h},\mathbf{r}};\rho/2) = \{p_2^* p_1 \,|\, p_1 \in C_{\mathbf{h},\mathbf{u}},\ p_2 \in C_{\mathbf{r},\mathbf{v}},\ \mathbf{u}\cdot\mathbf{v} = \cos\rho\} \tag{16}$$

Small circle of unit vectors (1)

Definition

Let $\mathbf{r} \in \mathbb{S}^2$ be a unit vector and

$$r(t) = \cos\frac{t}{2} + \mathbf{r}\sin\frac{t}{2},\quad t \in [0,2\pi),$$

represent the rotation about $\mathbf{r}$ by $t \in [0,2\pi)$. Then the set of unit vectors

$$\mathbf{r}'(t) = r(t)\,\mathbf{r}_0'\,r^*(t),\quad t \in [0,2\pi), \tag{17}$$

with $\mathbf{r}_0' \in \mathbb{S}^2$ in the plane spanned by $\mathbf{h}$ and $\mathbf{r}$ such that $\mathbf{r}\cdot\mathbf{r}_0' = \cos(\rho), \mathbf{h}\cdot\mathbf{r}_0' = \cos(\eta-\rho)$ parametrizes the small circle or cone

$$c(\mathbf{r};\rho) = \{\mathbf{r}' \in \mathbb{S}^2 \,|\, \mathbf{r}\cdot\mathbf{r}' = \cos\rho\} \subset \mathbb{S}^2$$

with angle ρ with respect to its centre $\mathbf{r}$.

Small circle of unit vectors (2)

Its parametrized form explicitly reads (e.g. Altmann, 1986)

$$\mathbf{r}'(t) = \mathbf{r}_0'\cos t + (\mathbf{r}\times\mathbf{r}_0')\sin t + (\mathbf{r}\cdot\mathbf{r}_0')\,\mathbf{r}\,(1-\cos t),\quad t \in [0,2\pi).$$

Analogously for $\mathbf{h} \in \mathbb{S}^2$,

$$h(t) = \cos\frac{t}{2} + \mathbf{h}\sin\frac{t}{2},\quad t \in [0,2\pi),$$

representing the rotation about $\mathbf{h}$ by $t \in [0,2\pi)$ and $\mathbf{h}_0' \in \mathbb{S}^2$ in the plane spanned by $\mathbf{h}$ and $\mathbf{r}$ such that $\mathbf{h}\cdot\mathbf{h}_0' = \cos(\rho), \mathbf{r}\cdot\mathbf{h}_0' = \cos(\eta+\rho)$ results in

$$\mathbf{h}'(t) = h(t)\,\mathbf{h}_0'\,h^*(t),\quad t \in [0,2\pi). \tag{18}$$

Point–to–point rotation by circle of quaternions (1)

Proposition

The fibre $G(\mathbf{h},\mathbf{r})$ of all rotations with $\mathbf{g}\,\mathbf{h} = \mathbf{r}$ is represented by the circle $C(q_1, q_2) \subset \mathbb{S}^3$ spanned by unit quaternions $q_1, q_2 \in \mathbb{S}^3$ given in terms of $\mathbf{h},\mathbf{r} \in \mathbb{S}^2$ by Eqs. (364), for example.

Since $q(t)$ and $-q(t)$ represent the same rotation, the circle $C(q_1, q_2)$ covers the fibre $G(\mathbf{h},\mathbf{r})$ twice.

Thus the major property of the circle $C(q_1, q_2) \equiv C_{\mathbf{h},\mathbf{r}}$ is that it is uniquely characterized by a pair $(\mathbf{h},\mathbf{r}) \in \mathbb{S}^2 \times \mathbb{S}^2$ and its antipodally symmetric $(-\mathbf{h},-\mathbf{r})$ in the way that it consists of all quaternions $q(t), t \in [0, 2\pi)$, with $q(t)\,\mathbf{h}\,q^*(t) = \mathbf{r}$ for all $t \in [0, 2\pi)$, and that it covers the fibre $G(\mathbf{h},\mathbf{r})$ twice.

Point–to–point rotation by circle of quaternions (2)

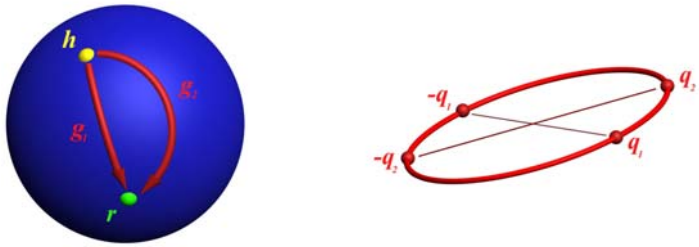

The fibre $G(\mathbf{h},\mathbf{r})$ of all rotations mapping $\mathbf{h} \in \mathbb{S}^2 \subset \mathbb{R}^3$ on $\mathbf{r} \in \mathbb{S}^2$ is represented by a great circle $C_{\mathbf{h},\mathbf{r}} \subset \mathbb{S}^3 \subset \mathbb{H}$.

Point–to–point rotation by circle of quaternions (3)

Proposition

The two circles $C(q_1, q_2)$ and $C(q_3, q_4)$ representing the fibres $G(\mathbf{h},\mathbf{r})$ and $G(-\mathbf{h},\mathbf{r})$, respectively, are orthonormal to one another.

Double fibration

Obviously, $G(\mathbf{h},\mathbf{r})$, $\mathbf{h},\mathbf{r} \in \mathbb{S}^2$, induces a double fibration or double covering of $\mathbf{SO}(3)$ as

$$\bigcup_{\mathbf{h}\in\mathbb{S}^2} G(\mathbf{h},\mathbf{r}) = \bigcup_{\mathbf{r}\in\mathbb{S}^2} G(\mathbf{h},\mathbf{r}) = \mathbf{SO}(3)$$

for any fixed $\mathbf{r}$ or fixed $\mathbf{h}$, respectively.

In the same way, the 1–dimensional geodesics, i.e. the great circles $C_{\mathbf{h},\mathbf{r}} \subset \mathbb{S}^3$, induce a double fibration of $\mathbb{S}^3$.

In fact, they are actually **Hopf** fibres.

Point–to–small circle rotation and vv by torus of quaternions (1)

Proposition

The set of all rotations mapping $\mathbf{h}$ *on the small circle* $c(\mathbf{r};\rho)$ *is equal to the set of all rotations mapping all elements of the small circle* $c(\mathbf{h};\rho)$ *onto* $\mathbf{r}$ *and represented by the spherical torus* $T(C(q_1,q_2);\frac{\rho}{2}) \subset \mathbb{S}^3$ *with core* $C(q_1,q_2)$.

The torus provides a multiple representation of the two sets of rotations.

Point–to–small circle rotation and vv by torus of quaternions (2)

The set of all rotations mapping $\mathbf{h} \in \mathbb{S}^2$ on the small circle $c(\mathbf{r};\rho) \subset \mathbb{S}^2$ is equal to the set of all rotations mapping the small circle $c(\mathbf{h};\rho)$ on $\mathbf{r}$, and it is represented by the torus $T(C;\rho/2) \subset \mathbb{S}^3$.

Point–to–small circle rotation and vv by torus of quaternions (3)

Proposition

The distance d *of an arbitrary* $q \in \mathbb{S}^3$ *from the circle* $C(q_1,q_2)$ *is given by*

$$d(q, C(q_1,q_2)) = \frac{1}{2}\arccos(q\mathbf{h}q^* \cdot \mathbf{r})$$

If $d(q, C(q_1,q_2)) = \rho$, then q and C are called ρ-incident.

Then, the torus $T(C(q_1,q_2);\frac{\rho}{2})$ consisting of all *quaternions* with distance $\frac{\rho}{2}$ from $C(q_1,q_2)$ essentially consists of all *circles* with distance $\frac{\rho}{2}$ from $C(q_1,q_2)$ representing all rotations mapping $\mathbf{h}$ on $c(\mathbf{r};\rho)$ and mapping $c(\mathbf{h};\rho)$ on $\mathbf{r}$.

Point–to–small circle rotation and vv by torus of quaternions (4)

Taking a second look at the equation

$$d(q, C(q_1,q_2)) = d(q, C_{\mathbf{h},\mathbf{r}}) = \frac{1}{2}\arccos(q\mathbf{h}q^* \cdot \mathbf{r}) = \frac{\rho}{2} \ ,$$

we may ask ourselves: Keeping q fixed, for which pairs $(\mathbf{h},\mathbf{r}) \in \mathbb{S}^2 \times \mathbb{S}^2$ is the equation above satisfied?

Obviously, the answer is:
It is satisfied for any $\mathbf{h} \in \mathbb{S}^2$, if $\mathbf{r} \in c(q\mathbf{h}q^*;\rho)$.
Equivalently, it is satisfied for any $\mathbf{r} \in \mathbb{S}^2$, if $\mathbf{h} \in c(q^*\mathbf{r}q;\rho)$.

Geometry of rotations

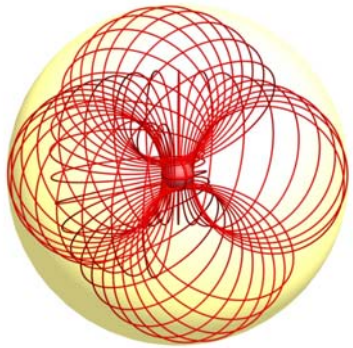

The set of all circles $C(p_1, p_2) \subset \mathbb{S}^3$ tangential to the sphere $s(q; \rho/2)$ with centre q and radius $\rho/2$.

Geometry of rotations

Eventually,

Proposition

The set of all circles $C(p_1, p_2) \subset \mathbb{S}^3$ with a fixed distance $\frac{\rho}{2}$ of a given $q \in \mathbb{S}^3$, i.e. the set of all circles tangential to the sphere $s(q; \rho/2)$ with centre q and radius $\rho/2$, is characterized by

$$\frac{\rho}{2} = d\Big(q, C(p_1, p_2)\Big) = \frac{1}{2}\arccos\Big(q\,\mathbf{h}\,q^* \cdot \mathbf{r}\Big), \qquad (19)$$

where $\mathbf{r} \in \mathbb{S}^2$ is uniquely defined in terms of $\mathbf{h}$ and p_1, p_2 by $\mathbf{r} := p(t)\,\mathbf{h}\,p^*(t)$ for all $p(t) \in C(p_1, p_2)$ and any arbitrary $\mathbf{h} \in \mathbb{S}^2$, i.e. each circle $C(p_1, p_2)$ represents all rotations mapping some $\mathbf{h} \in \mathbb{S}^2$ onto an element of the small circle $c(q\mathbf{h}q^*; \rho)$.

Geometry of rotations

Thus, for each $q \in \mathbb{S}^3$ and $\rho \in [0, \pi)$

$$\Big\{C(p_1, p_2) \,|\, d\Big(q, C(p_1, p_2)\Big) = \frac{\rho}{2}\Big\} = \bigcup_{\mathbf{h}\in\mathbb{S}^2} \bigcup_{\mathbf{r}\in c(q\,\mathbf{h}\,q^*;\rho)} C_{\mathbf{h},\mathbf{r}} \qquad (20)$$

$$= \bigcup_{\mathbf{h}\in\mathbb{S}^2} \bigcup_{\mathbf{r}\in c(q\,\mathbf{h}\,q^*;\rho)} C(p_1(\mathbf{h},\mathbf{r}), p_2(\mathbf{h},\mathbf{r}))$$

$$= \bigcup_{\mathbf{h}\in\mathbb{S}^2_+} \bigcup_{\mathbf{r}\in c(q\,\mathbf{h}\,q^*;\rho)} C(p_1(\mathbf{h},\mathbf{r}), p_2(\mathbf{h},\mathbf{r})),$$

where $\mathbb{S}^2_+$ denotes the upper hemisphere of $\mathbb{S}^2$. The last equation is due to the fact that $(\mathbf{h}, \mathbf{r})$ and $(-\mathbf{h}, -\mathbf{r})$ characterize the same great circle $C_{\mathbf{h},\mathbf{r}} \equiv C_{-\mathbf{h},-\mathbf{r}}$.

Geometry of rotations

Proposition

The distance of $q(t) \in C(q_1, q_2)$ from an arbitrary circle C_1 representing all rotations mapping $\mathbf{h}_1$ on $\mathbf{r}_1$ is given by spherical trigonometry

$$d(q(t), C_1) = \frac{1}{2}\arccos\Big(q(t)\mathbf{h}_1 q^*(t) \cdot \mathbf{r}_1\Big) \qquad (21)$$

$$= \frac{1}{2}\arccos\Big((\mathbf{h}\cdot\mathbf{h}_1)\,(\mathbf{r}\cdot\mathbf{r}_1) + \sqrt{1-(\mathbf{h}\cdot\mathbf{h}_1)^2}\sqrt{1-(\mathbf{r}\cdot\mathbf{r}_1)^2}\,\cos t\Big)$$

$$= \frac{1}{2}\arccos\Big(\cos\rho\,\cos\eta + \sin\rho\,\sin\eta\,\cos t\Big)\,. \qquad (22)$$

Geometry of rotations

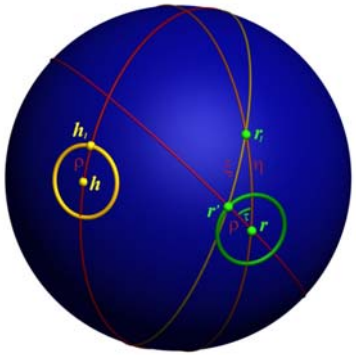

$$d(q(t), C_1) = \frac{1}{2}\arccos\Big(\cos\rho\,\cos\eta + \sin\rho\,\sin\eta\,\cos t\Big)\,.$$

Geometry of rotations

Preliminary conclusions

- One of the most beautiful features of quaternions is the role they play in the representation of rotations in low dimensional spaces $\mathbb{R}^3$ and $\mathbb{R}^4$.
- Representing rotations by quaternions yields an instructive and geometrically appealing clarification of the geometry of rotations.

Totally Geodesic Radon Transform

Application of the geometry of rotations to Radon transforms

Spherical Radon transform

Let $\mathcal{C}$ denote the set of all 1–dimensional totally geodesic submanifolds $C \subset \mathbb{S}^3$. Each $C \in \mathcal{C}$ is a 1–sphere, i.e. a circle with centre $\mathcal{O}$. Each circle is characterized by a unique pair of unit vectors $(\mathbf{h}, \mathbf{r}) \in \mathbb{S}^2 \times \mathbb{S}^2$ by virtue of $q\,\mathbf{h}\,q^* = \mathbf{r}$ for all $q \in C$.

Definition

The 1–dimensional spherical (totally geodesic) Radon transform of a real $f : \mathbb{S}^3 \mapsto \mathbb{R}^1$ is defined as

$$\mathcal{R}f(C) = \frac{1}{2\pi}\int_C f(q)\,d\omega_1(q) \equiv \mathcal{R}f(\mathbf{h}, \mathbf{r}).$$

It associates with the function f its mean values over circles $C \in \mathcal{C}$.

Then

$$\mathcal{X}f(\mathbf{h}, \mathbf{r}) = \frac{1}{2}\Big(\mathcal{R}f(C_{\mathbf{h},\mathbf{r}}) + \mathcal{R}f(C_{-\mathbf{h},\mathbf{r}})\Big), \qquad (23)$$

where $\mathcal{X}f$ is referred to as **basic crystallographic X–ray transform**.

Properties of the spherical Radon transform

As a function of $\boldsymbol{g} \mapsto \mathcal{R}f(\mathbf{h}, \boldsymbol{g}\mathbf{h})$, the 1d Radon transform is constant on the fibres $G(\mathbf{h}, \mathbf{r})$, i.e. for all $\boldsymbol{g} \in G(\mathbf{h}, \mathbf{r})$.

The 1d Radon transform $\mathcal{R}f(\mathbf{h}, \mathbf{r})$ satisfies the Darboux–type differential equation

$$(\Delta_{\mathbf{h}} - \Delta_{\mathbf{r}})\, \mathcal{R}f(\mathbf{h}, \mathbf{r}) = 0$$

where $\Delta_{\mathbf{h}}$ stands for the Laplace–Beltrami operator with respect to the spherical coordinates of $\mathbf{h}$.

Generalized spherical Radon transform

Definition

The generalized 1–dimensional spherical Radon transform of a real function $f : \mathbb{S}^3 \mapsto \mathbb{R}^1$ is defined as

$$\mathcal{R}^{(\rho)} f(C) = \frac{1}{4\pi^2 \sin\rho} \int_{d(q,C)=\rho} f(q)\, dq.$$

It associates with f its mean values over the torus $T(C, \rho)$ with core $C \equiv C_{\mathbf{h},\mathbf{r}}$ and radius ρ.

Spherically generalized translation

Definition

The spherically generalized translation of a function $F : \mathbb{S}^2 \mapsto \mathbb{R}^1$ is defined

$$\mathcal{T}_\rho F(\mathbf{r}) = \frac{1}{2\pi\sqrt{1-\cos^2\rho}} \int_{\mathbf{r}\mathbf{r}'=\cos\rho} F(\mathbf{r}')\, d\omega_2(\mathbf{r}').$$

It can be determined by

$$\mathcal{T}_\rho F(\mathbf{r}) = \frac{1}{2\pi\sqrt{1-\cos^2\rho}} \int_0^{2\pi} F(\mathbf{r}'(t))\, dt,$$

with $\mathbf{r}'(t)$ given according to

$$\mathbf{r}'(t) = r(t)\, \mathbf{r}'_0\, r^*(t), \quad t \in [0, 2\pi),$$

with $\mathbf{r}'_0 \in \mathbb{S}^2$ in the plane spanned by $\mathbf{h}$ and $\mathbf{r}$ such that $\mathbf{r} \cdot \mathbf{r}'_0 = \cos(\rho), \mathbf{h} \cdot \mathbf{r}'_0 = \cos(\eta - \rho)$.

Spherically generalized translation of a Radon transfom

When the translation $\mathcal{T}_\rho$ is applied to the Radon transform with respect to one of its arguments, then the geometry of rotations represented by quaternions amounts to

$$\begin{aligned}
\Big(\mathcal{T}_\rho[\mathcal{R}f]\Big)(\mathbf{h}, \mathbf{r}) &= \frac{1}{2\pi \sin\rho} \int_{c(\mathbf{h};\rho)} \mathcal{R}f(\mathbf{h}', \mathbf{r}) d\mathbf{h}' \\
&= \frac{1}{2\pi \sin\rho} \int_{c(\mathbf{r};\rho)} \mathcal{R}f(\mathbf{h}, \mathbf{r}') d\mathbf{r}' \qquad (24) \\
&= \frac{1}{4\pi^2 \sin\rho} \int_{T(C(q_1(\mathbf{h},\mathbf{r}), q_2(\mathbf{h},\mathbf{r})); \frac{\rho}{2})} f(q) dq \qquad (25) \\
&= \mathcal{R}^{(\rho/2)} f(C_{\mathbf{h},\mathbf{r}}). \qquad (26)
\end{aligned}$$

Eq. 39, cf. (Bunge, 1969, p. 47; Bunge, 1982, p. 76), is an Ásgeirsson–type mean value theorem (cf. Ásgeirsson, 1937; John, 1938) justifying the application of $\mathcal{T}_\rho$ to $\mathcal{R}f$ regardless of the order of its arguments, and Eq. 40 is instrumental to the inversion of the spherical Radon transform (Helgason, 1994; 1999).

The angle density function

We have just accomplished

Proposition

The generalized 1*–dimensional spherical Radon transform is equal to the translated spherical Radon transform*

$$\Big(\mathcal{T}_\rho[\mathcal{R}f]\Big)(\mathbf{h},\mathbf{r}) = \mathcal{R}^{(\rho/2)}f(C_{\mathbf{h},\mathbf{r}})$$

and it can be identified with the angle density function

$$\mathcal{R}^{(\rho/2)}f(C_{\mathbf{h},\mathbf{r}}) = \mathcal{A}f(\mathbf{h},\mathbf{r};\rho) = \frac{1}{2\pi\sin\rho}\int_{c(\mathbf{r};\rho)} \mathcal{R}f(\mathbf{h},\mathbf{r}')d\mathbf{r}' \quad (27)$$

The "angle distribution function" has been introduced in (Bunge, 1969, p. 44; Bunge, 1982, p. 74) (with a false normalization). It is the probability density that the crystallographic direction $\mathbf{h}$ statistically encloses the angle $\rho, 0 \leq \rho \leq \pi$, with the specimen direction $\mathbf{r}$ given the orientation probability density function f.

Crystallographic Orientation

Crystallographic orientation (1)

Neglecting crystal symmetry or assuming triclinic crystal symmetry, the crystallographic orientation $\boldsymbol{g}$ of an individual crystal is the active rotation $\boldsymbol{g} \in G \subset \mathbf{SO}(3)$ which brings a right–handed orthogonal coordinate system $K_\mathcal{S}$ fixed to the specimen into coincidence with a right–handed orthogonal coordinate system $K_\mathcal{C}$ fixed to the crystal,

$$\boldsymbol{g} \in \mathbf{SO}(3): \; K_\mathcal{S} \mapsto K_\mathcal{C}.$$

Texture analysis is the analysis of the crystallographic orientation distribution of a polycrystalline specimen.

Orientation imaging is the spatial analysis of the crystallographic orientation distribution of a polycrystalline specimen.

Crystallographic orientation (2)

If the right–handed specimen coordinate system $K_\mathcal{S} = <\mathbf{x},\mathbf{y},\mathbf{z}>$ and the right–handed crystallographic coordinate system $K_\mathcal{C} = <\mathbf{a},\mathbf{b},\mathbf{c}>$ are related to one another as

$$\boldsymbol{g}\,K_\mathcal{S} = K_\mathcal{C}$$

in the sense that

$$\boldsymbol{g}\,\mathbf{x} = \mathbf{a}, \;\; \boldsymbol{g}\,\mathbf{y} = \mathbf{b}, \;\; \boldsymbol{g}\,\mathbf{z} = \mathbf{c}$$

i.e. the crystallographic orientation $\boldsymbol{g}$ brings the specimen coordinate system $K_\mathcal{S}$ into coincendence with the crystal coordinate system $K_\mathcal{C}$ of an individual crystal, then the vector of coordinates $\mathbf{r}_{K_\mathcal{S}} \in \mathbb{S}^2$ with respect $K_\mathcal{S}$ of a unique vector and the vector $\mathbf{h}_{K_\mathcal{C}} \in \mathbb{S}^2$ of its coordinates with respect to $K_\mathcal{C}$ are related to one another by

$$\boldsymbol{g}\,\mathbf{h}_{K_\mathcal{C}} = \mathbf{r}_{K_\mathcal{S}}$$

Crystallographic Orientation (3)

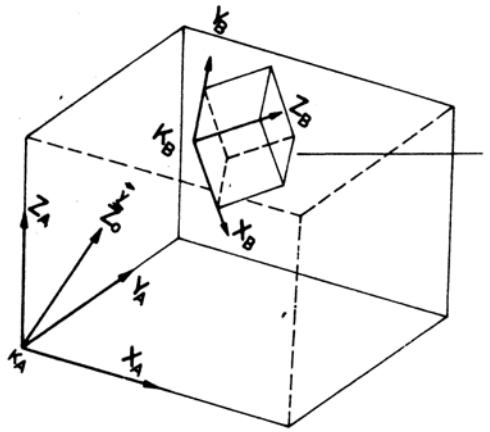

$$g \in G : \; K_S \mapsto K_C$$

(from Matthies, S., 1982, p. 16)

Crystallographic Orientation (4)

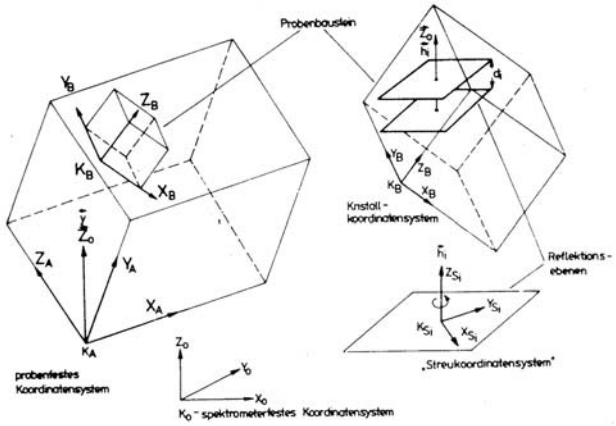

$$g\,K_S = K_C : \; g\,\mathbf{h}_{K_C} = \mathbf{r}_{K_S}$$

(from Matthies, S., 1982, p. 16)

Crystallographic Orientation (5)

In case of crystal symmetry several symmetrically equivalent crystal coordinate systems K_C, K'_C exist, which can be distinguished mathematically but not physically.

To each crystallographic direction $\mathbf{h}$ corresponds a set H of crystal symmetrically equivalent directions, which can be distinguished mathematically but not physically.

If the crystal symmetry class was given by a finite subgroup $\dot{G} \subset \mathbf{SO}(3)$ of rotations, then $H = \{\dot{g}\mathbf{h}_0 \,|\, \dot{g} \in \dot{G}\}$ for a given crystallographic direction $\mathbf{h}_0$. Thus we are interested in the sets

$$gH = \{g\dot{g}\mathbf{h}_0 \,|\, g \in \mathbf{SO}(3), \dot{g} \in \dot{G}, \mathbf{h}_0 \in \mathbb{S}^2\}\,,$$

and in particular in the sets $g\dot{G}$.

Crystallographic Orientation (6)

Applying the results of linear algebra, it is

$$M_{\mathcal{B}'_C}(\mathbf{v}) = M^{\mathcal{B}_{C'}}_{\mathcal{B}_C}(id)\; M^{\mathcal{B}_C}_{\mathcal{B}_S}(id) M_{\mathcal{B}_S}(\mathbf{v})\,.$$

Thus

$$M^{\mathcal{B}_{C'}}_{\mathcal{B}_S}(id) = M^{\mathcal{B}_{C'}}_{\mathcal{B}_C}(id)\; M^{\mathcal{B}_C}_{\mathcal{B}_S}(id)\,.$$

Then

$$M^{\mathcal{B}}_{\mathcal{B}}(g_e) = M^{\mathcal{B}}_{\mathcal{B}}(g)\, M^{\mathcal{B}}_{\mathcal{B}}(\dot{g}) = (B_S^t B_C)\,(B_C^t B'_C) = B_S^t B'_C$$

Crystallographic Orientation (7)

For an arbitrary $\mathbf{g} \in \mathbf{SO}(3)$ the set

$$\mathbf{g}\dot{G} = \{\mathbf{g}\dot{\mathbf{g}} | \dot{\mathbf{g}} \in \dot{G}\}$$

is called a left coset of $\dot{G}$.

Any two cosets have the same number of elements (cardinality), and their cardinality is equal to the cardinality of $\dot{G}$.

The left cosets of $\dot{G}$ induce a partition of $\mathbf{SO}(3)$ into equivalence classes. We may choose a representative of each equivalence class and refer to it as coset representative. The set of representatives is denoted $\mathbb{G}$.

The total number of cosets is called the index of $\dot{G}$ in $\mathbf{SO}(3)$ (and is infinite).

Crystallographic Orientation (8)

The set of all cosets is denoted $\mathbf{SO}(3)/\dot{G}$ and

$$\mathbf{SO}(3)/\dot{G} = \{\mathbf{g}\dot{G} \,|\, \mathbf{g} \in \mathbf{SO}(3)\}\,.$$

In group theory, one can proof that

$$\begin{aligned} \mathbf{SO}(3)/\dot{G} &= \Big(\mathbf{SO}(3) \otimes \{id, -id\}\Big)/\Big(\dot{G} \otimes \{id, -id\}\Big) \\ &= O(3)/\Big(\dot{G} \otimes \{id, -id\}\Big)\,. \end{aligned}$$

A function $f : \mathbf{SO}(3) \mapsto \mathbb{R}$ with the property

$$f(\mathbf{g}) = f(\mathbf{g}\dot{\mathbf{g}}) \text{ for all } \dot{\mathbf{g}} \in \dot{G}$$

is essentially defined on the set of cosets $\mathbf{SO}(3)/\dot{G}$.

Crystallographic Orientation (9)

Let $\mathbf{SO}(3)$ denote the special orthogonal group of (proper) rotations, and $O(3)$ the orthogonal group comprising rotations and inversions, thus $O(3) = \mathbf{SO}(3) \otimes \{id, -id\}$, where $-id$ denotes the symmetry operation of inversion.

Crystallographic Orientation (10)

Let $\mathcal{G}_\mathcal{C}$ denote the the crystallographic symmetry class, i.e. a finite point symmetry group; there exist 32 different symmetry classes. They are given by 11 purely rotational groups, 11 Laue groups, and 10 others.

Let

$$G_\mathcal{C} := \mathcal{G}_\mathcal{C} \cap \mathbf{SO}(3)$$

denote the finite point subgroup of proper rotations associated with the crystal symmetry class $\mathcal{G}_\mathcal{C}$, and $\#G_\mathcal{C}$ the total number of its elements.

Crystallographic Orientation (11) – Symmetry–Classes

The 32 crystallographic point groups and their symbols

System	Class		Symbol	
		Hermann-Mauguin	Schönflies	Mathematical
tricline	tricline - pedial	1	C_1	$\mathcal{C}_1$
	tricline - pinacoidal	$\overline{1}$	C_i	$\overline{\mathcal{C}_1}$
monocline	monocline - sphenoidal	2	C_2	$\mathcal{C}_2$
	monocline - domatic	m	C_s	$\mathcal{C}_2\mathcal{C}_1$
	monocline - prismatic	$2/m$	C_{2h}	$\overline{\mathcal{C}_2}$
rhombic	rhombic - disphenoidal	222	D_2	$\mathcal{D}_2$
	rhombic - pyramidal	$2mm$	C_{2v}	$\mathcal{D}_2\mathcal{C}_2$
	rhombic - dipyramidal	$2/m2/m2/m$	D_{2h}	$\overline{\mathcal{D}_2}$
tetragonal	tetragonal - pyramidal	4	C_4	$\mathcal{C}_4$
	tetragonal - disphenoidal	$\overline{4}$	S_4	$\mathcal{C}_4\mathcal{C}_2$
	tetragonal - dipyramidal	$4/m$	C_{4h}	$\overline{\mathcal{C}_4}$
	tetragonal - trapezohedral	422	D_4	$\mathcal{D}_4$
	ditetragonal - pyramidal	$4mm$	C_{4v}	$\mathcal{D}_4\mathcal{C}_4$
	tetragonal - scalenohedral	$\overline{4}2m$	D_{2d}, V_d	$\mathcal{D}_4\mathcal{D}_2$
	ditetragonal - dipyramidal	$4/m2/m2/m$, $4/mmm$	D_{4h}	$\overline{\mathcal{D}_4}$
trigonal	trigonal - pyramidal	3	C_3	$\mathcal{C}_3$
	trigonal - rhombohedral	$\overline{3}$	C_{3i}, S_6	$\overline{\mathcal{C}_3}$
	trigonal - trapezohedral	32	D_3	$\mathcal{D}_3$
	ditrigonal - pyramidal	$3m$	C_{3v}	$\mathcal{D}_3\mathcal{C}_3$
	ditrigonal - scalenohedral	$\overline{3}2/m$	D_{3d}	$\overline{\mathcal{D}_3}$
hexagonal	hexagonal - pyramidal	6	C_6	$\mathcal{C}_6$
	hexagonal - dipyramidal	$6/m$	C_{6h}	$\overline{\mathcal{C}_6}$

Crystallographic Orientation (12)

Due to Friedel's law the *effective* crystal symmetry is described by the point group

$$\widetilde{\mathcal{G}}_{\mathcal{C}} = \mathcal{G}_{\mathcal{C}} \otimes \{id, -id\},$$

which is also referred to as (associated) Laue class. Out of the 32 symmetry classes the 11 Laue groups contain the operation of inversion as an element of symmetry such that $\mathcal{G}_{\mathcal{C}} = \widetilde{\mathcal{G}}_{\mathcal{C}}$.

Let

$$\widetilde{G}_{\mathcal{C}} := \widetilde{\mathcal{G}}_{\mathcal{C}} \cap \mathbf{SO}(3) = \Big(\mathcal{G}_{\mathcal{C}} \otimes \{id, -id\}\Big) \cap \mathbf{SO}(3)$$

denote the finite subgroup of proper rotations with respect to the effective crystal symmetry class $\widetilde{\mathcal{G}}_{\mathcal{C}}$.

Crystallographic Orientation (13) – Laue–Classes

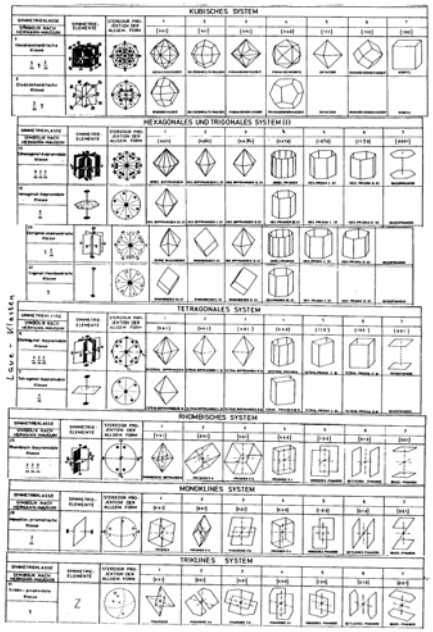

Crystallographic Orientation (14)

For the 11 purely rotational groups and the 11 Laue groups

$$\widetilde{\mathcal{G}}_{\mathcal{C}} = \mathcal{G}_{\mathcal{C}} \otimes \{id, -id\} = \Big(\mathcal{G}_{\mathcal{C}} \cap \mathbf{SO}(3)\Big) \otimes \{id, -id\} = G_{\mathcal{C}} \otimes \{id, -id\}$$

holds, implying

$$\widetilde{G}_{\mathcal{C}} = \widetilde{\mathcal{G}}_{\mathcal{C}} \cap \mathbf{SO}(3) = \Big(G_{\mathcal{C}} \otimes \{id, -id\}\Big) \cap \mathbf{SO}(3) = G_{\mathcal{C}}.$$

Therefore, the total number of their elements is

$$\#\widetilde{\mathcal{G}}_{\mathcal{C}} = 2\,\#G_{\mathcal{C}}\,.$$

For the remaining 10 groups

$$\widetilde{\mathcal{G}}_{\mathcal{C}} \neq G_{\mathcal{C}} \otimes \{id, -id\}, \qquad \widetilde{G}_{\mathcal{C}} \neq G_{\mathcal{C}}$$

In this case, restriction to $G_{\mathcal{C}}$ means an essential loss of information.

Crystallographic Orientation (15)

Example (cf. Matthies and Helming, 1982)

$$\mathcal{G}_\mathcal{C} = C_s = \{id, m\}$$

then

$$G_\mathcal{C} = \mathcal{G}_\mathcal{C} \cap \mathbf{SO}(3) = \{id, m\} \cap \mathbf{SO}(3) = \{id\} = C_1\,,$$

and

$$\widetilde{\mathcal{G}}_\mathcal{C} = \mathcal{G}_\mathcal{C} \otimes \{id, -id\} = \{id, m\} \otimes \{id, -id\} = \{id, m, -id, C_2\} = C_{2h}\,.$$

However,

$$G_\mathcal{C} \otimes \{id, -id\} = \{id, -id\}\,,$$

and is thus different from $\widetilde{\mathcal{G}}_\mathcal{C}$.
Also

$$\widetilde{G}_\mathcal{C} = \widetilde{\mathcal{G}}_\mathcal{C} \cap \mathbf{SO}(3) = \{id, m, -id, C_2\} \cap \mathbf{SO}(3) = \{id, C_2\} \neq G_\mathcal{C}\,.$$

Crystallographic Orientation (16)

From group theory it is known that

$$\begin{aligned} O(3)/\widetilde{\mathcal{G}}_\mathcal{C} &= \Big(\mathbf{SO}(3) \otimes \{id, -id\}\Big) / \Big(\mathcal{G}_\mathcal{C} \otimes \{id, -id\}\Big) \\ &= \mathbf{SO}(3) / \Big(\widetilde{\mathcal{G}}_\mathcal{C} \cap \mathbf{SO}(3)\Big) = \mathbf{SO}(3)/\widetilde{G}_\mathcal{C}\,. \end{aligned}$$

Eventually, for the 11 purely rotational groups and the 11 Laue groups

$$O(3)/\widetilde{\mathcal{G}}_\mathcal{C} = \mathbf{SO}(3)/G_\mathcal{C}\,.$$

For the remaining 10 groups

$$O(3)/\widetilde{\mathcal{G}}_\mathcal{C} = \mathbf{SO}(3)/\widetilde{G}_\mathcal{C} \neq \mathbf{SO}(3)/G_\mathcal{C}\,,$$

and the restriction to $\mathbf{SO}(3)/G_\mathcal{C}$ means an essential loss of information.

Crystallographic Orientation (17)

Tabelle 8.4. Kristallsysteme, Punktgruppen, Symmetrieabhängigkeit physikalischer Eigenschaften

Kristallsysteme	Nr.	Sch[a]	H.-M.[b]	Symmetrie-Elemente[c]		Symmetrie-Elemente und Bezugsrichtungen[d] a	b	c	Enantiomorphie	opt. Aktivität	Piezoelektriz.	Pyroelektriz.	Laue-Gruppen
triklin $a \neq b \neq c \neq a$, $\alpha \neq \beta \neq \gamma \neq \alpha$, $\alpha, \beta, \gamma \neq 90°$	1	C_1	1			–	–	–	+	+	+	+	$\bar{1}$
	2	C_i	$\bar{1}$		$\bar{1}$	–	–	–					
monoklin $a \neq b \neq c \neq a$, $\alpha = \gamma = 90°$, $\beta > 90°$	3	C_2	2	$\|_p$		–	2	–	+	+	+	+	2/m
	4	C_s	m	m		–	m	–		(+)	+	+	
	5	C_{2h}	2/m	$\|\perp$m	$\bar{1}$	–	2/m	–					
orthorhombisch $a \neq b \neq c \neq a$, $\alpha = \beta = \gamma = 90°$	6	D_2	222	$\|+\|+\|$		2	2	2	+	+	+		mmm
	7	C_{2v}	mm2	m+m+$\|_p$		m	m	2		(+)	+	+	
	8	D_{2h}	mmm (2/m2/m2/m)	($\|\perp$m)+($\|\perp$m)+($\|\perp$m)	$\bar{1}$	2/m	2/m	2/m					
tetragonal $a = b \neq c$, $\alpha = \beta = \gamma = 90°$						c	⟨a⟩	⟨110⟩					
	9	C_4	4	$\|_p$		4	–	–	+	+	+	+	4/m
	10	S_4	$\bar{4}$	◪		$\bar{4}$	–	–		(+)	+		

Crystallographic Orientation (18)

Tabelle 8.4 (Fortsetzung)

Kristallsysteme	Nr.	Sch[a]	H.-M.[b]	Symmetrie-Elemente[c]		Symmetrie-Elemente und Bezugsrichtungen[d] c	⟨a⟩	⟨110⟩	Enantiomorphie	opt. Aktivität	Piezoelektriz.	Pyroelektriz.	Laue-Gruppen
tetragonal $a = b \neq c$, $\alpha = \beta = \gamma = 90°$ (Fortsetzung)	11	C_{4h}	4/m	■$\perp$m	$\bar{1}$	4/m	–	–					4/m
	12	D_4	422	■+2$\|$+2$\|$		4	2	2	+	+	+		4/mmm
	13	C_{4v}	4mm	■$_p$+2m+2m		4	m	m			+	+	
	14	D_{2d}	$\bar{4}$2m	◪+2$\|$+2m		$\bar{4}$	2	m		(+)	+		
	15	D_{4h}	4/mmm (4/m2/m2/m)	(■$\perp$m)+2($\|\perp$m)+2($\|\perp$m)	$\bar{1}$	4/m	2/m	2/m					
trigonal $a = b \neq c$, $\alpha = \beta = 90°$, $\gamma = 120°$						c	⟨a⟩	–					
	16	C_3	3	▲$_p$		3	–	–	+	+	+	+	$\bar{3}$
	17	C_{3i}	$\bar{3}$	△	$\bar{1}$	$\bar{3}$	–	–					
	18	D_3	32	▲+3$\|_p$		3	2	–	+	+	+		$\bar{3}$m
	19	C_{3v}	3m	▲$_p$+3m		3	m	–			+	+	
	20	D_{3d}	$\bar{3}$m ($\bar{3}$2/m)	△+3($\|\perp$m)	$\bar{1}$	$\bar{3}$							

Crystallographic Orientation (18)

Tabelle 8.4 (Fortsetzung)

						c	⟨a⟩	⟨210⟩					
hexagonal $a = b \neq c$ $\alpha = \beta = 90°$ $\gamma = 120°$	21	C_6	6	●$_P$		6	–	–	+	+	+	+	6/m
	22	C_{3h}	$\bar{6}$	♣=(▲⊥m)		$\bar{6}$	–	–			+		
	23	C_{6h}	6/m	● ⊥m	$\bar{1}$	6/m	–	–					
	24	D_6	622	● +3◖ +3◖		6	2	2	+	+	+		6/mmm
	25	C_{6v}	6mm	●$_P$ +3m +3m		6	m	m			+	+	
	26	D_{3h}	$\bar{6}$m2	♣+3m+3◖$_P$ | ♣=(▲⊥m)		$\bar{6}$	m	2			+		
	27	D_{6h}	6/mmm (6/m 2/m 2/m)	(● ⊥m)+3(◖ ⊥m)+3(◖ ⊥m)	$\bar{1}$	6/m	2/m	2/m					
							⟨a⟩	⟨111⟩	⟨110⟩				
kubisch $a = b = c$ $\alpha = \beta = \gamma = 90°$	28	T	23	3◖ +4▲$_P$		2	3	–	+	+	+		m$\bar{3}$
	29	T_h	m$\bar{3}$ (2/m$\bar{3}$)	3(◖ ⊥m)+4▲	$\bar{1}$	2/m	$\bar{3}$	–					
	30	O	432	3■ +4▲ +6◖		4	3	2	+	+			m$\bar{3}$m
	31	T_d	$\bar{4}$3m	3◪ +4▲$_P$ +6m		$\bar{4}$	3	m			+		
	32	O_h	m$\bar{3}$m (4/m$\bar{3}$2/m)	3(■ ⊥m)+4▲+6(◖ ⊥m)	$\bar{1}$	4/m	$\bar{3}$	2/m					

The end

Thank you for your attention!

helmut.schaeben@geo.tu-freiberg.de

The end

≫ **Alles Gerade ist vom Teufel** ≪
Kant?, Leibniz?

≫ **Alles Leben ist in Kreisen** ≪
Indianisches Sprichwort

References

References (1)

Altmann, S.L., 1986, Rotations, Quaternions, and Double Groups: Oxford University Press, Oxford

Bigalke, H.G., 1984, Kugelgeometrie: Verlag Sauerländer

Burckhardt, J.J., 1947, Die Bewegungsgruppen der Kristallographie: Birkhäuser

Curtis, C.W., Reiner, J., 1962, Representation Theory of Finite Groups and Associative Algebras: Interscience, New York

Delanghe, R., Sommen, F., Souček, V., 1992, Clifford Algebra and Spinor-Valued Functions, A Function Theory for the Dirac Operator: Kluwer Academic Publishers, Dordrecht, Boston, London

References (2)

Gel'fand, I.M., Minlos, R.A., Shapiro, Z. Ya., 1963, Representations of the Rotation and Lorentz Groups and Their Applications: Pergamon Press

Gürlebeck, K., Sprößig, W., 1997, Quaternionic Calculus for Physicists and Engineers: Wiley

Hanson, A.J., 2006, Visualizing Quaternions: Morgan Kaufmann Publishers

Henderson, D.W., 1996, Experiencing Geometry on Plane and Sphere: Prentice Hall

Kleber, W., 1969, Einführung in die Kristallographie: VEB Verlag Technik

References (3)

Kuipers, J.B., 1999, Quaternions and Rotation Sequences - A Primer with Applications to Orbits, Aerospace, and Virtual Reality: Princeton University Press

Lang, S., 1969, Linear Algebra, 3rd printing: Addison–Wesley Publishing Company

Matthies, S., Helming, K., 1982, General considerations of the loss of information on the orientation distribution function of texturized samples in pole figure measurements: phys. stat. sol. (b), 113, 569-582

Meister, L., Schaeben, H., 2004, A concise quaternion geometry of rotations, MMAS 28, 101–126

References (4)

Mirman, R., 1999, Point Groups, Space Groups, Crystals, Molecules: World Scientific

Moran, P.A.P., 1975, Quaternions, Haar measure, and the estimation of a paleomagnetic rotation, in Gani, J., (ed.), Perspectives in Probability and Statistics, Applied Probability Trust, 295-301

Morawiec, A., 2004, Orientations and Rotations: Computations in Crystallographic Textures: Springer

Vilenkin, N.J., 1968, Special Functions and the Theory of Group Representations: Am. Math. Soc. Transl. 22

Visualization of Preferred Crystallographic Orientation, ω–Sections

Contents

Introduction

Since the domain of crystallographic orientations is three–dimensional and spherical, their insightful visualization or visualization of related probability density functions requires

- to exploit the effect of a given orientation on crystallographic axes,
- to consider pole point and pole density plots, respectively, and
- to apply projections from the two–dimensional unit spheres $S^2 \subset \mathbb{R}^3$ onto the unit disk $D = \{\mathbf{x} \in \mathbb{R}^2 \,|\, \|\mathbf{x}\| \leq 1\} \subset \mathbb{R}^2$.

Visualization of Preferred Crystallographic Orientation, ω–Sections

Pole point plots, pole density plots, pole figures

Pole point plots, Schmidt's Net (1)

Crystallographic directions may be represented by unit vectors; more specifically, by polar vectors $\mathbf{h} \in \mathbb{S}^2$ or axial vectors $\pm\mathbf{h} \in \mathbb{S}^2$. They may be visualized as points on the surface of the upper and/or lower hemisphere $\mathbb{S}^2 \subset \mathbb{R}^3$.

Pole point plots, Schmidt's Net (2)

Usually, they are projected onto the unit disk $D \subset \mathbb{R}^2$ and displayed in Schmidt's net (equal area projection)

$$\mathbf{r} = \begin{pmatrix} \cos\varphi \sin\vartheta \\ \sin\varphi \sin\vartheta \\ \cos\vartheta \end{pmatrix} \mapsto \mathbf{r}' = \begin{pmatrix} 2\sin\frac{\vartheta}{2}\cos\varphi \\ 2\sin\frac{\vartheta}{2}\sin\varphi \end{pmatrix}$$

$$\begin{pmatrix} 2\sin\frac{\vartheta}{2}\cos\varphi \\ 2\sin\frac{\vartheta}{2}\sin\varphi \end{pmatrix} = \begin{pmatrix} \frac{\sqrt{2}}{\sqrt{1+\cos\vartheta}} & 0 & 0 \\ 0 & \frac{\sqrt{2}}{\sqrt{1+\cos\vartheta}} & 0 \end{pmatrix} \begin{pmatrix} \cos\varphi \sin\vartheta \\ \sin\varphi \sin\vartheta \\ \cos\vartheta \end{pmatrix}$$

Equal–Area Projection

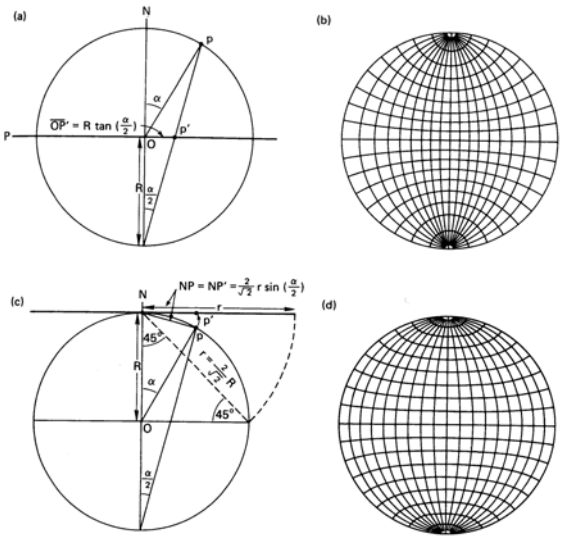

(from Wenk, H.-R., 1985, p. 13)

Pole–Density Diagrams, Schmidt's Net

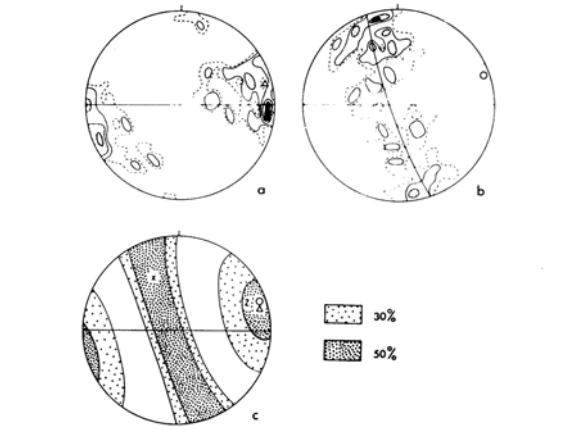

FIG. 6.—*a* and *b*, Orientation density diagrams (*lower hemisphere*) of olivine in a deformed peridotite; sample SQ 1-29. The foliation plane is vertical E-W and the lineation is horizontal E-W. 100 measurements; Counting area 1/220 of the hemisphere area. (*a*), [100] olivine, contours 1, 2, 4, 6 and 10%, *triangle* = best axis. (*b*), [010] olivine, contours, 1, 2, 4 and 6%, *circle* = best plane pole. *c* Synthetic diagram corresponding to figs. 6*a* (*Z*) and 6*b* (*X*) (lower hemisphere). Best [100] = *triangle*: best plane pole of [010] = *circle*.

(from Darot, M., Bouchez, J.L., 1976, J. Geol. 84, 239-247)

Pole Figures (1)

Display

$$P(\mathbf{h},\mathbf{r}) = \frac{1}{4\pi}\int_{G(\mathbf{h},\mathbf{r})\cup G(-\mathbf{h},\mathbf{r})} f(\boldsymbol{g})\,d\boldsymbol{g} = P_{\mathbf{h}}(\mathbf{r})$$

graphically as a function of the specimen direction **r** depending on the parameter given by the crystallographic direction **h** by contour lines of equal density in equal area projection.

Pole Figures (2)

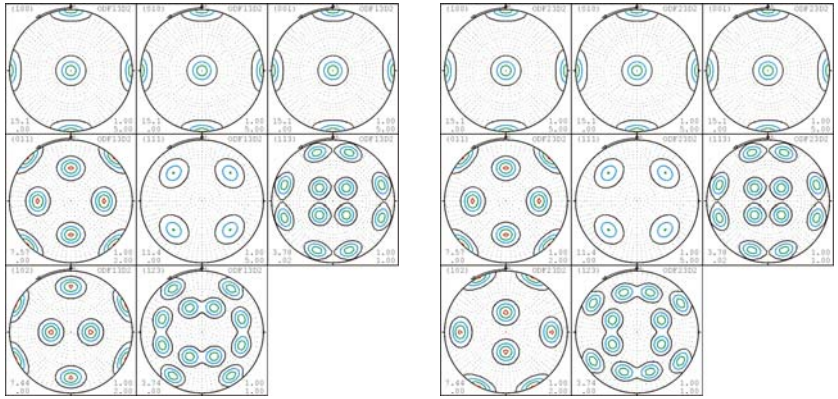

Pole figures $P_{\mathbf{h}}(\mathbf{r})$ of $f_1(\boldsymbol{g};\boldsymbol{g}^o_{11},\boldsymbol{g}^o_{12},\boldsymbol{g}^o_{13})$ and pole figures $P_{\mathbf{h}}(\mathbf{r})$ of $f_2(\boldsymbol{g};\boldsymbol{g}^o_{21},\boldsymbol{g}^o_{22},\boldsymbol{g}^o_{23})$, respectively, for several crystal forms with orthorhombic crystal symmetry imposed.

Visualization of Preferred Crystallographic Orientation, ω–Sections

Visualizing orientations and their probability density function

Domains and Visualizations of ODFs (1)

An odf f may be thought of as a function of the Euler angles $(\varphi_1, \Phi, \varphi_2)$. The domain of this function is usually displayed as a 3d rectangular box.

Then the odf is usually visualized as contour lines of equal density in series of cross–sections perpendicular to one of the three axes.

Domains and Visualizations of ODFs (2)

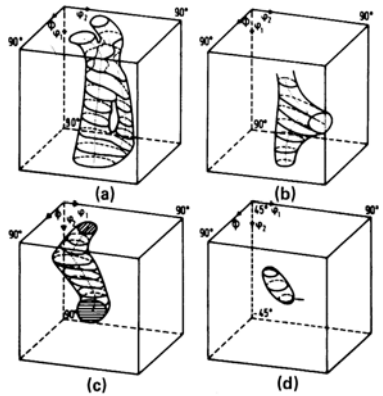

(from Bunge, in Wenk, H.-R., 1985, p. 84)
Just a cartoon!

Domains and Visualizations of ODFs (3)

An odf f may be thought of as a function of the Euler angles (α, β, γ). The domain of this function is usually displayed as a cylinder.

Then the ODF is usually visualized as contour lines of equal density in series of cross–sections perpendicular to the γ–axis, i.e. in γ–sections.

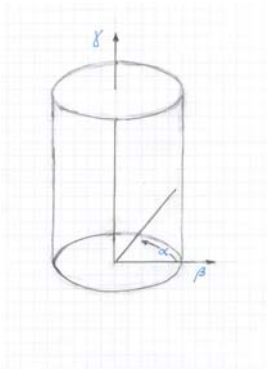

Domains and Visualizations of ODFs (4)

An odf f may be thought of as a function of unit quaternions $q \in \mathbb{S}^3$. The essential domain of this function is the upper (lower) unit hypersphere $\mathbb{S}^3_+ \subset \mathbb{R}^4$.

Then the ODF is usually visualized as contour lines of equal density on the upper (lower) hypersphere.

Domains and Visualizations of ODFs (5)

If the odf f depends on the angle ω of the orientation $\boldsymbol{g}(\omega, \mathbf{n})$ only, it may be thought of as a function of $\cos\omega$. The domain of this function is the real interval $[-1, 1]$.
Then it is referred to as "rotationally symmetric", " rotationally invariant ", "spherically radial", "central", or "zonal".

In this special case, the odf can be visualized as a simple graph of f over the interval $[-1, 1]$.

Visualization by Averaging ODFs (1)

An odf $f : \mathbb{S}^2 \times [0, \pi] \mapsto \mathbb{R}^1_+$ given in terms of axis and angle of an orientation

$$f(\boldsymbol{g}) = f(\omega, \mathbf{n}), \quad \omega \in [0, \pi], \ \mathbf{n} \in \mathbb{S}^2$$

may be averaged with respect to $\mathbf{n} \in \mathbb{S}^2$ and transformed into a new univariate function $f_2 : [0, \pi] \mapsto \mathbb{R}^1_+$ by

$$f_{\text{zonal}}(\omega(\boldsymbol{g})) = \frac{1}{4\pi} \int_{\mathbb{S}^2} f(\omega, \mathbf{n})\, d\mathbf{n}$$

f_{zonal} is by definition independent of the axis $\mathbf{n}$, but depends on the angle $\omega(\boldsymbol{g})$ of the orientation $\boldsymbol{g} = \boldsymbol{g}(\omega, \mathbf{n})$ only.

Visualization by Averaging ODFs (2)

$$f_{\text{zonal}}(\omega(\boldsymbol{g})) = \frac{1}{4\pi} \int_{\mathbb{S}^2} f(\omega, \mathbf{n})\, d\mathbf{n}$$

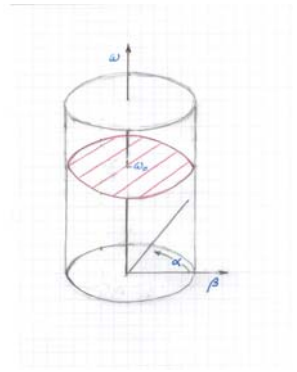

Visualization by Averaging ODFs (3)

Are there more interesting projections?

Let $\boldsymbol{g} = \boldsymbol{g}(\alpha, \beta, \gamma) \in \mathbf{SO}(3)$,
and let $\mathbf{r} \in \mathbb{S}^2 \subset \mathbb{R}^3$ with $\mathbf{r} = (\cos\alpha \sin\beta, \sin\alpha \sin\beta, \cos\beta)^t_{Ks}$.
Then $\boldsymbol{g}\,\mathbf{c} = \mathbf{r}$ for all $\gamma \in [0, 2\pi]$.

Analogously, let $\boldsymbol{g} = \boldsymbol{g}(\alpha, \beta, \gamma) \in \mathbf{SO}(3)$.
Then $\boldsymbol{g}^{-1}\mathbf{z} = \mathbf{h}'$ with
$\mathbf{h}' := (\cos\gamma' \sin\beta, \sin\gamma' \sin\beta, \cos\beta)^t_{Kc}, \quad \gamma' = \pi - \gamma$, for all $\alpha \in [0, 2\pi]$, i.e. $\boldsymbol{g}\mathbf{h}' = \mathbf{z}$

Visualization of Preferred Crystallographic Orientation, ω–Sections

γ–sections

γ–sections (1)

Since

$$\boldsymbol{g}(\alpha,\beta,\gamma)\,\mathbf{c} = \boldsymbol{g}(\alpha,\beta,\gamma)\begin{pmatrix}0\\0\\1\end{pmatrix}_{K_C} = \begin{pmatrix}\cos\alpha\sin\beta\\ \sin\alpha\sin\beta\\ \cos\beta\end{pmatrix}_{K_S} =: \mathbf{r}_{K_S}$$

for all $\gamma \in [0, 2\pi)$ it holds that

$$\begin{aligned}\frac{1}{2\pi}\int_{[0,2\pi]} f(g(\alpha,\beta,\gamma))d\gamma &= \frac{1}{2\pi}\int_{\{\boldsymbol{g}\in\mathbf{SO}(3)\,|\,\boldsymbol{g}\,\mathbf{c}=\mathbf{r}_{K_S}\}} f(\boldsymbol{g})d\boldsymbol{g}\\ &= \mathcal{R}f(\mathbf{c},\mathbf{r}_{K_S}),\end{aligned}$$

which gives rise to γ–sections, the superposition of which is the **c**–pole figure.

What is the physical meaning of γ?

γ–sections (2)

Formally, γ–sections may be defined with respect to an equidistant partition $0 = \gamma_0 < \gamma_1 < \ldots < \gamma_{n+1} = \pi$ with $\gamma_{i+1} - \gamma_i = \Delta\gamma$ of the range $[0, \pi]$ of γ by

$$\Gamma_i f(\mathbf{c},\mathbf{r}) = \frac{1}{2\pi}\int_{[\gamma_i,\gamma_{i+1}]} f(\boldsymbol{g}(\alpha,\beta,\gamma))d\gamma,\ i = 1,\ldots,n$$

with

$$\sum_{i=1}^{n}\Gamma_i f(\mathbf{c},\mathbf{r}) = \mathcal{R}f(\mathbf{c},\mathbf{r})$$

γ–sections (3)

As a function of $\boldsymbol{g} \mapsto \mathcal{R}f(\mathbf{c},\boldsymbol{g}\,\mathbf{c})$, it is constant for all $\boldsymbol{g} \in G(\mathbf{c},\mathbf{r}) := \{\boldsymbol{g} \in \mathbf{SO}(3)\,|\,\boldsymbol{g}\,\mathbf{c} = \mathbf{r}\}$.

If f is constant on the set $G(\mathbf{c},\mathbf{r})$ for all $\mathbf{r}$, then $\mathcal{R}f(\mathbf{c},\mathbf{r})$ contains the entire information carried by f; actually

$$f(\boldsymbol{g}) = \mathcal{R}f(\mathbf{c},\boldsymbol{g}\,\mathbf{c}).$$

If an odf f does not depend on $\boldsymbol{g}$ but only on the dot product $\mathbf{r}_0 \cdot \boldsymbol{g}\mathbf{h}_0$, then it is referred to as a $(\mathbf{h}_0,\mathbf{r}_0)$–fibre texture. Fibres are a special case of the situation described above.

γ–sections (4)

The projection of $\mathbf{z}_{K_S}$ onto the tangential plane at $\mathbf{r}$

$$(\mathbf{z}_{K_S})_T(\mathbf{r}) \quad = \quad \frac{\mathbf{z}_{K_S} - (\mathbf{z}_{K_S} \cdot \mathbf{r})\,\mathbf{r}}{\|\mathbf{z}_{K_S} - (\mathbf{z}_{K_S} \cdot \mathbf{r})\,\mathbf{r}\|}$$

and the projection of $\boldsymbol{g}\mathbf{a}_{K_C}$ onto the tangential plane at $\mathbf{r}$

$$(\boldsymbol{g}\mathbf{a}_{K_C})_T(\mathbf{r}) = \boldsymbol{g}\mathbf{a}_{K_C} - (\mathbf{a}_{K_C} \cdot \mathbf{c}_{K_C})\,\mathbf{r} = \boldsymbol{g}\mathbf{a}_{K_C}$$

enclose the angle $\pi - \gamma$ to be interpreted as the angle ω between the orthogonal projection of $\boldsymbol{g}\mathbf{a}_{K_C}$, being counterclockwise rotated by γ about $\mathbf{r}$, and the orthogonally projected $\mathbf{z}_{K_S}$ when $(\boldsymbol{g}\mathbf{a}_{K_C})_T(\mathbf{r}), (\mathbf{z}_{K_S})_T(\mathbf{r})$, and $\mathbf{r}$ are thought of as a right-handed system.

γ–sections (5)

Is it possible to define sections of an orientation space such that their superposition is any user–specified pole figure?
Is it possible to spread any pole figure into corresponding sections of an orientation space?

Visualization of Preferred Crystallographic Orientation, ω–Sections

Generalization: ω–sections

Crystallographic orientation – pole points

The orientation $\boldsymbol{g}$ of an individual crystal is the rotation $\boldsymbol{g} \in \mathbf{SO}(3) : K_S \mapsto K_C$ which maps a right–handed orthonormal coordinate system K_S fixed to the specimen onto another right–handed orthonormal coordinate system K_C fixed to the crystal,

$$\boldsymbol{g}\,K_S = K_C, \;\; \boldsymbol{g} \in \mathbf{SO}(3). \tag{28}$$

If a unique direction is represented by $\mathbf{h}$ with respect to the crystal frame K_C, and by $\mathbf{r}$ with respect to the specimen frame K_S, and the two coordinate systems transform by $K_C = \boldsymbol{g}\,K_S$, then the coordinates of the unique direction transform according to

$$\mathbf{r}_{K_S} = \boldsymbol{g}\,\mathbf{h}_{K_C}. \tag{29}$$

Double fibration of $\mathbf{SO}(3)$

The sets

$$G(\mathbf{h},\mathbf{r}) = \{\boldsymbol{g} \in \mathbf{SO}(3) \,|\, \boldsymbol{g}\mathbf{h} = \mathbf{r},\ \ (\mathbf{h},\mathbf{r}) \in \mathbb{S}^2 \times \mathbb{S}^2\} \qquad (30)$$

provide a double fibration of $\mathbf{SO}(3)$ as
(i) given $\mathbf{h}_0$, it holds that $G(\mathbf{h}_0,\mathbf{r}_1) \cap G(\mathbf{h}_0,\mathbf{r}_2) = \emptyset$ if $\mathbf{r}_1 \neq \mathbf{r}_2$, and, analogously, given $\mathbf{r}_0$, it holds that $G(\mathbf{h}_1,\mathbf{r}_0) \cap G(\mathbf{h}_2,\mathbf{r}_0) = \emptyset$ if $\mathbf{h}_1 \neq \mathbf{h}_2$;
(ii)

$$\bigcup_{\mathbf{r}\in\mathbb{S}^2} G(\mathbf{h}_0,\mathbf{r}) = \bigcup_{\mathbf{h}\in\mathbb{S}^2} G(\mathbf{h},\mathbf{r}_0) = \mathbf{SO}(3);$$

(iii) given $\boldsymbol{g} \in \mathbf{SO}(3)$ and $\mathbf{h}_0$, there exists a vector $\mathbf{r}$ such that $\boldsymbol{g} \in G(\mathbf{h}_0,\mathbf{r})$, and, analogously, given $\boldsymbol{g} \in \mathbf{SO}(3)$ and $\mathbf{r}_0$, there exists a vector $\mathbf{h}$ such that $\boldsymbol{g} \in G(\mathbf{h},\mathbf{r}_0)$.

Parametrization of a fibre $G(\mathbf{h},\mathbf{r})$ (1)

The elements $\boldsymbol{g} \in G(\mathbf{h},\mathbf{r})$ can be factorized and the factorization provides a parametrization of $G(\mathbf{h},\mathbf{r})$

$$\begin{aligned} G(\mathbf{h},\mathbf{r}) &= \{\boldsymbol{g}_0\, \boldsymbol{g}(\omega;\mathbf{h}) \,|\, \boldsymbol{g}_0 \in G(\mathbf{h},\mathbf{r}),\ \omega \in [0,2\pi)\} \\ G(\mathbf{h},\mathbf{r}) &= \{\boldsymbol{g}(\omega;\mathbf{r})\, \boldsymbol{g}_0 \,|\, \boldsymbol{g}_0 \in G(\mathbf{h},\mathbf{r}),\ \omega \in [0,2\pi)\} \end{aligned} \qquad (31)$$

The elements of $G(\mathbf{h},\mathbf{r})$ may be thought of as to differ by an initial rotation about $\mathbf{h}$, or a final rotation about $\mathbf{r}$, respectively, by an arbitrary angle $\omega \in [0,2\pi)$.

What is the physical meaning of ω?

To which rotation does ω refer?

How to control ω to use it for visualization?

ω–sections (1)

Since an orientation $\boldsymbol{g}$ is uniquely determined by two pairs of directions $(\mathbf{h},\mathbf{r})$ and $(\mathbf{h}_1,\mathbf{v})$, each of which consists of one crystallographic and one specimen direction, provided that $(\mathbf{h}\times\mathbf{r})\times(\mathbf{h}_1\times\mathbf{v}) \neq 0$, the angle ω is determined as the angle enclosed by the orthogonal projection $(\boldsymbol{g}\mathbf{h}_1)_T(\mathbf{r})$ of $\boldsymbol{g}\mathbf{h}_1$ and the orthogonal projection $(\mathbf{v})_T(\mathbf{r})$ of a second variable user–defined specimen direction $\mathbf{v}$ onto the tangential plane at $\mathbf{r}$ when looking at the tangential plane from outside the pole sphere, provided that $\mathbf{v} \neq \mathbf{r}$.

$\omega = 0$ refers to the unique orientation $\boldsymbol{g}_0$ such that

$$\boldsymbol{g}_0\,\mathbf{h} = \mathbf{r} \text{ and } \boldsymbol{g}_0\,\mathbf{h}_1 = \mathbf{v}$$

ω–sections (2)

Formally

$$\omega(\mathbf{r}) := \angle(\ (\mathbf{v})_T(\mathbf{r}),\ \ (\boldsymbol{g}\mathbf{h}_1)_T(\mathbf{r})\ ) \qquad (32)$$

with

$$\begin{aligned} (\mathbf{v})_T(\mathbf{r}) &:= \mathbf{v} - (\mathbf{v}\cdot\mathbf{r})\,\mathbf{r} \\ (\boldsymbol{g}\mathbf{h}_1)_T(\mathbf{r}) &:= \boldsymbol{g}\mathbf{h}_1 - (\boldsymbol{g}\mathbf{h}_1\cdot\mathbf{r})\,\mathbf{r} = \boldsymbol{g}(\mathbf{h}_1 - (\mathbf{h}_1\cdot\mathbf{h})\,\mathbf{h}) \end{aligned}$$

ω–sections (3)

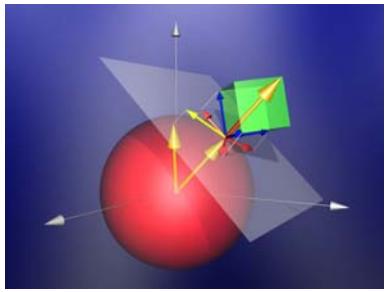

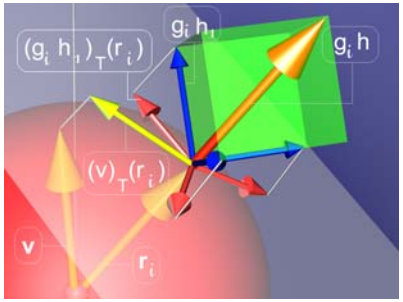

(111)–pole sphere displaying $(111)^t = \mathbf{h} = \boldsymbol{g}_i^{-1}\,\mathbf{r}_i$, and the associated tangential plane with the orthogonal projection of the crystal direction $\mathbf{h}_1 = (100)^t$, represented by $\boldsymbol{g}_i\,\mathbf{h}_1$ with respect to the specimen coordinate system $K_{\mathcal{S}}$, as well as $(010)^t$ and $(001)^t$, and the orthogonal projection of the specimen direction $\mathbf{v}$, enclosing the angle ω (Figures by courtesy of Heiko Kost, Anidesk Digitalvisualization, Webenheim, Germany).

ω–sections (4)

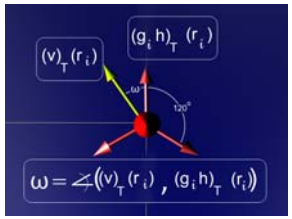

Top view of tangential plane with the orthogonal projection of the crystal direction $\mathbf{h}_1 = (100)^t$, represented by $\boldsymbol{g}_i\,\mathbf{h}_1$ with respect to the specimen coordinate system $K_{\mathcal{S}}$, as well as $(010)^t$ and $(001)^t$, and the orthogonal projection of the specimen direction $\mathbf{v}$ enclosing the angle ω (Figure by courtesy of Heiko Kost, Anidesk Digitalvisualization, Webenheim, Germany).

ω–sections (5)

$\omega = 0$ refers to the unique orientation $\boldsymbol{g}_0$ such that

$$\boldsymbol{g}_0\,\mathbf{h} = \mathbf{r} \text{ and } \boldsymbol{g}_0\,\mathbf{h}_1 = \mathbf{v}$$

A subsequent rotation about $\mathbf{r}$ by $\omega \in [0, 2\pi)$ results in the orientation $\boldsymbol{g} = \boldsymbol{g}(\omega, \mathbf{r})\,\boldsymbol{g}_0$ such that

$$\begin{aligned} \omega(\boldsymbol{g}, \boldsymbol{g}_0) &= \omega \\ \angle(\,(\mathbf{v})_{\mathcal{T}}(\mathbf{r}),\ (\boldsymbol{g}\,\mathbf{h}_1)_{\mathcal{T}}(\mathbf{r})\,) &= \omega \\ \boldsymbol{g}\mathbf{h} = \boldsymbol{g}(\omega, \mathbf{r})\,\boldsymbol{g}_0\mathbf{h} &= \mathbf{r} \end{aligned}$$

ω–sections (6)

An ω–section of the orientation space is defined in terms of

1. a crystallographic direction $\mathbf{h}$ characterizing the pole point or pole density plot, which is the superposition of all sections. An orientation $\boldsymbol{g}$ is initially displayed at location $\mathbf{r} = \boldsymbol{g}\mathbf{h}$ and at all locations corresponding to crystal–symmetrically equivalent directions of $\mathbf{h}$;
2. a second crystallographic direction $\mathbf{h}_1$ not parallel to $\mathbf{h}$, a specimen direction $\mathbf{v}$ not parallel to $\mathbf{r}$, an angle $\omega \in [0, 2\pi]$, and an angular tolerance $\Delta\omega$. An orientation is actually displayed if and only if the angle of $\boldsymbol{g}\mathbf{h}_1$ and $\mathbf{v}$ both orthogonally projected onto the tangential plane of the $\mathbf{h}$–pole sphere at $\mathbf{r}$ is in $[\omega - \Delta\omega, \omega + \Delta\omega]$, i.e.

$$\angle(\,(\mathbf{v})_{\mathcal{T}}(\mathbf{r})\ ,\ (\boldsymbol{g}\,\mathbf{h}_1)_{\mathcal{T}}(\mathbf{r})\,) \in [\omega - \Delta\omega, \omega + \Delta\omega].$$

ω–sections (7)

Formally, an ω–section of the orientation space is defined for integral measurements by

$$\Omega f(\mathbf{h},\mathbf{r};\mathbf{h}_1,\mathbf{v},\omega,\Delta\omega) = \frac{1}{2\pi}\int_{[\omega-\Delta\omega,\,\omega+\Delta\omega]} f(\boldsymbol{g}(\varpi;\mathbf{r})\boldsymbol{g}_0)\,d\varpi \quad (33)$$

and for individual measurements by

$$P_n(\boldsymbol{g};\mathbf{h},\mathbf{r};\mathbf{h}_1,\mathbf{v},\omega,\Delta\omega) = \sum_{i=1}^{n} \mathbb{1}_{\{\boldsymbol{g}(\omega,\mathbf{r})\boldsymbol{g}_0\,|\,\omega\in[\omega-\Delta\omega,\omega+\Delta\omega]\}}(\boldsymbol{g}) \quad (34)$$

with the rotation $\boldsymbol{g}_0$ such that $\boldsymbol{g}_0\mathbf{h} = \mathbf{r}$ and $(\boldsymbol{g}_0\mathbf{h}_1)_T(\mathbf{r}) = \boldsymbol{g}_0((\mathbf{h}_1)_T(\mathbf{r})) = (\mathbf{v})_T(\mathbf{r})$, where $(\mathbf{h},\mathbf{r})$ and $(\mathbf{h}_1,\mathbf{v})$ are two pairs of a crystallographic and a specimen direction, which are presumed to be given, i.e. they have to be specified by the user as have ω and $\Delta\omega$, respectively.

ω–sections (8)

If

$$\mathbf{h} = \mathbf{c}_{K_C} \quad \text{and} \quad \boldsymbol{g}(\alpha,\beta,\gamma)\,\mathbf{c}_{K_C} = \mathbf{r}_{K_S}$$
$$\mathbf{h}_1 = \mathbf{a}_{K_C} \quad \text{and} \quad \mathbf{v} = \mathbf{z}_{K_S}$$

then ω–sections reduce to γ–sections with

$$\omega = \pi - \gamma$$

Moreover, σ–sections can be interpreted as ω–sections with a varying specimen direction $\mathbf{v} = \boldsymbol{g}(-\alpha;\mathbf{r})\mathbf{z}_{K_S}$, because then it holds

$$\omega - \alpha = \pi - \gamma - \alpha = \pi - 2\sigma$$

Visualization of Preferred Crystallographic Orientation, ω–Sections

Bingham distribution of a random unit quaternion

Bingham distribution of a random unit quaternion von Mises – Fisher 3×3 matrix distribution

Employing the one-one correspondence between $\mathbf{SO}(3)$ and $\mathbb{S}^3$ the following theorem (Prentice, 1986) has been deduced.

Let μ be the mapping that assigns to each quaternion representation $q \in \mathbb{S}^3$ the matrix representation $X \in \mathbf{SO}(3)$ of a rotation. Then $X \in \mathbf{SO}(3)$ has a von Mises – Fisher matrix distribution $M_3(F)$ if and only if $q \in \mathbb{S}^3$ with $\mu(q) = X$ has a Bingham distribution $B_4(\Lambda, A)$.

Bingham distribution of a random unit quaternion (1)

Let $q \in \mathbb{S}^3 \subset \mathbb{R}^4$ be a unit quaternion representing a random rotation. Then $q \in \mathbb{S}^3$ is said to be distributed according to the (even) Bingham distribution $B_4(\Lambda, A)$ (Bingham, 1964; 1974) if it has the probability density function

$$f_{\mathrm{B}}(q; \Lambda, A) \;=\; c_B^{-1}(\Lambda)\, \exp\left\{ \sum_{i=1}^{4} \lambda_i \left(\mathrm{Sc}(a_i^* q) \right)^2 \right\} \, [\, ds_3 \,] \;,$$

where ds_3 represents the Lebesgue invariant area element on $\mathbb{S}^3$, $A \in SO(4)$ is a (4×4) orthogonal matrix with unit column quaternions $a_i \in \mathbb{S}^3 \subset \mathbb{H}$ such that

$$\sum_{i=1}^{4} \left(\mathrm{Sc}(a_i^* q) \right)^2 = 1,$$

Λ is a (4×4) diagonal matrix with entries $\lambda_1, \ldots, \lambda_4$, and $c_B(\Lambda)$ is a normalizing constant depending on Λ only.

Bingham distribution of a random unit quaternion (2)

$B_4(\Lambda + \alpha I_4, A)$ and $B_4(\Lambda, A)$ are indistinguishable for any $\alpha \in \mathbb{R}^1$, i. e. the shape parameters λ_i, $i = 1, \ldots, 4$, are determined only up to an additive constant. Uniqueness can be imposed by some convention.

Bingham distribution of a random unit quaternion (3)

The spherical Radon transform $\mathcal{R}$ of the Bingham distribution

$$\left(\mathcal{R} \left[f_{\mathrm{B}}(\circ; \Lambda, A) \right] \right)(\mathbf{h}, \mathbf{r}) \;=\; \frac{1}{2\pi} \int_{\{q \in \mathbb{S}^3 \,|\, q\,\mathbf{h}\,q^* = \mathbf{r}\}} f_{\mathrm{B}}(q; \Lambda, A)\; ds_3(q)$$

follows from integration along the circle $C(q_1, q_2)$ as

$$\begin{aligned} \mathcal{R} f_{\mathrm{B}}(\mathbf{h}, \mathbf{r}) \;&=\; c_B^{-1}(\Lambda)\, \frac{1}{2\pi} \int_0^{2\pi} \exp\left(\sum_{i=1}^{4} \lambda_i \left(\mathrm{Sc}(a_i^* q(t)) \right)^2 \right) dt \\ &=\; c_B^{-1}(\Lambda)\, \exp(\xi)\, I_0(\sqrt{\upsilon^2 + \zeta^2}) \end{aligned}$$

with

$$\begin{aligned} \xi \;&=\; \frac{1}{2} \sum_{i=1}^{4} \lambda_i \left((\mathrm{Sc}(a_i^* q_1))^2 + (\mathrm{Sc}(a_i^* q_2))^2 \right), \\ \upsilon \;&=\; \frac{1}{2} \sum_{i=1}^{4} \lambda_i \left((\mathrm{Sc}(a_i^* q_1))^2 - (\mathrm{Sc}(a_i^* q_2))^2 \right), \\ \zeta \;&=\; \sum \lambda_i\, \mathrm{Sc}(a_i^* q_1)\, \mathrm{Sc}(a_i^* q_2)\,. \end{aligned}$$

Bingham distribution of a random unit quaternion (4)

Special cases related to "Ideal–Lagen"

Unimodal standard orientation density function

$$\begin{aligned} f_b(\omega_b; S_b) \;&=\; C_b^{-1}(S_b)\, \exp\,(S_b\, \cos\,\omega_b)\, [\, ds_3(\omega_b) \,], \\ \mathcal{R} f_b(\mathbf{h}, \mathbf{r}) \;&=\; C_b^{-1}(2\lambda)\, \exp(\lambda\,(z_4 - 1))\, I_0(\lambda(1 + z_4)), \;\; z_4 = a_4\,\mathbf{h}\,a_4^* \cdot \mathbf{r}. \end{aligned}$$

Circular ("fibre") standard orientation density function

$$\begin{aligned} f_c(\omega_c;\, \lambda) \;&=\; C_c^{-1}(\lambda)\, \exp(\,\lambda\, \cos\omega_c\,)\, [ds_3(\omega_{\mathbf{c}})], \\ \mathcal{R} f_c(\mathbf{h}, \mathbf{r}) \;&=\; C_c^{-1}(\lambda)\, \exp\,(\,\lambda\, z_h\, z_r\,)\, I_0\Big(\,\lambda\, \sqrt{1 - z_h^2}\, \sqrt{1 - z_r^2}\,\Big) \\ &\qquad z_h = \mathbf{h} \cdot \mathbf{h}_c, z_r = \mathbf{r} \cdot \mathbf{r}_c. \end{aligned}$$

Spherical ("surface") standard orientation density function

$$\begin{aligned} f_s(\omega_s; S_s) \;&=\; C_s^{-1}(S_s)\, \exp\,(S_s\, \cos\,\omega_s)\, [\, ds_3(\omega_s) \,], \\ \mathcal{R} f_s(\mathbf{h}, \mathbf{r}) \;&=\; C_s^{-1}(2\lambda)\, \exp(\lambda\,(1 - z_1))\, I_0(\lambda(1 + z_1)), \;\; z_1 = a_1\,\mathbf{h}\,a_1^* \cdot \mathbf{r}. \end{aligned}$$

Example

The Bingham disribution

$$f_{\mathrm{B}}(q;\Lambda,A) \;=\; c_B^{-1}(\Lambda)\,\exp\left\{\sum_{i=1}^{4}\lambda_i\left(\mathrm{Sc}(a_i^* q)\right)^2\right\}\,[\,ds_3\,]\;,$$

for rotations represented by unit quaternions in $S^3 \subset \mathbb{R}^4$ or, equivalently, the von Mises–Fisher matrix distribution

$$f_{\mathrm{vMF}}(X;F) = C_{\mathrm{vMF}}^{-1}(D_\kappa)\exp[\,\mathrm{tr}(FX^t)\,]\,[\,dX\,]$$

provide a model for three different patterns of preferred crystallographic orientation called

- bimodal axial,
- multimodal circular, and
- multimodal spherical.

If the distribution is rotationally symmetric, the three cases refer to a simple texture, a fibre texture, and a spherical or surface texture (component), cf. (Schaeben, 1996; Schaeben and Kunze, 2003).

Example (cont.)

Individual rotation data according to the three cases have been simulated with parameter matrix

$$F = KM \tag{35}$$

decomposed into the elliptical component K and the polar component M. In all tree cases, M has been chosen to represent the identical rotation

$$M = \begin{pmatrix} 1 & 0 & 0 \\ 0 & 1 & 0 \\ 0 & 0 & 1 \end{pmatrix}$$

Example (cont.)

To simulate rotationally symmteric distributions, the elliptical component has been chosen

1. in case (i) of a axial simple texture

$$K_1 = \kappa \begin{pmatrix} 1 & 0 & 0 \\ 0 & 1 & 0 \\ 0 & 0 & 1 \end{pmatrix}, \quad \kappa = 50$$

2. in case (ii) of a fibre texture

$$K_2 = \kappa \begin{pmatrix} 0 & 0 & 0 \\ 0 & 0 & 0 \\ 0 & 0 & 1 \end{pmatrix}, \quad \kappa = 50$$

3. in case (iii) of a spherical or surface texture texture

$$K_3 = -\kappa \begin{pmatrix} 1 & 0 & 0 \\ 0 & 1 & 0 \\ 0 & 0 & 1 \end{pmatrix}, \quad \kappa = 50$$

Example (cont.)

For all three cases,

1. first the spherical Radon transform is displayed for $\mathbf{h} = (001)^t$ and $\mathbf{h} = (111)^t$ in equal area projection of the lower and upper hemisphere, both as pole point plot and pole density plot;
2. then the pole point plot of the spherical Radon transform for $\mathbf{h} = (001)^t$ augmented by $\mathbf{h}_1 = (111)^t$ and $\mathbf{v} = (010)^t$ is depicted,
3. then the spreading of the $(001)^t$–figure into ω–sections is exposed .

Example (cont.)

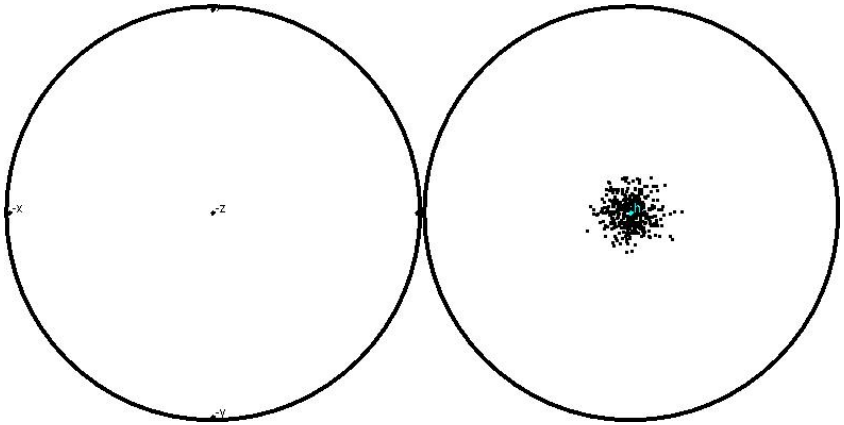

Fig. 3: Pole point plot of the spherical Radon transform of the axial distribution for $\mathbf{h} = (001)^t$ in equal area projection of lower (left) and upper (right) hemisphere.

Example (cont.)

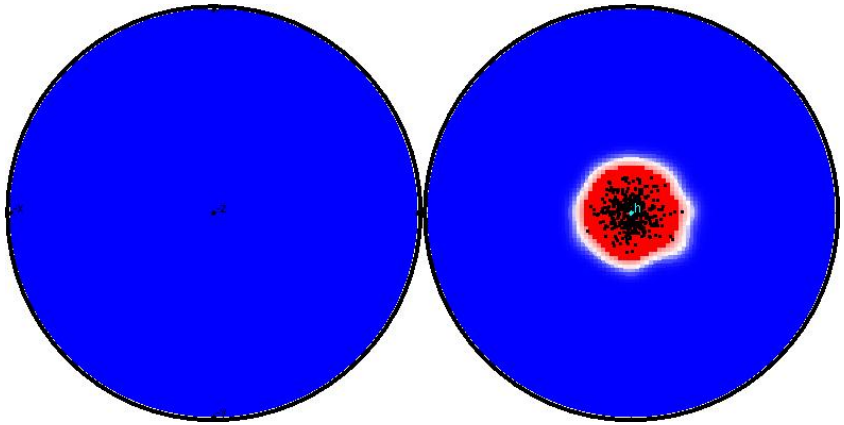

Fig. 4: Pole density plot of the spherical Radon transform of the axial distribution for $\mathbf{h} = (001)^t$ in equal area projection of lower (left) and upper (right) hemisphere.

Example (cont.)

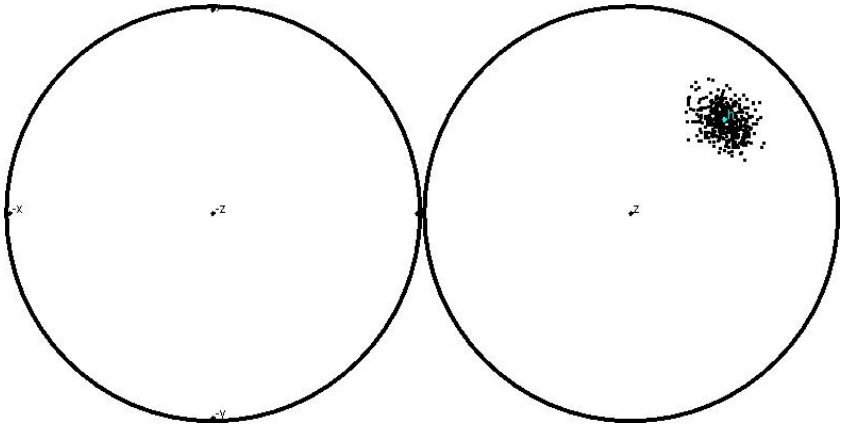

Fig. 5: Pole point plot of the spherical Radon transform of the axial distribution for $\mathbf{h} = (111)^t$ in equal area projection of lower (left) and upper (right) hemisphere.

Example (cont.)

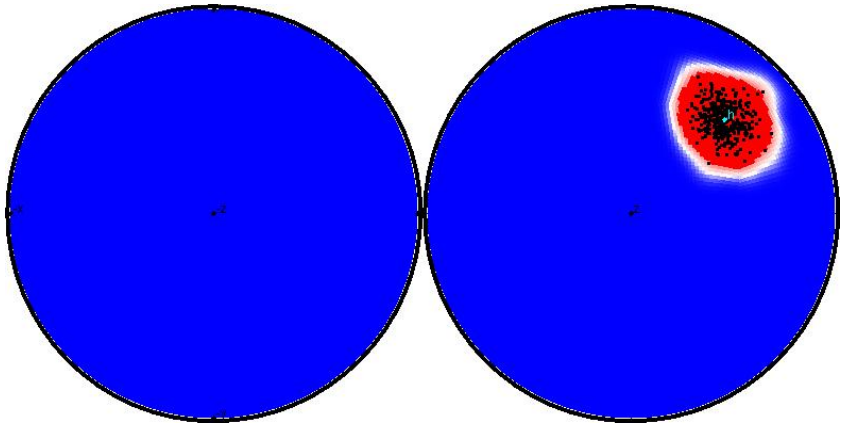

Fig. 6: Pole density plot of the spherical Radon transform of the axial distribution for $\mathbf{h} = (111)^t$ in equal area projection of lower (left) and upper (right) hemisphere.

Example (cont.)

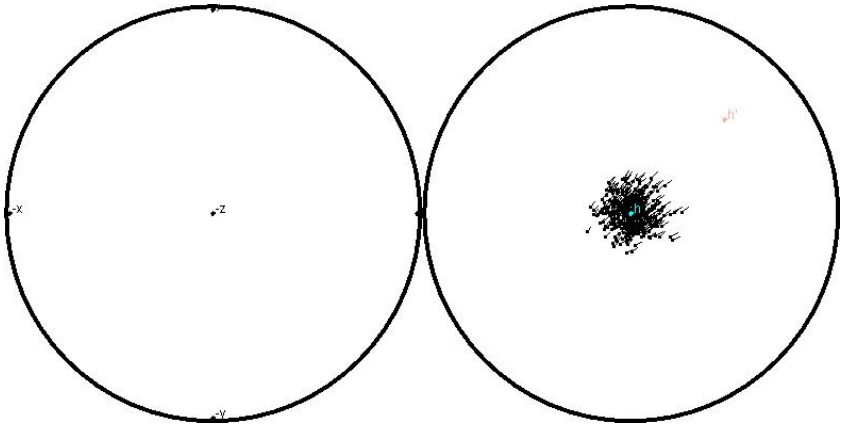

Fig. 7: Augmented pole point plot of the spherical Radon transform of the axial distribution for $\mathbf{h} = (001)^t$ in equal area projection of lower (left) and upper (right) hemisphere displaying the direction of (111) at each pole point $\mathbf{h}_i = \boldsymbol{g}_i\mathbf{h}$.

Example (cont.)

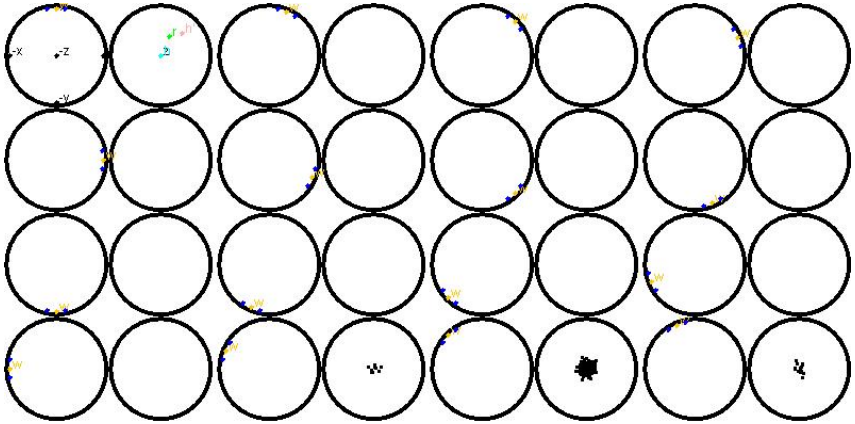

Fig. 8: ω–sections of (001) pole point plot of the spherical Radon transform of the axial distribution with stepsize $\Delta\omega = 11.25$.

Example (cont.)

For the symmetrical bimodal axial case of the von Mises–Fisher distribution (simple texture) both the $\mathbf{h} = (001)^t$ and the $\mathbf{h} = (111)^t$ pole point (Fig. 3 and Fig. 5) and pole density plots (Fig. 4 and Fig. 6) show a strong circularly symmetrical maximum at $\mathbf{r} = (001)^t$ and $\mathbf{r} = 1/\sqrt{3}(111)^t$, respectively. The augmented $(001)^t$–pole point plot (Fig. 7) shows that $\boldsymbol{g}_i(111)^t$ displayed at $\mathbf{r}_i = \boldsymbol{g}_i(001)^t$ point to $1/\sqrt{3}(111)^t$ with little deviations. The ω–sections (Fig. 8) reveal that the distribution of the angles enclosed by the orthogonal projections of $\mathbf{h}_1 = (111)^t$ and $\mathbf{v} = (010)^t$ onto the tangential plane at $\mathbf{r}_i = \boldsymbol{g}_i(001)^t$ is unimodally symmetrically and strongly concentrated at $-\pi/4$.

Example (cont.)

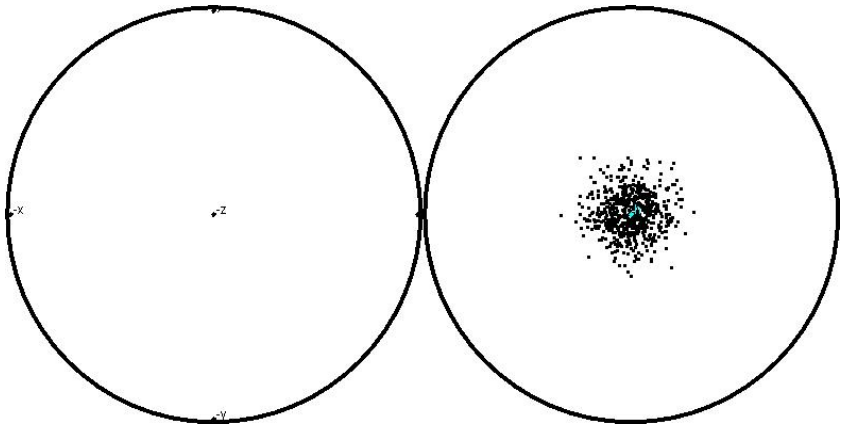

Fig. 9: Pole point plot of the spherical Radon transform of the circular distribution for $\mathbf{h} = (001)^t$ in equal area projection of lower (left) and upper (right) hemisphere.

Example (cont.)

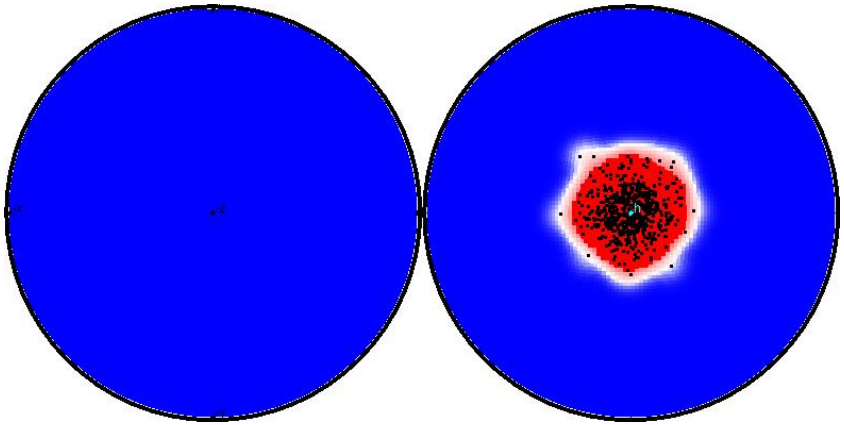

Fig. 10: Pole density plot of the spherical Radon transform of the circular distribution for $\mathbf{h} = (001)^t$ in equal area projection of lower (left) and upper (right) hemisphere.

Example (cont.)

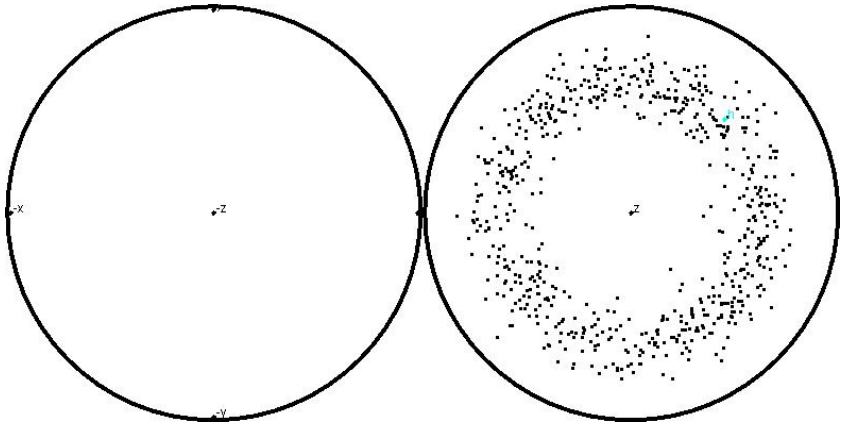

Fig. 11: Pole point plot of the spherical Radon transform of the circular distribution for $\mathbf{h} = (111)^t$ in equal area projection of lower (left) and upper (right) hemisphere.

Example (cont.)

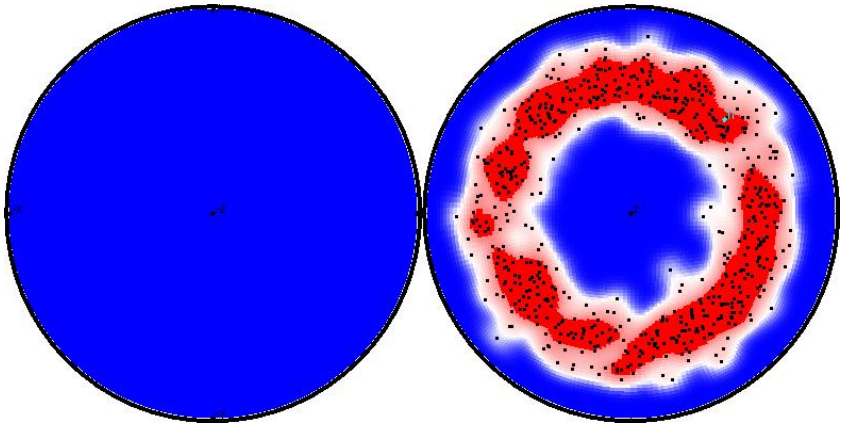

Fig. 12: Pole density plot of the spherical Radon transform of the circular distribution for $\mathbf{h} = (111)^t$ in equal area projection of lower (left) and upper (right) hemisphere.

Example (cont.)

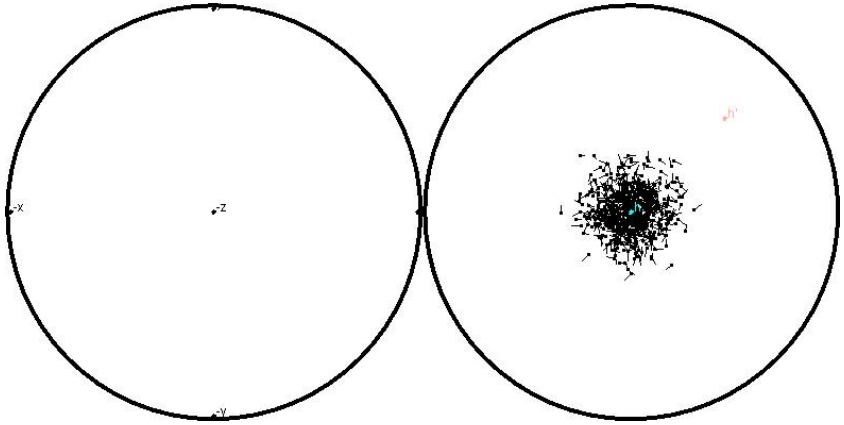

Fig. 13: Augmented pole point plot of the spherical Radon transform of the circular distribution for $\mathbf{h} = (001)^t$ in equal area projection of lower (left) and upper (right) hemisphere displaying the direction of (111) at each pole point $\mathbf{h}_i = \boldsymbol{g}_i\mathbf{h}$.

Example (cont.)

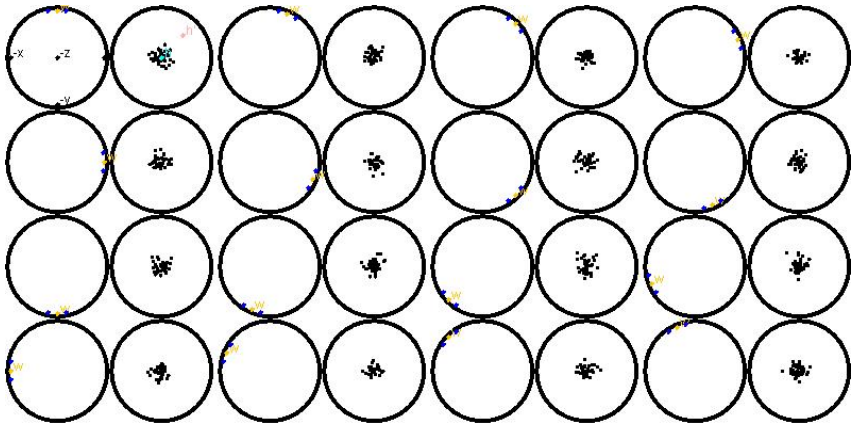

Fig. 14: ω–sections of (001) pole point plot of the spherical Radon transform of the circular distribution with stepsize $\Delta\omega = 11.25$.

Example (cont.)

For the symmetrical circular case of the von Mises–Fisher distribution (fibre texture) the $\mathbf{h} = (001)^t$–pole point (Fig. 9) and the pole density (Fig. 10) plots show a strong circular symmetrical maximum at $\mathbf{r} = (001)^t$. The $\mathbf{h} = (111)^t$ pole point (Fig. 11) and pole density (Fig. 12) plot show a symmetrical small circle distribution with an aperture angle of 54 degrees. The augmented $(001)^t$–pole point plot (Fig. 13) indicates a uniform distribution of the angles enclosed by the orthogonal projections of $\mathbf{h}_1 = (111)^t$ and $\mathbf{v} = (010)^t$ onto the tangential plane at $\mathbf{r}_i = \mathbf{g}_i(001)^t$. The ω–sections (Fig. 14) confirm the uniform distribution.

Example (cont.)

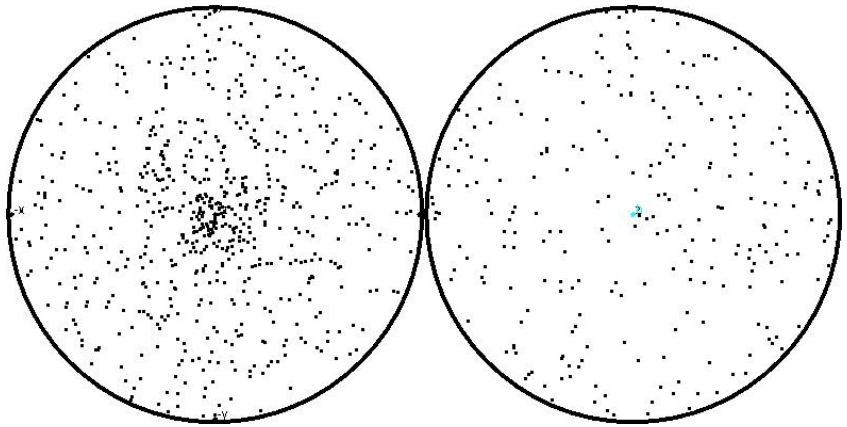

Fig. 15: Pole point plot of the spherical Radon transform of the spherical distribution for $\mathbf{h} = (001)^t$ in equal area projection of lower (left) and upper (right) hemisphere.

Example (cont.)

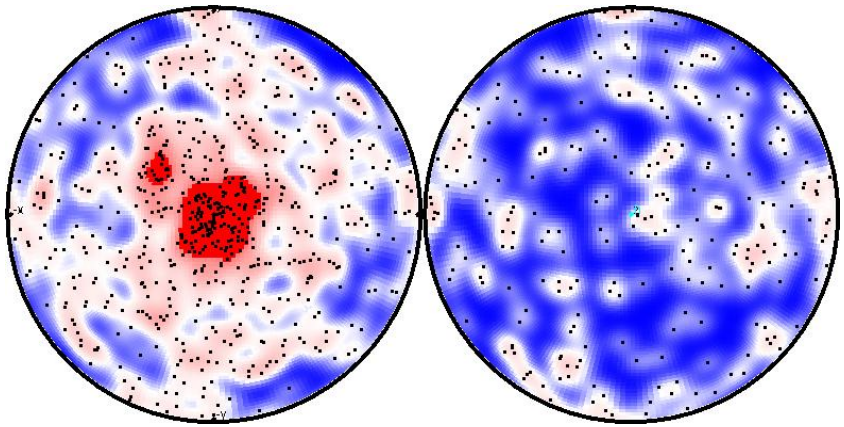

Fig. 16: Pole density plot of the spherical Radon transform of the spherical distribution for $\mathbf{h} = (001)^t$ in equal area projection of lower (left) and upper (right) hemisphere.

Example (cont.)

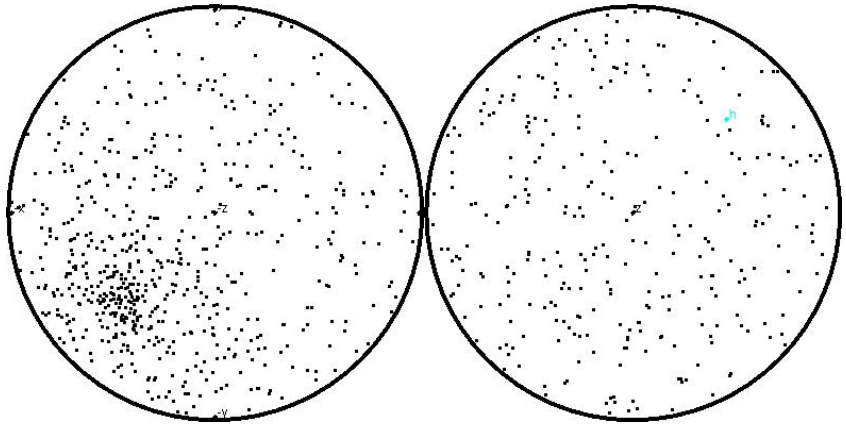

Fig. 17: Pole point plot of the spherical Radon transform of the spherical distribution for $\mathbf{h} = (111)^t$ in equal area projection of lower (left) and upper (right) hemisphere.

Example (cont.)

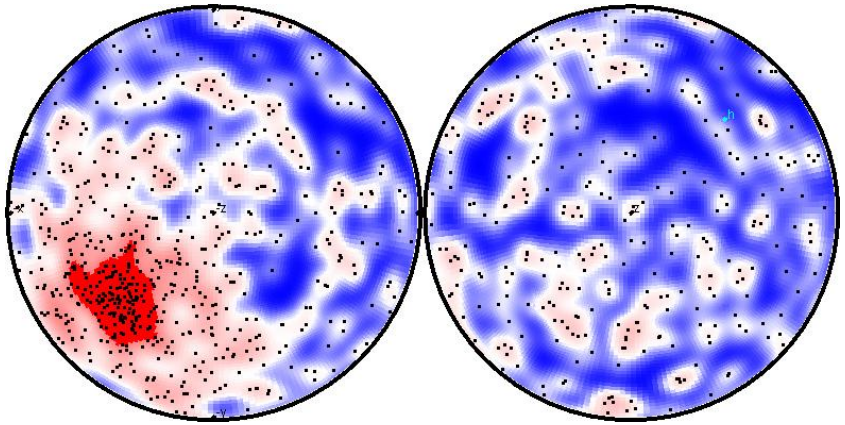

Fig. 18: Pole density plot of the spherical Radon transform of the spherical distribution for $\mathbf{h} = (111)^t$ in equal area projection of lower (left) and upper (right) hemisphere.

Example (cont.)

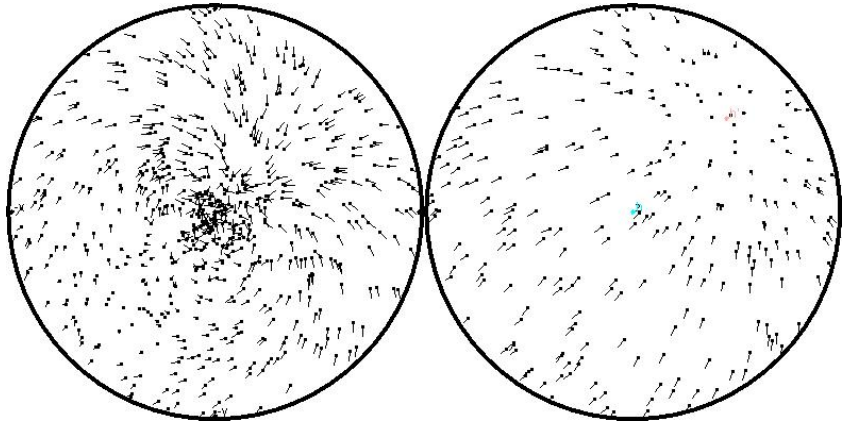

Fig. 19: Augmented pole point plot of the spherical Radon transform of the spherical distribution for $\mathbf{h} = (001)^t$ in equal area projection of lower (left) and upper (right) hemisphere displaying the direction of (111) at each pole point $\mathbf{h}_i = \boldsymbol{g}_i\mathbf{h}$.

Example (cont.)

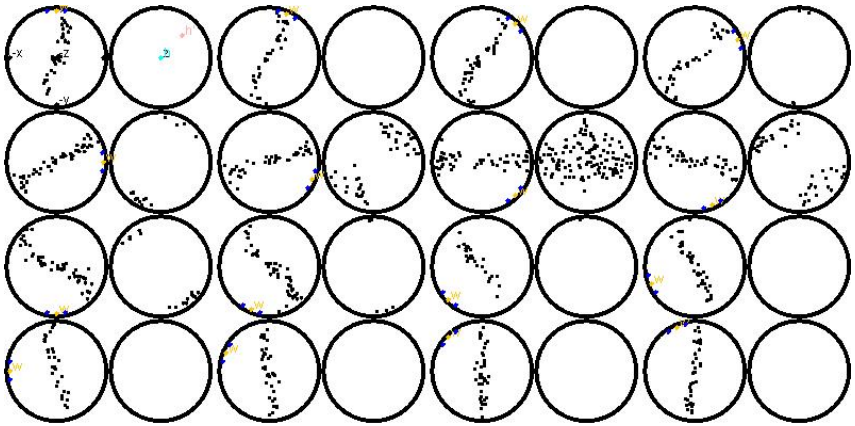

Fig. 20: ω–sections of (001) pole point plot of the spherical Radon transform of the spherical distribution with stepsize $\Delta\omega = 11.25$.

Example (cont.)

For the symmetrical spherical case of the von Mises–Fisher distribution (spherical or surface texture) both the $\mathbf{h} = (001)^t$ and the $\mathbf{h} = (111)^t$ pole point (Fig. 15 and Fig. 17) and pole density plots (Fig. 16 and Fig. 18) show a weak circularly symmetrical maximum at $\mathbf{r} = -(001)^t$ and $\mathbf{r} = -1/\sqrt{3}(111)^t$, respectively. The augmented $(001)^t$–pole point plot (Fig. 19) exposes a distinguished pattern of $\mathbf{g}_i(111)^t$ directions displayed at $\mathbf{r}_i = \mathbf{g}_i(001)^t$. The ω–sections (Fig. 20) show that the distribution of the angles enclosed by the orthogonal projections of $\mathbf{h}_1 = (111)^t$ and $\mathbf{v} = (010)^t$ onto the tangential plane at $\mathbf{r}_i = \mathbf{g}_i(001)^t$ is unimodally symmetrically and weakly concentrated at $3\pi/4$.

Visualization of Preferred Crystallographic Orientation, ω–Sections

Properties of ω–sections

Properties of ω–sections (1)

- ω–sections preserve volume, respectively area;
- the direction of any given axis with respect to the reference frame is geometrically visible,
- the defining parameters have a simple geometrical interpretation,
- the user can choose the most informative sections in a fast and interactive way,
- ω–sections add up to a user–specified pole probability density function,
- the set of sections visualizes the complete information of the orientation probability density function.

Properties of ω–sections (2)

If $\omega = 0$, then all orientations are actually displayed for which $\mathbf{h}_1$ is perfectly aligned with $\mathbf{v}$ and $\mathbf{h}$ coincides with the direction $\mathbf{r}$ displayed in the pole point plot.

Continuously varying ω along the circle $[0, 2\pi]$ of angles for fixed $\mathbf{v}$ and $\mathbf{h}_1$ displays continuous sections of the orientation space, each displayed with equal area and in the same amount of cpu–time.

For fixed $\omega = 0$, or $\omega = \pi/2$, and fixed $\mathbf{h}_1$, varying $\mathbf{v}$ over the whole pole sphere corresponds to exploring "where is $\mathbf{h}_1$ headed to?". The answer is provided by the most dense clusters of orientations.

Exchanging the roles of $\mathbf{v}$ and $\mathbf{h}_1$ allows exploring the data according to "which crystallographic direction heads to $\mathbf{v}$?".

Properties of ω–sections (3)

Dynamically linked views of ω–sections and their superposition will provide easy–to–read and instructive displays of the orientation data, their probability density function and corresponding pole probability density functions.

Visualization of Preferred Crystallographic Orientation, ω–Sections

Conclusions

Conclusions

The display of pole point or pole density plots conveys only summary information about the texture. Therefore, orientations and their probability density functions should be displayed in the most sensible possible way, revealing the best possible insight by exhibiting simultaneous orientational relationships of two different crystal axes with two different specimen directions in ω–sections such that their superposition yields a user–specified pole probability density function.

The end

Thank you for your attention!

helmut.schaeben@geo.tu-freiberg.de

Visualization of Preferred Crystallographic Orientation, ω–Sections

References

References (1)

Boogaart, K.G.v.d. and Schaeben, H., 2004, Exploratory orientation data analysis with ω–sections: J. Appl. Cryst. 37, 683–697

Helming, K., Matthies, S., and Vinel, G.W., 1988, ODF representation by means of σ–sections: in Kallend, J.S., Gottstein, G., (eds.), Proceedings of the 8th Internatl. Conf. on Textures of Materials 1987, American Institue of Mining, Metallurgical, and Petroleum Engineers, 55–60

Matthies, S., Helming, K., and Kunze, K., 1990, On the representation of orientation distributions in texture analysis by σ–sections: I. General properties of σ–sections: phys. stat. sol. (b) 157, 71–83

References (2)

Matthies, S., Helming, K., and Kunze, K., 1990, On the representation of orientation distributions in texture analysis by σ–sections: II. Consideration of crystal and sample symmetry, examples, sigma sections: phys. stat. sol. (b) 157, 489–507

Kocks, U.F., Tomé, C.N., and Wenk, H.R., 1998, Texture and Anisotropy - Preferred Orientations in Polycrystals and their Effect on Materials Properties: Cambridge University Press, Cambridge

Kunze, K., 1991, Zur quantitativen Texturanalyse von Gesteinen: Bestimmung, Interpretation und Simulation von Quarzteilgefügen: Diss. RWTH Aachen

References (3)

Kunze, K. and Schaeben, H., 2004, The Bingham distribution of quaternions and its spherical Radon transform in texture analysis: Math. Geol. 36, 917–944

Wenk, H.R., (ed.), 1985, Preferred Orientation in Deformed Metals and Rocks - An Introduction to Modern Texture Analysis: Academic Press, Orlando

Mathematical Texture Analysis

PDF-to-ODF Inversion – Applied Spherical Tomography

PDF-to-ODF Inversion

Contents

PDF-to-ODF Inversion

ODF-to-PDF Projection
The totally geodesic Radon–Transform

Origins of Spherical Tomography

The papers by **Paul Funk**
Über Flächen mit lauter geschlossenen geodätischen Linien: Math. Ann. 74 **(1913)**, *278–300*
Über eine geometrische Anwendung der Abel'schen Integral–gleichung: Math. Ann. 77 **(1916)**, *129–135*
deal with it.

They appeared earlier than
Johann Radon, *Über die Bestimmung von Funktionen durch ihre Integralwerte längs gewisser Mannigfaltigkeiten: Berichte über die Verhandlungen der Königlich Sächsischen Gesellschaft der Wissenschaften zu Leipzig, Math.-Phys. Klasse 69* **(1917)**, *262–277*

Radon Transform for $\mathbf{SO}(3)$ (1)

Let $f : \mathbf{SO}(3) \mapsto [0, \infty)$ be a probability density function of a random rotation $\boldsymbol{g} \in \mathbf{SO}(3)$.

For any given direction $\mathbf{h} \in \mathbb{S}^2$ the probability density function of coincidence of the random direction $\boldsymbol{g}\mathbf{h} \in \mathbb{S}^2$ with a given direction $\mathbf{r} \in \mathbb{S}^2$ is provided by the 1d spherical Radon transform

$$\mathcal{R}f(\mathbf{h}, \mathbf{r}) = \frac{1}{2\pi} \int_{G(\mathbf{h},\mathbf{r})} f(\boldsymbol{g}) d\boldsymbol{g} \tag{36}$$

with fibres

$$G(\mathbf{h}, \mathbf{r}) = \{\boldsymbol{g} \in \mathbf{SO}(3) \,|\, \boldsymbol{g}\mathbf{h} = \mathbf{r}\}$$

The spherical Radon transform is a function on $\mathbb{S}^2 \times \mathbb{S}^2$, where a pair $(\mathbf{h}, \mathbf{r}) \in \mathbb{S}^2 \times \mathbb{S}^2$ refers to a 1d great circle of $\mathbb{S}^3 \subset \mathbb{H}$.

Radon Transform for $\mathbf{SO}(3)$ (2)

Application of the invariant Haar measure $d\boldsymbol{g}$ in Eq. (62) ensures that the Radon transform is independent of the choices of the involved coordinate systems $K_{\mathcal{S}}$, $K_{\mathcal{C}}$, and in fact of any additional joint external rotation, which in turn implies a basic invariance of the form

$$\mathcal{R}[f(\circ)](\mathbf{h}, \mathbf{r}) = \mathcal{R}[f(\boldsymbol{g}_s \circ \boldsymbol{g}_c^{-1})](\boldsymbol{g}_c\mathbf{h}, \boldsymbol{g}_s\mathbf{r}) \,,$$

where $\boldsymbol{g}_s$ and $\boldsymbol{g}_c$ refer to rotations of the crystal and the specimen coordinate system, respectively.

It implies that the spherical Radon transform $\mathcal{R}f$ is zonal with respect to $\boldsymbol{g}_0\mathbf{h}$ or $\boldsymbol{g}_0^{-1}\mathbf{r}$, respectively, if f is zonal with respect to $\boldsymbol{g}_0$.

Pole Figure Projection

The *crystallographic* X–ray transform associated with the crystal form H of an orientation probability density function f is defined as

$$\mathcal{X}f(\mathbf{h}, \mathbf{r}) = \frac{1}{2 \ \mathrm{card}(H)} \sum_{\mathbf{h} \in H} \Big(\mathcal{R}f(\mathbf{h}, \mathbf{r}) + \mathcal{R}f(-\mathbf{h}, \mathbf{r}) \Big) = P(\mathbf{h}, \mathbf{r}) \tag{37}$$

These *pole figures* are experimentally accessible by diffraction with X–, neutron– or synchrotron–radiation.

Inverse Spherical Radon Transform – Problems (1)

To which extent and for which assumptions is it possible to determine f globally or locally in a neighbourhood $\mathcal{U}(\boldsymbol{g}_0)$ numerically from data sampled from $\mathcal{R}f(\mathbf{h}, \mathbf{r})$, more specifically from

$$\iota_{ij} = \iota(\mathbf{h}_i, \mathbf{r}_{j_i}) = a(\mathbf{h}_i)\mathcal{R}f(\mathbf{h}_i, \mathbf{r}_{j_i}) + b(\mathbf{h}_i, \mathbf{r}_{j_i})$$

Corresponding mathematical problems are

- existence and uniqueness of an inverse $\mathcal{R}^{-1}$ with respect to function spaces
- condition of the problem – ill posed problem
- localization
- data
- numerical methods

Pole Figure Inversion – Problems (2)

To which extent and for which appropriate additional modeling assumptions is it possible to determine f globally on $\mathbf{SO}(3)$ or locally in a neighbourhood $\mathcal{U}(\mathbf{g}_0) \subset \mathbf{SO}(3)$ numerically from data sampled from $\mathcal{X}f(\mathbf{h}, \mathbf{r})$, more specifically from

$$\iota_{ij} = \iota(\mathbf{h}_i, \mathbf{r}_{j_i}) = a(\mathbf{h}_i)\mathcal{X}f(\mathbf{h}_i, \mathbf{r}_{j_i}) + b(\mathbf{h}_i, \mathbf{r}_{j_i})$$

Mathematical Tomography

In mathematical tomography the transform assigning to a function defined on a d–dimensional manifold its mean values with respect to the family of d'–dimensional submanifolds with $1 \leq d' \leq d-1$ is casually referred to as Radon transform, or more specifically also as d'–plane transform. If $d' = 1$, it is explicitly called X–ray transform; if $d' = d-1$, it is explicitly called Radon–transform (cf. Helgason, 1994; 1999). For $d = 2$ the two cases coincide. The start of spherical mathematical tomography dates back to the pioneering papers by Paul Funk (1913, 1916), while mathematical tomography in an Euclidean setting commenced later with the classic paper by Johann Radon (1917). In this sense, the term "X–ray transform" applies to texture analysis and is used by us, even though it does not refer to the actual radiation which could be γ, neutron, or synchrotron as well. In mathematics it is well understood that under reasonable assumptions the Radon transform has a unique inverse such that a function f can be recovered from its Radon transform (cf. Helgason, 1999; Ramm, 1996; Müller, 1998). Quite obviously, the uniqueness is lost for the even axial pole probability density function, Eq. (37), where another mean is involved.

First example (1)

We define two different orientation probability density functions in terms of superposed δ–distributions by

$$f_1(\mathbf{g}; \mathbf{g}_{11}, \mathbf{g}_{12}, \mathbf{g}_{13}, \mathbf{g}_{14}, \mathbf{g}_{15}, \mathbf{g}_{16}) := \frac{1}{6}\sum_{j=1}^{6} \mathbb{1}_{\mathbf{g}_{1i}}(\mathbf{g})$$

$$f_2(\mathbf{g}; \mathbf{g}_{21}, \mathbf{g}_{22}, \mathbf{g}_{23}, \mathbf{g}_{24}, \mathbf{g}_{25}, \mathbf{g}_{26}) := \frac{1}{6}\sum_{j=1}^{6} \mathbb{1}_{\mathbf{g}_{2i}}(\mathbf{g})$$

where

$$\mathbb{1}_{\mathbf{g}_{ij}}(\mathbf{g}) = \begin{cases} 1 & \text{if } \mathbf{g} = \mathbf{g}_{ij} \\ 0 & \text{otherwise} \end{cases}, \; i = 1, 2, \; j = 1, \ldots, 6$$

First example (2)

with

$$\begin{aligned} \mathbf{g}_{11} &:= (\pi/2, \pi/2, 0), & \mathbf{g}_{21} &:= (3\pi/2, \pi/2, 0), \quad \text{light–blue} \\ \mathbf{g}_{12} &:= (3\pi/2, \pi/2, \pi/2), & \mathbf{g}_{22} &:= (\pi/2, \pi/2, \pi/2), \quad \text{green} \\ \mathbf{g}_{13} &:= (\pi, \pi/2, \pi), & \mathbf{g}_{23} &:= (0, \pi/2, \pi) \quad \text{red} \\ \mathbf{g}_{14} &:= (0, \pi/2, 3\pi/2), & \mathbf{g}_{24} &:= (\pi, \pi/2, 3\pi/2), \quad \text{yellow} \\ \mathbf{g}_{15} &:= (0, \pi, \pi/2), & \mathbf{g}_{25} &:= (0, \pi, 3\pi/2), \quad \text{grey} \\ \mathbf{g}_{16} &:= (0, 0, \pi), & \mathbf{g}_{26} &:= (0, 0, 0) \quad \text{dark–blue} \end{aligned}$$

in terms of Euler angles (α, β, γ) according to the "**y**–convention" observing that (α, β, γ) results in the same state as $(\alpha \pm \pi, 2\pi - \beta, \gamma \pm \pi)$.

First example (3)

Then

$$M(\boldsymbol{g}_{11}) = \begin{pmatrix} 0 & -1 & 0 \\ 0 & 0 & 1 \\ -1 & 0 & 0 \end{pmatrix} \quad \text{and} \quad M(\boldsymbol{g}_{21}) = \begin{pmatrix} 0 & 1 & 0 \\ 0 & 0 & -1 \\ -1 & 0 & 0 \end{pmatrix}$$

$$M(\boldsymbol{g}_{12}) = \begin{pmatrix} 1 & 0 & 0 \\ 0 & 0 & -1 \\ 0 & 1 & 0 \end{pmatrix} \quad \text{and} \quad M(\boldsymbol{g}_{22}) = \begin{pmatrix} -1 & 0 & 0 \\ 0 & 0 & 1 \\ 0 & 1 & 0 \end{pmatrix}$$

$$M(\boldsymbol{g}_{13}) = \begin{pmatrix} 0 & 0 & -1 \\ 0 & 1 & 0 \\ 1 & 0 & 0 \end{pmatrix} \quad \text{and} \quad M(\boldsymbol{g}_{23}) = \begin{pmatrix} 0 & 0 & 1 \\ 0 & -1 & 0 \\ 1 & 0 & 0 \end{pmatrix}$$

$$M(\boldsymbol{g}_{14}) = \begin{pmatrix} 0 & 0 & 1 \\ -1 & 0 & 0 \\ 0 & -1 & 0 \end{pmatrix} \quad \text{and} \quad M(\boldsymbol{g}_{24}) = \begin{pmatrix} 0 & 0 & -1 \\ 1 & 0 & 0 \\ 0 & -1 & 0 \end{pmatrix}$$

$$M(\boldsymbol{g}_{15}) = \begin{pmatrix} 0 & 1 & 0 \\ 1 & 0 & 0 \\ 0 & 0 & -1 \end{pmatrix} \quad \text{and} \quad M(\boldsymbol{g}_{25}) = \begin{pmatrix} 0 & -1 & 0 \\ -1 & 0 & 0 \\ 0 & 0 & -1 \end{pmatrix}$$

$$M(\boldsymbol{g}_{16}) = \begin{pmatrix} -1 & 0 & 0 \\ 0 & -1 & 0 \\ 0 & 0 & 1 \end{pmatrix} \quad \text{and} \quad M(\boldsymbol{g}_{26}) = \begin{pmatrix} 1 & 0 & 0 \\ 0 & 1 & 0 \\ 0 & 0 & 1 \end{pmatrix}$$

First example (4)

and

$$\boldsymbol{g}_{2i} = \boldsymbol{g}(\pi; \mathbf{z})\, \boldsymbol{g}_{1i}, \quad i = 1, 2, 3,$$

i.e. the two sets of orientations differ by a rotation about $\mathbf{z}$ by π represented by

$$M(\pi; \mathbf{z}) = \begin{pmatrix} -1 & 0 & 0 \\ 0 & -1 & 0 \\ 0 & 0 & 1 \end{pmatrix}.$$

First example (5)

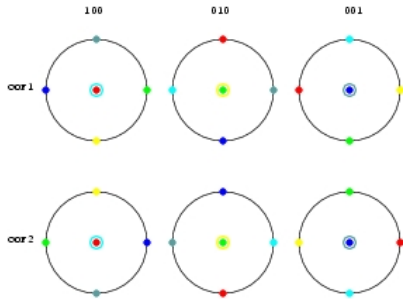

Fig. 1, top row: Pole point plots corresponding to $\boldsymbol{g}_{11}, \boldsymbol{g}_{12}, \boldsymbol{g}_{13}, \boldsymbol{g}_{14}, \boldsymbol{g}_{15}, \boldsymbol{g}_{16}$ colour coded light–blue, green, red, yellow, grey, dark–blue, respectively;
bottom row: Pole point plots corresponding to $\boldsymbol{g}_{21}, \boldsymbol{g}_{22}, \boldsymbol{g}_{23}, \boldsymbol{g}_{24}, \boldsymbol{g}_{25}, \boldsymbol{g}_{26}$ colour coded light–blue, green, red, yellow, grey, dark–blue, respectively.

First example (6)

Reading the pole point plots as pole figures of two different orientation probability density functions, each composed of six "Ideal–Lagen", i.e. neglecting the colour coding, the three pole figures cannot be distinguished.

First example (7)

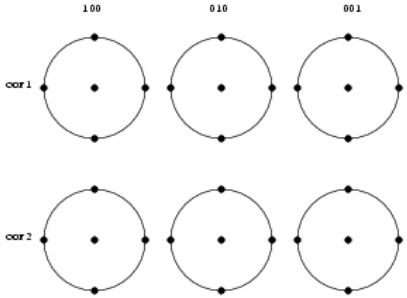

Fig. 2: Pole figure plots of crystal forms (100), (010), and (001) corresponding to the superpositions of two different sets of six distinct "Ideal–Lagen".

Thus, we have shown by example that two different orientation probability density functions exist which have three pole figures in common for which the crystallographic directions **h** are not coplanar.

Second example with reference to crystal symmetry (1)

Ideal–Lagen

$$f_1(\boldsymbol{g};\boldsymbol{g}^o_{11},\boldsymbol{g}^o_{12},\boldsymbol{g}^o_{13}) := \frac{1}{3}\sum_{j=1}^{3} \mathbb{1}_{\boldsymbol{g}^o_{1i}}(\boldsymbol{g}), \quad f_2(\boldsymbol{g};\boldsymbol{g}^o_{21},\boldsymbol{g}^o_{22},\boldsymbol{g}^o_{23}) := \frac{1}{3}\sum_{j=1}^{3} \mathbb{1}_{\boldsymbol{g}^o_{2i}}(\boldsymbol{g})$$

with

$$\mathbb{1}_{\boldsymbol{g}^o_{ij}}(\boldsymbol{g}) = \begin{cases} 1 & \text{if } \boldsymbol{g} = \boldsymbol{g}^o_{ij} \\ 0 & \text{otherwise} \end{cases}, \; i = 1,2, \; j = 1,2,3$$

with

$$\begin{aligned} \boldsymbol{g}^o_{11} &:= (\pi/2, 0, 0), & \boldsymbol{g}^o_{21} &:= (0, 0, 0), \quad \text{(blue)} \\ \boldsymbol{g}^o_{12} &:= (\pi/2, \pi/2, \pi/2), & \boldsymbol{g}^o_{22} &:= (0, \pi/2, \pi/2), \quad \text{(green)} \\ \boldsymbol{g}^o_{13} &:= (0, \pi/2, 0), & \boldsymbol{g}^o_{23} &:= (\pi/2, \pi/2, 0) \quad \text{(red)} \end{aligned}$$

in terms of Euler angles (α, β, γ) according to the "**y**–convention".

The two sets of Ideal–Lagen and their corresponding orientation probability density functions differ by a rotation about **z** by $\pi/2$.

Second example with reference to crystal symmetry (2)

Then

$$M(\boldsymbol{g}^o_{11}) = \begin{pmatrix} 0 & -1 & 0 \\ 1 & 0 & 0 \\ 0 & 0 & 1 \end{pmatrix} \quad \text{and} \quad M(\boldsymbol{g}^o_{21}) = \begin{pmatrix} 1 & 0 & 0 \\ 0 & 1 & 0 \\ 0 & 0 & 1 \end{pmatrix}$$

$$M(\boldsymbol{g}^o_{12}) = \begin{pmatrix} -1 & 0 & 0 \\ 0 & 0 & 1 \\ 0 & 1 & 0 \end{pmatrix} \quad \text{and} \quad M(\boldsymbol{g}^o_{22}) = \begin{pmatrix} 0 & 0 & 1 \\ 1 & 0 & 0 \\ 0 & 1 & 0 \end{pmatrix}$$

$$M(\boldsymbol{g}^o_{13}) = \begin{pmatrix} 0 & 0 & 1 \\ 0 & 1 & 0 \\ -1 & 0 & 0 \end{pmatrix} \quad \text{and} \quad M(\boldsymbol{g}^o_{23}) = \begin{pmatrix} 0 & -1 & 0 \\ 0 & 0 & 1 \\ -1 & 0 & 0 \end{pmatrix}$$

and

$$\boldsymbol{g}^o_{1i} = \boldsymbol{g}(\pi/2; \mathbf{z})\, \boldsymbol{g}^o_{2i}, \quad i = 1,2,3.$$

Second example with reference to crystal symmetry (3)

Ideal–Lagen

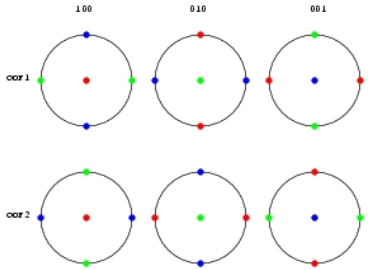

Fig. 3, top row: Pole point plots corresponding to $\boldsymbol{g}^o_{11}, \boldsymbol{g}^o_{12}, \boldsymbol{g}^o_{13}$ colour coded blue, green, red, respectively;
bottom row: Pole point plots corresponding to $\boldsymbol{g}^o_{21}, \boldsymbol{g}^o_{22}, \boldsymbol{g}^o_{23}$ colour coded blue, green, red, respectively.

Second example with reference to crystal symmetry (4)

The two orientation probability density functions differ by a rotation about $\mathbf{z}$ by $\pi/2$. Therefore, any pole point plot of f_2 initially differs by a rotation about $\mathbf{z}$ by $\pi/2$ from the corresponding pole point plot of f_1.

Without explicit consideration of any symmetry, any $\mathbf{h}$–pole figure of f_i

$$\mathcal{X} f_i(\mathbf{h}, \mathbf{r}) = \frac{1}{2 \ \mathrm{card}(H)} \sum_{j=1}^{3} \mathbb{1}_{(\mathbf{h}, \pm \boldsymbol{g}_{ij}^{o} \mathbf{h})}(\mathbf{h}, \mathbf{r}).$$

is a δ–distribution which vanishes everywhere except in $\mathbf{r}_j = \pm \boldsymbol{g}_{ij}^{o} \mathbf{h}$, $j = 1, 2, 3$, (and their crystal symmetrically equivalent pole points in case of crystal symmetry).

Second example with reference to crystal symmetry (5)

Next we impose orthorhombic crystal symmetry and additionally assume (i) constant ratios of axes equal to 1, and (ii) all angles of the unit cell to be $\pi/2$. It should be noted that orthorhombic crystals with all ratios of axes equal to 1 and all angles equal to $\pi/2$ exist; there are often referred to as pseudo–cubic as the apparent symmetry is cubic: the rhombic dipyramids look like octahedra, the combination of the three pinacoids (100), (010), and (001) look like a cube, the combination of the two prisms (011) and (101) look like a dodecahedron (rhombododecaeder). Analogously, any actual crystal symmetry appears to be of higher order.

Second example with reference to crystal symmetry (6)

Calculating all crystallographic pole points $\boldsymbol{g}^{o}\mathbf{h}$, i.e. the specimen directions $\mathbf{r} = \boldsymbol{g}^{o}\mathbf{h}$, according to the δ–distributions composing f_1, f_2 yields the correspnding pole figures composed of "Ideal–Lagen"

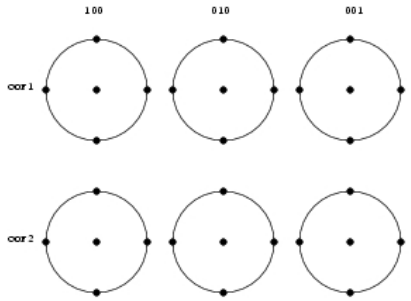

Fig. 4, top row: Pole figures corresponding to $f_1(\boldsymbol{g}, \boldsymbol{g}_{11}^{o}, \boldsymbol{g}_{12}^{o}, \boldsymbol{g}_{13}^{o})$; bottom row: Pole figures corresponding to $f_2(\boldsymbol{g}, \boldsymbol{g}_{21}^{o}, \boldsymbol{g}_{22}^{o}, \boldsymbol{g}_{23}^{o})$.

Second example with reference to crystal symmetry (7)

Then we model each of the two different orientation probability density functions $f_i, i = 1, 2$, by the equally weighted superposition of three bell–shaped unimodal von Mises–Fisher probability density functions with modes $\boldsymbol{g}_{ij}^{o}, j = 1, 2, 3$, and constant halfwidth of 20 degrees corrsponding to a spherical variance $\kappa = 45.62505$.

Any two $\mathbf{h}$ pole figures corresponding to f_1 and f_2, respectively, differ by a rotation about $\mathbf{z}$ by $\pi/2$ for orthorhombic crystal symmetry. Thus, the example is again designed to exploit an intricate interplay of crystal symmetry and two distinct orientation probability density functions differing by a rotation about $\mathbf{z}$ by $\pi/2$. It is emphasized that none of the given six different orientations are equivalent with respect to crystal symmetry.

Second example with reference to crystal symmetry (8)

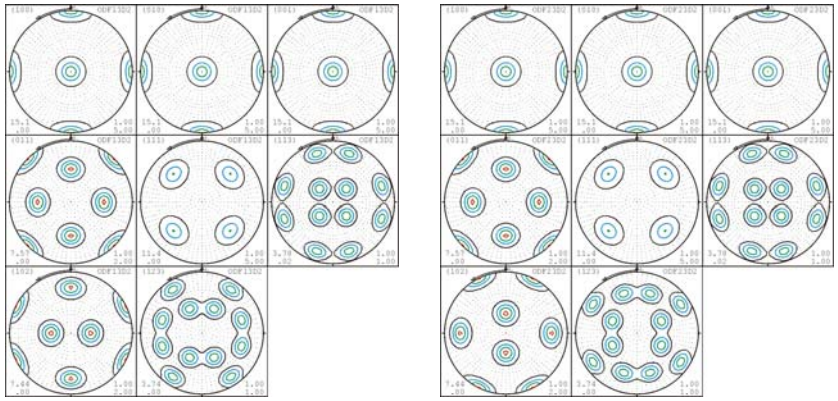

Figure 5: Pole figures $\mathcal{X}[f_1(\circ;\mathbf{g}^o_{11},\mathbf{g}^o_{12},\mathbf{g}^o_{13})](\mathbf{h},\mathbf{r})$ and pole figures $\mathcal{X}[f_2(\circ;\mathbf{g}^o_{21},\mathbf{g}^o_{22},\mathbf{g}^o_{23})](\mathbf{h},\mathbf{r})$, respectively, for several crystal forms with orthorhombic crystal symmetry imposed.

Second example with reference to crystal symmetry (9)

Summarizingly, for orthorhombic crystal symmetry, pole figures $\mathcal{X}f_i(\mathbf{h},\circ)$ agree for crystal forms e.g. $(100),(010),(001),(011),(111),(113)$, but differ in e.g. (102), and (123). More generally, pole figures $\mathcal{X}f_i(\mathbf{h},\circ)$ agree if a rotation about the axis $\mathbf{z}$ by the angle $\pi/2$ is compatible for the crystal form H with the symmetry elements of the orthorhombic crystal symmetry group, i.e. if a symmetry element $\mathbf{g}_c$ exists such that $\mathbf{g}^o_{1i}\mathbf{h} = \mathbf{g}^o_{2p(i)}\mathbf{g}_c\mathbf{h}$ for every $i \in \{1,2,3\}$ and $p(i) \in p(\{1,2,3\})$ in a permuted set of $\{1,2,3\}$.

It is emphasized that the three pole figures of crystal forms (100), (010), and (001) are coincident for any ratios of axes. If the ratios of axes are different from 1, then only these three pole figures are coincident.

Second example with reference to crystal symmetry (10)

These examples substantiate earlier criticism that the "texture component fit" method cannot resolve the ambiguity of the inverse problem to determine an orientation from pole density functions.

PDF-to-ODF Inversion

Properties of the Radon Transform

- Antipodal Symmetry
- Preservation of Radial Symmetry
- Effect of Crystal Symmetry
- Loss of Non–Negativity
- Darboux Differential Equation
- Range Theorems
- Finite Support Theorem
- Localization

Representation of Fibres G(**h**, **r**)

The set $G(\mathbf{h},\mathbf{r}) \subset \mathbf{SO}(3)$ of all rotations with $\mathfrak{g}\mathbf{h} = \mathbf{r}$ is represented by the circle $C(q_1, q_2) \subset \mathbb{S}^3$

$$C(q_1, q_2) = q_1 \cos t + q_2 \sin t = C_{\mathbf{h},\mathbf{r}}, \quad t \in [0, 2\pi)$$

spanned by unit quaternions $q_1, q_2 \in \mathbb{S}^3$ given in terms of $\mathbf{h}, \mathbf{r} \in \mathbb{S}^2$.

An obvious choice of $q_1, q_2 \in \mathbb{S}^3$ are the orthogonal unit quaternions

$$\begin{aligned} q_1 &:= \frac{1}{\|1 - rh\|}(1 - rh) = \cos\frac{\eta}{2} + \frac{\mathbf{h}\times\mathbf{r}}{\|\,\mathbf{h}\times\mathbf{r}\,\|}\sin\frac{\eta}{2} \\ q_2 &:= \frac{1}{\|h + r\|}(h + r) = 0 + \frac{\mathbf{h}+\mathbf{r}}{\|\,\mathbf{h}+\mathbf{r}\,\|} \end{aligned}$$

where η denotes the angle between $\mathbf{h}$ and $\mathbf{r}$, and

$$\|1 - rh\| = \sqrt{2(1 + \cos\eta)} = 2\cos\frac{\eta}{2}, \quad \|h + r\| = 2\cos\frac{\eta}{2}$$

Another Parametrization of Fibres $G(\mathbf{h}, \mathbf{r})$

With the unit quaternions

$$\begin{aligned} h(t) &:= \cos\frac{t}{2} + \mathbf{h}\sin\frac{t}{2}, \quad t \in [0, 2\pi) \\ r(t) &:= \cos\frac{t}{2} + \mathbf{r}\sin\frac{t}{2}, \quad t \in [0, 2\pi) \end{aligned}$$

the elements of the circle $C(q_1, q_2)$ can obviously be factorized by virtue of

$$\begin{aligned} C(q_1, q_2) &= \{q_0\, h(t)\,;\; q_0 \in C(q_1, q_2),\; t \in [0, 2\pi)\} \\ C(q_1, q_2) &= \{r(t)\, q_0\,;\; q_0 \in C(q_1, q_2),\; t \in [0, 2\pi)\} \end{aligned}$$

Totally Geodesic Radon Transform (1)

Let $\mathcal{C}$ denote the set of all 1–dimensional totally geodesic submanifolds $C \subset \mathbb{S}^3$. Each $C \in \mathcal{C}$ is a 1–sphere, i.e. a circle with centre $\mathcal{O}$. Each circle is characterized by a unique pair of unit vectors $(\mathbf{h}, \mathbf{r}) \in \mathbb{S}^2 \times \mathbb{S}^2$ (and equivalently by its antipodally symmetric) by virtue of $q\,\mathbf{h}\,q^* = \mathbf{r}$ for all $q \in C$. Thus, referring to the quaternion representation, Eq. (37) can be rewritten in a parametric form as

$$P(\mathbf{h}, \mathbf{r}) = \frac{1}{8\pi}\int_{C\cup C^\perp} f(q)\, d\omega_1(q),$$

where the circle $C \subset S^3$ represents all rotations mapping $\mathbf{h} \in \mathbb{S}^2$ on $\mathbf{r} \in \mathbb{S}^2$ and where $C^\perp(q_1, q_2)$ is the orthogonal circle representing all rotations mapping $-\mathbf{h}$ on $\mathbf{r}$, and where ω_1 denotes the usual one–dimensional circular Riemann measure.

Totally Geodesic Radon Transform (2)

It should be noted that no distinction has been made whether f refers to $\mathbf{SO}(3)$ or $\mathbb{S}^3$, even though the form of f depends on the representation of $\mathfrak{g}$; in particular, with respect to $\mathbb{S}^3$ only even functions f could be orientation probability density functions as $q \in \mathbb{S}^3$ and $-q$ represent the same orientation. Then

$$\mathcal{X}f(\mathbf{h}, \mathbf{r}) = \frac{1}{4}\Big(\mathcal{R}f(C_{\mathbf{h},\mathbf{r}}) + \mathcal{R}f(C_{-\mathbf{h},\mathbf{r}})\Big) = P(\mathbf{h}, \mathbf{r}). \qquad (38)$$

Totally Geodesic Radon Transform (3)

The geometry of rotations amounts to

$$\begin{aligned}
\int_{c(\mathbf{h};2\rho)} \mathcal{R}f(\mathbf{h}',\mathbf{r})d\mathbf{h}' &= \int_{c(\mathbf{r};2\rho)} \mathcal{R}f(\mathbf{h},\mathbf{r}')d\mathbf{r}' \qquad (39)\\
&= \int_{c(\mathbf{r};2\rho)} \int_{C(\,q_1(\mathbf{h},\mathbf{r}'),q_2(\mathbf{h},\mathbf{r}')\,)} f(q)dq\,d\mathbf{r}'\\
&= \int_{T(C(q_1(\mathbf{h},\mathbf{r}),q_2(\mathbf{h},\mathbf{r}));\rho)} f(q)dq \qquad (40)\\
&= \int_{d(\,q,\,C(q_1(\mathbf{h},\mathbf{r}),q_2(\mathbf{h},\mathbf{r}))\,)=\rho} f(q)dq
\end{aligned}$$

where Eq. 39 is an Ásgeirsson–type mean value theorem, and where Eq. 40 is instrumental to the inversion of the spherical Radon transform.

Properties of the Radon transform for $\mathbf{SO}(3)$ or $\mathbb{S}^3$ (1)

As a function of $\boldsymbol{g} \mapsto \mathcal{R}f(\mathbf{h},\boldsymbol{g}\mathbf{h})$, the 1d Radon transform

$$\mathcal{R}f(\mathbf{h},\mathbf{r}) = \frac{1}{2\pi}\int_{G(\mathbf{h},\mathbf{r})} f(\boldsymbol{g})d\boldsymbol{g}$$

is constant for all $\boldsymbol{g} \in G(\mathbf{h},\mathbf{r})$.

Properties of the Radon transform for $\mathbf{SO}(3)$ or $\mathbb{S}^3$ (2)

Obviously,

$$\begin{aligned}
\mathcal{R}f(-\mathbf{h},\mathbf{r}) &= \mathcal{R}f(\mathbf{h},-\mathbf{r})\\
\mathcal{R}f(-\mathbf{h},-\mathbf{r}) &= \mathcal{R}f(\mathbf{h},\mathbf{r})
\end{aligned}$$

$\mathcal{R}f$ is an even function on $\mathbb{S}^2 \times \mathbb{S}^2$.
However, it is emphasized that for a given $\mathbf{h} \in \mathbb{S}^2$

$$\mathcal{R}f(\mathbf{h},\mathbf{r}) \neq \mathcal{R}f(-\mathbf{h},\mathbf{r})$$

holds.

For the crystallographic transform, it is

$$\mathcal{X}f(\mathbf{h},\mathbf{r}) = \mathcal{X}f(-\mathbf{h},\mathbf{r}) = \mathcal{X}f(\mathbf{h},-\mathbf{r})$$

$\mathcal{X}f$ is an even function in each individual variable $\mathbf{h} \in \mathbb{S}^2$ or $\mathbf{r} \in \mathbb{S}^2$.

Properties of the Radon transform for $\mathbf{SO}(3)$ or $\mathbb{S}^3$ (3)

For any fixed orientations $\boldsymbol{g}_c,\boldsymbol{g}_s,\boldsymbol{g}_0 \in \mathbf{SO}(3)$

$$\begin{aligned}
\mathcal{R}[f(\circ\boldsymbol{g}_c](\mathbf{h},\mathbf{r}) &= \mathcal{R}[f(\circ)](\boldsymbol{g}_c\mathbf{h},\mathbf{r})\\
\mathcal{R}[f(\boldsymbol{g}_s^{-1}\circ))](\mathbf{h},\mathbf{r}) &= \mathcal{R}[f(\circ)](\mathbf{h},\boldsymbol{g}_s\mathbf{r})\\
\mathcal{R}[f(\boldsymbol{g}_s^{-1}\circ\boldsymbol{g}_c)](\mathbf{h},\mathbf{r}) &= \mathcal{R}[f(\circ)](\boldsymbol{g}_c\mathbf{h},\boldsymbol{g}_s\mathbf{r})\\
\mathcal{R}[f(\circ)](\boldsymbol{g}_0\mathbf{h},\mathbf{r}) &= \mathcal{R}[f(\boldsymbol{g}_0^{-1}\circ\boldsymbol{g}_0)](\mathbf{h},\boldsymbol{g}_0^{-1}\mathbf{r})
\end{aligned}$$

where the last equation reduces for rotationally invariant functions $f(\boldsymbol{g}) = f(\omega(\boldsymbol{g}))$ which depend only on the angle ω of the rotation $\boldsymbol{g}$ to

$$\mathcal{R}f(\boldsymbol{g}_0\mathbf{h},\mathbf{r}) = \mathcal{R}f(\mathbf{h},\boldsymbol{g}_0^{-1}\mathbf{r})$$

Thus, rotational invariance ("zonality") is preserved by the spherical $\mathcal{R}$ transform.

Properties of the Radon transform for $\mathbf{SO}(3)$ or $\mathbb{S}^3$ (4)

Thus, if f is rotationally invariant with respect to $\boldsymbol{g}_0$, i.e. if

$$f(\boldsymbol{g},\boldsymbol{g}_0) = f(d(\boldsymbol{g},\boldsymbol{g}_0)) = f(\omega(\boldsymbol{g}\boldsymbol{g}_0^{-1}))$$

then the Radon transform $\mathcal{R}f$ defined on $\mathbb{S}^2 \times \mathbb{S}^2$ is rotationally invariant with respect to $\mathbf{r}_0 = \boldsymbol{g}_0\mathbf{h}$. It reduces to a real function $\mathcal{R}f(\boldsymbol{g}_0\mathbf{h}\cdot\mathbf{r})$ depending on the angle $\angle(\boldsymbol{g}_0\mathbf{h},\mathbf{r}) \in [0,\pi]$ and may be thought of as being defined on $[-1,1]$ by virtue of the inner (dot) product $\boldsymbol{g}_0\mathbf{h}\cdot\mathbf{r}$.

It should be noted that the rotational invariance of f with respect to $\boldsymbol{g}_0 \in \mathbf{SO}(3)$ is necessary and sufficient for the rotational invariance of the transform $\mathcal{R}f(\mathbf{h},\mathbf{r})$ with respect to $\mathbf{r}_0 = \boldsymbol{g}_0\mathbf{h}$.

Properties of the Radon transform for $\mathbf{SO}(3)$ or $\mathbb{S}^3$ (5)

Let $\boldsymbol{g}$ be an arbitrary element of $\mathbf{SO}(3)$. In case of crystallographic symmetry the left coset of orientations

$$\boldsymbol{g}G_{\mathcal{C}} = \{\boldsymbol{g}\boldsymbol{g}_{\mathcal{C}_j} \,|\, \boldsymbol{g}_{\mathcal{C}_j} \in G_{\mathcal{C}}, j = 1,\ldots,\#G_{\mathcal{C}}\}$$

of the subgroup $G_{\mathcal{C}} \subset \mathbf{SO}(3)$ consists of all orientations which are physically indistinguishable with respect to the coordinate system $K_{\mathcal{S}}$ fixed to the specimen; $\boldsymbol{g}$ may be referred to as representative of the coset $\boldsymbol{g}G_{\mathcal{C}}$.

Properties of the Radon transform for $\mathbf{SO}(3)$ or $\mathbb{S}^3$ (6)

Therefore, the property

$$f(\boldsymbol{g}\boldsymbol{g}_{\mathcal{C}_j}) = f(\boldsymbol{g}),\ \ \boldsymbol{g}_{\mathcal{C}_j} \in G_{\mathcal{C}}, j = 1,\ldots,\#G_{\mathcal{C}}$$

is imposed on f, that is, f is constant on each coset. Since the cosets of $G_{\mathcal{C}}$ provide a partition of $\mathbf{SO}(3)$ into sets which do not contain any two symmetrically equivalent orientations, it will eventually be sufficient to consider f on the elementary set $\mathbb{G} \subset \mathbf{SO}(3)$ of representatives of all cosets.

Properties of the Radon transform for $\mathbf{SO}(3)$ or $\mathbb{S}^3$ (7)

If for a subgroup $G_{\mathcal{C}} \subset \mathbf{SO}(3)$ a function f satisfies $f(\boldsymbol{g}\boldsymbol{g}_{\mathcal{C}_j}) = f(\boldsymbol{g})$ for all $\boldsymbol{g}_{\mathcal{C}_j} \in G_{\mathcal{C}}, j = 1,\ldots,\#G_{\mathcal{C}}$, its corresponding transform $\mathcal{R}f$ satisfies

$$\mathcal{R}f(\boldsymbol{g}_{\mathcal{C}_j}\mathbf{h},\mathbf{r}) = \Big(\mathcal{R}[f(\circ\boldsymbol{g}_{\mathcal{C}})]\Big)(\mathbf{h},\mathbf{r}) = \Big(\mathcal{R}[f(\circ)]\Big)(\mathbf{h},\mathbf{r}) = \mathcal{R}f(\mathbf{h},\mathbf{r})$$

for all $\boldsymbol{g}_{\mathcal{C}_j} \in G_{\mathcal{C}}, j = 1,\ldots,\#G_{\mathcal{C}}$.

Spherical Mean Value Theorem (1)

$\mathcal{R}f(\mathbf{h},\mathbf{r})$ satisfies a spherical variant of Ásgeirsson's mean value theorem which may be stated as follows. Let $\mu(\mathbf{h},\mathbf{r};\rho)$, $\nu(\mathbf{h},\mathbf{r};\rho)$, and $w(\mathbf{h},\mathbf{r};\rho,\tau)$ be defined as

$$\begin{aligned}
\mu(\mathbf{h},\mathbf{r};\rho) &:= \int_{c(\mathbf{h};\rho)} \mathcal{R}f(\mathbf{h}',\mathbf{r})dt(\mathbf{h}') \\
\nu(\mathbf{h},\mathbf{r};\rho) &:= \int_{c(\mathbf{r};\rho)} \mathcal{R}f(\mathbf{h},\mathbf{r}')dt(\mathbf{r}') \\
w(\mathbf{h},\mathbf{r};\rho,\tau) &:= \int_{c(\mathbf{r};\tau)} \int_{c(\mathbf{h};\rho})\mathcal{R}f(\mathbf{h}',\mathbf{r}')dt(\mathbf{h}')dt(\mathbf{r}')
\end{aligned}$$

Then

$$\begin{aligned}
\mu(\mathbf{h},\mathbf{r};\rho) &= w(\mathbf{h},\mathbf{r};\rho,1) \\
\nu(\mathbf{h},\mathbf{r};\rho) &= w(\mathbf{h},\mathbf{r};1,\rho)
\end{aligned}$$

and

$$\mu(\mathbf{h},\mathbf{r},\rho) = \nu(\mathbf{h},\mathbf{r},\rho).$$

Spherical Mean Value Theorem (2)

More generally

$$w(\mathbf{h},\mathbf{r};\rho,\tau) = w(\mathbf{h},\mathbf{r};\tau,\rho)$$

the double mean value is symmetric in the radii ρ and τ.

Since $\mu(\mathbf{h},\mathbf{r},\rho) = \nu(\mathbf{h},\mathbf{r},\rho)$ holds for all $\rho \in (-1,1)$, it provides at once a mean value theorem for the spherical surface element $\Omega_{\mathbf{h},\rho} = \{\mathbf{h}' \in S^2 \mid \cos\rho \leq \mathbf{h}'\cdot\mathbf{h}\}$ with center $\mathbf{h} \in S^2_+$ by integration with respect to ρ

$$\int_{[1,\delta]} \mu(\mathbf{h},\mathbf{r},\rho)d\rho = \int_{[1,\delta]} \nu(\mathbf{h},\mathbf{r},\rho)d\rho$$

Loss of Non–Negativity

Obviously, if $f \geq 0$, then $\mathcal{R}f \geq 0$.

However, the non–negativity of $\mathcal{R}f$ does not imply the non–negativity of f.

Is there a criterion in terms of $\mathcal{R}f$ that it is the projection of a non–negative f?

How to construct a non–negative f from experimental data of $\mathcal{R}f$?

N.B.: This loss of non–negativity causes the essential problems of the harmonic method for inversion of the crystallographic X–ray transform, since once a non–negative, even interpolant of the pole figures has been found its is not clear whether there exists an odd complement such that the resulting ODF is non–negative, too.

Darboux Differential Equation

$\mathcal{R}f(\mathbf{h},\mathbf{r})$ satisfies the differential equation

$$(\Delta_{\mathbf{h}} - \Delta_{\mathbf{r}})\,\mathcal{R}f(\mathbf{h},\mathbf{r}) = 0$$

where $\Delta_{\mathbf{h}}$ stands for the spherical Laplacian with respect to the spherical coordinates of $\mathbf{h}$.

Elementarily, it can be seen by interchanging $\mathbf{h},\mathbf{r}$, replacing $q \in \mathbf{SO}(3)$ by $q^* \in \mathbf{SO}(3)$, and applying elementary properties as follows

$$\Delta_{\mathbf{h}}\,\mathcal{R}f(\mathbf{h},\mathbf{r}) = \Delta_{\mathbf{r}}\,(\mathcal{X}[f(\circ^*)])(\mathbf{r},\mathbf{h}) = \Delta_{\mathbf{r}}\,\mathcal{R}f(\mathbf{h},\mathbf{r})$$

General Solution of Darboux Differential Equation

The general solution of the Darboux differential equation is in terms of spherical harmonics

$$\mathcal{R}f(\mathbf{h},\mathbf{r}) = \sum_{\ell=0}^{\infty} \sum_{m=-\ell}^{\ell} \sum_{n=-\ell}^{\ell} C_\ell^{mn}\, Y_\ell^m(\mathbf{h})\, Y_\ell^n(\mathbf{r}) \qquad (41)$$

and in terms of characteristics

$$\mathcal{R}f(\mathbf{h},\mathbf{r}) = \sum_{\ell} \sum_{k} u_\ell(\mathbf{h} \cdot {q^*}_k \mathbf{r} q_k) \qquad (42)$$

where $q_k \in S^3$ are arbitrary unit quaternions and $u_\ell \in C^2(\mathbb{R}^1)$ are some appropriately chosen real twice differentiable functions (Nikolayev and Schaeben, 1999). u_ℓ are zonal with respect to ${q^*}_k \mathbf{r} q_k$, or $q_k \mathbf{h} q_k^*$, $k = 1, \ldots, K$, respectively.

Singular Value Decomposition

Let T_ℓ^{mn} denote the generalized harmonics for $\mathbf{SO}(3)$ of order ℓ. Then

$$\mathcal{R}\, T_\ell^{mn}(\mathbf{h},\mathbf{r}) = \frac{1}{\sqrt{2\ell+1}} Y_\ell^m(\mathbf{h}) Y_\ell^n(\mathbf{r})$$

Furthermore

$$\mathcal{X}\, T_\ell^{mn}(\mathbf{h},\mathbf{r}) = \begin{cases} \frac{1}{\sqrt{2\ell+1}} Y_\ell^m(\mathbf{h}) Y_\ell^n(\mathbf{r}) & \text{if } \ell \text{ even} \\ 0 & \text{if } \ell \text{ odd} \end{cases}$$

Thus, the kernel of the operator $\mathcal{X}$ consists of all generalized harmonics T_ℓ of odd order ℓ, and therefore $\mathcal{X}$ is not invertible.

Range Theorem (1)

A range theorem characterizing the image of the spherical Radon transform in terms of the differential equation states that any function $u \in \mathcal{C}^\infty(S^2 \times S^2)$ satisfying $(\Delta_{\mathbf{h}} - \Delta_{\mathbf{r}})\, u(\mathbf{h},\mathbf{r}) = 0$ is the spherical Radon transform of some function $f \in \mathcal{C}^\infty(S^3)$ (Nikolayev and Schaeben, 1999).

In particular, that function f is given in terms of generalized harmonics T by

$$f(\boldsymbol{g}) = \sum_{\ell=0}^{\infty} \sum_{m=-\ell}^{\ell} \sum_{n=-\ell}^{\ell} C_\ell^{mn}\, T_\ell^{mn}(\boldsymbol{g})$$

Range Theorem (2)

More specifically, the image of $\mathcal{R}$ is characterized by

$$\begin{aligned} \mathcal{R}\, \mathcal{L}^2(\mathbb{S}^3) &= \{u(\mathbf{h},\mathbf{r}) = \sum C_\ell^{mn}\, Y_\ell^m(\mathbf{h})\, Y_\ell^n(\mathbf{r}) \mid \sum (2\ell+1)(C_\ell^{mn})^2 < \infty\} \\ &= \{u \in \mathcal{H}^{\frac{1}{2}} \mid \Delta_{\mathbf{h}}^{1/2} u(\mathbf{h},\mathbf{r}) = \Delta_{\mathbf{r}}^{1/2} u(\mathbf{h},\mathbf{r})\} \end{aligned}$$

Inverse Radon Transform – Inversion formulae

The Dual Spherical Radon Transform (1)

The Radon transform $\mathcal{R}f(\mathbf{h},\mathbf{r})$ may be thought of as a function $P : \mathcal{C} \mapsto \mathbb{R}$ where $\mathcal{C}$ denotes the set of all 1d great circles of $\mathbb{S}^3$.

Then the dual spherical Radon transform of a real continuous function $P : \mathcal{C} \mapsto \mathbb{R}$ is defined as

$$\widetilde{\mathcal{R}}P(q) = \int_{C \ni q} P(C)\, d\mu(C)$$

$\widetilde{\mathcal{R}}P$ is the mean value of the function P over the set of circles $C \in \mathcal{C}$ passing through $q \in \mathbb{S}^3$.

The Dual Spherical Radon Transform (2)

In terms of $(\mathbf{h},\mathbf{r}) \in \mathbb{S}^2 \times \mathbb{S}^2$ parametrizing the 1d great circle $C \in \mathcal{C}$, the dual Radon transform is given by

$$\begin{aligned}(\widetilde{\mathcal{R}}[P(\circ,\circ)])(q) &= \int_{\{(\mathbf{h},\mathbf{r})\in\mathbb{S}^2\times\mathbb{S}^2 \,|\, \boldsymbol{g}\mathbf{h}=\mathbf{r}\}} P(\mathbf{h},\mathbf{r})\, d(\mathbf{h},\mathbf{r}) \\ &= \int_{\mathbb{S}^2} P(\mathbf{h},\boldsymbol{g}\mathbf{h})\, d\mathbf{h}\end{aligned}$$

Inverse Spherical Radon transform (1)

Eventually it holds

$$f(\boldsymbol{g}) = \frac{1}{8}\int_{S^2} (-2\Delta_{\mathbb{S}^2\times\mathbb{S}^2}+1)^{1/2}\mathcal{R}f(\mathbf{h},\,\boldsymbol{g}\mathbf{h})\, d\mathbf{h}.$$

equivlent to the formula by Matthies, 1979, 1982, 1987

$$\begin{aligned}f(\boldsymbol{g}) &= \frac{1}{4\pi}\int_{\mathbf{H}} \bar{f}(\mathbf{h}',\boldsymbol{g})\, d\mathbf{h}', \\ \text{with}\quad \bar{f}(\mathbf{h}',\boldsymbol{g}) &= \mathcal{P}_{\boldsymbol{g}\cdot\mathbf{h}'}(-\mathbf{h}') + \frac{1}{\pi}\int_0^\pi d\theta\, \cos\left(\frac{\theta}{2}\right)\frac{d}{d\cos\theta}\bar{R}(\cos\theta,\mathbf{h}',\boldsymbol{g} \\ \text{and}\quad \bar{R}(\cos\theta,\mathbf{h}',\boldsymbol{g}) &= \int_0^{2\pi} \mathcal{P}_{\boldsymbol{g}\cdot\mathbf{h}'}(\{\mathbf{h}',0\}^{-1}\cdot y)\, d\phi; \quad y=(\theta,\phi).\end{aligned}$$

or Muller, Esling, Bunge, 1981, 1982

$$f(\boldsymbol{g}) = \int_{\mathbf{H}} P_{\mathbf{h}}(-\boldsymbol{g}\mathbf{h})\, d\mathbf{h} + 2\int_0^\pi d\theta \cos\left(\frac{\theta}{2}\right)\frac{d}{d\cos\theta}\int_{\mathbf{H}} W_{\mathbf{h},\boldsymbol{g}\mathbf{h}}(\cos\theta)\, d\mathbf{h}$$

Inverse Spherical Radon transform (2)

In texture analysis, i.e. in material science and engineering, the best known inversion formula dates back right to the beginning of "quantitative" texture analysis (Bunge, 1965; Roe, 1965). The formula may be rewritten in a rather abstract way as

$$f = \mathcal{F}^{-1}_{\mathbf{SO}(3)}\, \mathcal{S}\, \mathcal{F}_{\mathbb{S}^2\times\mathbb{S}^2}\, \mathcal{R} f \quad , \tag{43}$$

where $\mathcal{S}$ denotes a scaling matrix with entries $\sqrt{2\ell+1}$ indicating the ill-posedness of the inverse problem. It states that the harmonic coefficients of f are up to a scaling equal to the harmonic coefficients of its Radon transform. In the context of texture analysis and experimentally accessible "pole figures", the former statement is true only for even–order coefficients.

Inverse Spherical Radon transform (3)

In integral geometry the following inversion formulae are known

$$\begin{aligned} f &= \frac{1}{8\pi}\int_{S^2} (-2\Delta_{\mathbb{S}^2\times\mathbb{S}^2}+1)^{1/2}\mathcal{R}f(\mathbf{h}, \boldsymbol{g}\mathbf{h})\, d\omega_2(\mathbf{h}) \\ &= \frac{1}{4\pi}\widetilde{\mathcal{R}}\left[(-2\Delta_{\mathbb{S}^2\times\mathbb{S}^2}+1)^{1/2}\,\mathcal{R}f\right] \end{aligned} \tag{44}$$

where $\widetilde{\mathcal{R}}$ denotes the adjoint operator of $\mathcal{R}$ with respect to L^2.

Also,

$$f = \frac{1}{4\pi}(-4\Delta_{\mathbb{S}^3}+1)^{1/2}\,\widetilde{\mathcal{R}}\,\mathcal{R}f \tag{45}$$

cf. (Helgason, 1994; 1999).

The equivalence of all these formula is explicitly shown in (Bernstein and Schaeben, 2005).

Finite Support Theorem

If f vanishes outside the spherical cap

$$U_\epsilon(\boldsymbol{g}_0) := \{\boldsymbol{g}\in\mathbf{SO}(3)\,|\,\angle(\boldsymbol{g}_0,\boldsymbol{g})\le\epsilon\},$$

then its Radon transform $\mathcal{R}f$ vanishes outside the corresponding spherical cap

$$V_\epsilon(\boldsymbol{g}_0) := \{(\mathbf{h},\mathbf{r})\in\mathbb{S}^2\times\mathbb{S}^2\,|\,\angle(\boldsymbol{g}_0\mathbf{h},\mathbf{r})<\epsilon\},$$

where $V_\epsilon(\boldsymbol{g}_0)$ denotes the set of all fibres intersecting $U_\epsilon(\boldsymbol{g}_0)$ because $\angle(\boldsymbol{g}_0\mathbf{h},\mathbf{r})$ is the distance of a fibre $G(\mathbf{h},\mathbf{r})$ from $\boldsymbol{g}_0$.

If f vanishes outside the spherical cap $K(q_0;\kappa) := \{q\in S^3\,|\,\mathrm{Sc}(q_0q^*)\ge\cos\epsilon\}$, then $\mathcal{R}f$ vanishes outside the corresponding spherical cap of $S^2\times S^2$.

Inversion and Localization

Let $\boldsymbol{g}_0\in\mathbf{SO}(3)$ denote an arbitrary rotation, $U_\epsilon(\boldsymbol{g}_0)\subset\mathbf{SO}(3)$ a neighborhood of $\boldsymbol{g}_0$ and $V_\epsilon(\boldsymbol{g}_0)$ the corresponding neighborhood in $\mathbb{S}^2\times\mathbb{S}^2$.

Then $\mathcal{R}f(\mathbf{h},\mathbf{r})=\mathbf{0}$ for all $(\mathbf{h},\mathbf{r})\in V_\epsilon(\boldsymbol{g}_0)$ implies $f(\boldsymbol{g})=0$ for all $\boldsymbol{g}\in U_\epsilon(\boldsymbol{g}_0)$ for any **non–negative** function $f\in C(\mathbf{SO}(3))$.

It should be noted that localization of the inverse Radon transform cannot be inferred.

In fact, one can conclude from inversion formula (**??**) that the inverse Radon transform cannot be localized.

Inverse Radon Transform – Special cases

Inversion: Special cases (1)

Under mild conditions the spherical Radon transform is invertible.

In general, f is defined on the 3–dimensional manifold $\mathbf{SO}(3)$, and $\mathcal{R}f$ is defined on $\mathbb{S}^2 \times \mathbb{S}^2$, which is apparently 4–dimensional; however, due to the Darboux–type differential equation governing $\mathcal{R}f$, the domain of definition is effectively 3–dimensional.

The inversion formulae indicate that $\mathcal{R}f$ must be known as a function on $\mathbb{S}^2 \times \mathbb{S}^2$. In the practice of texture analysis, $\mathcal{X}f$ can be experimentally sampled for a few axes $\pm\mathbf{h}$ only. Therefore, we are interested to characterize special cases where the knowledge of $\mathcal{X}f$ for a small total number of axes $\pm\mathbf{h}$ is sufficient to determine the even portion of f unanimously.

Inversion: Special cases (2)

The corresponding special cases concerning $\mathcal{R}f$ are constructed imposing constraints on the support of f directly or by rotational symmetry, and employing the geometry of rotations involved in the spherical Radon transform.

Next we shall compile a list of special cases where the inversion of the Radon transform is especially simple. In a descriptive way the following special cases may be distinguished.

Inversion: Special cases (3)

Proposition

If $\mathbf{h}_0 \in \mathbb{S}^2$ *exists such that* $f : \mathbb{G} \mapsto \mathbb{R}^1_+$ *is constant on* $G(\mathbf{h}_0, \mathbf{r})$ *for every* $\mathbf{r} \in \mathbb{S}^2$*, then*

$$f(\boldsymbol{g}) = \mathcal{R}f(\mathbf{h}_0, \boldsymbol{g}\mathbf{h}_0) \tag{46}$$

Since the transform $\mathcal{R}f(\mathbf{h}, \boldsymbol{g}\mathbf{h})$ as a function of $\boldsymbol{g} \in \mathbb{G}$ is constant on each $G(\mathbf{h}, \mathbf{r})$, the proof is obvious.

Analogously, if $\mathbf{r}_0 \in \mathbb{S}^2$ exists such that $f : \mathbb{G} \mapsto \mathbb{R}^1_+$ is constant on $G(\mathbf{h}, \mathbf{r}_0)$ for every $\mathbf{h} \in \mathbb{S}^2$, then

$$f(\boldsymbol{g}) = \mathcal{R}f(\boldsymbol{g}^{-1}\mathbf{r}_0, \mathbf{r}_0) \tag{47}$$

Inversion: Special cases (4)

An orientation probability density function f is called a fibre texture if there is a pair $(\mathbf{h}_0, \mathbf{r}_0)$ of a specific crystallographic direction $\mathbf{h}_0$ and a specific specimen direction $\mathbf{r}_0$ such that f is rotationally symmetric with respect to the one–dimensional set of modes $G(\mathbf{h}_0, \mathbf{r}_0)$, i.e. it depends only on the orientation distance

$$\text{dist}\,(\boldsymbol{g}, G(\mathbf{h}_0, \mathbf{r}_0)) = \inf_{\tilde{\boldsymbol{g}} \in G(\mathbf{h}_0, \mathbf{r}_0)} \omega(\boldsymbol{g}\tilde{\boldsymbol{g}}^{-1}) = \eta(\boldsymbol{g}\mathbf{h} \cdot \mathbf{r}) = \arccos(\boldsymbol{g}\mathbf{h} \cdot \mathbf{r})$$

of $\boldsymbol{g}$ and $G(\mathbf{h}_0, \mathbf{r}_0)$ (Grewen and Wassermann, 1955).

If f is represents a rotationally symmetric fibre texture with respect to a given pair $(\mathbf{h}_0, \mathbf{r}_0) \in \mathbb{S}^2 \times \mathbb{S}^2$, then a function $f_c : [-1, 1] \mapsto \mathbb{R}^1_+$ exists such that $f(\boldsymbol{g}) = f_c(\boldsymbol{g}\mathbf{h}_0 \cdot \mathbf{r}_0)$.

Inversion: Special cases (5)

Proposition

If $f : \mathbb{G} \mapsto \mathbb{R}^1_+$ represents a symmetrical fibre texture with respect to a given pair $(\mathbf{h}_0, \mathbf{r}_0) \in \mathbb{S}^2 \times \mathbb{S}^2$, then f is uniquely determined by $\mathcal{R}f(\boldsymbol{g}\mathbf{h}_0 \cdot \mathbf{r}_0)$.

Since f is presumed to be a rotatinally symmetrical fibre textures, we can immediately conclude from Eq. (46) that

$$\begin{aligned} f(\boldsymbol{g}) &= f_c(\boldsymbol{g}\mathbf{h}_0 \cdot \mathbf{r}_0) = \mathcal{R}f(\mathbf{h}_0, \mathbf{r}), \ \boldsymbol{g} \in G(\mathbf{h}_0, \mathbf{r}) \\ f(\boldsymbol{g}) &= f_c(\mathbf{h}_0 \cdot \boldsymbol{g}^{-1}\mathbf{r}_0) = \mathcal{R}f(\mathbf{h}, \mathbf{r}_0), \ \boldsymbol{g} \in G(\mathbf{h}, \mathbf{r}_0) \end{aligned}$$

indicating that $\mathcal{R}f(\mathbf{h}_0, \circ)$ is rotationally symmetric with respect to $\mathbf{r}_0$, and analogously that $\mathcal{R}f(\circ, \mathbf{r}_0)$ is rotationally symmetric with respect to $\mathbf{h}_0$.

Inversion: Special cases (6)

If $f : \mathbb{G} \mapsto \mathbb{R}^1_+$ represents a rotationally symmetric or, synonymously, zonal, central, texture with respect to a given $\boldsymbol{g}_0 \in \mathbb{G}$, then a function $f_a : [0, \pi] \mapsto \mathbb{R}^1_+$ exists such that $f(\boldsymbol{g}) = f_a(\omega(\boldsymbol{g}\boldsymbol{g}_0^{-1}))$.

Proposition

If $f : \mathbb{G} \mapsto \mathbb{R}^1_+$ represents a central texture with respect to a given $\boldsymbol{g}_0 \in \mathbb{G}$, then $\mathcal{R}f$ is central with respect to $\boldsymbol{g}_0\mathbf{h}$ (or $\boldsymbol{g}_0^{-1}\mathbf{r}$) and f is uniquely determined by $(\mathcal{R}f_a)(\boldsymbol{g}_0\mathbf{h} \cdot \mathbf{r}) = (\mathcal{R}[f(\circ\boldsymbol{g}_0^{-1})])(\mathbf{h}, \mathbf{r})$.

Inversion: Special cases (7)

Proof. Since f is presumed to be central it holds that $f(\boldsymbol{g}\boldsymbol{g}_0^{-1}) = f(\tilde{\boldsymbol{g}}\boldsymbol{g}\boldsymbol{g}_0^{-1}\tilde{\boldsymbol{g}}^{-1})$. Then Eq. (242) implies that for an arbitrary $\tilde{\boldsymbol{g}} \in \mathbb{G}$

$$\begin{aligned} \left(\mathcal{R}[f(\circ)]\right)(\boldsymbol{g}_0\mathbf{h}, \mathbf{r}) &= \left(\mathcal{R}[f(\circ\boldsymbol{g}_0^{-1})]\right)(\mathbf{h}, \mathbf{r}) \\ &= \left(\mathcal{R}[f(\tilde{\boldsymbol{g}} \circ \boldsymbol{g}_0^{-1}\tilde{\boldsymbol{g}}^{-1})]\right)(\mathbf{h}, \mathbf{r}) \\ &= \left(\mathcal{R}[f(\circ)]\right)(\tilde{\boldsymbol{g}}\boldsymbol{g}_0\mathbf{h}, \tilde{\boldsymbol{g}}\mathbf{r}) = \left(\mathcal{R}[f(\circ)]\right)(\tilde{\boldsymbol{g}}\mathbf{h}_0, \tilde{\boldsymbol{g}}\mathbf{r}) \end{aligned}$$

holds, thus showing that $\mathcal{R}f$ depends only on $\boldsymbol{g}_0\mathbf{h} \cdot \mathbf{r}$ and moreover that any $\mathcal{R}f(\mathbf{h}, \circ)$ is only a rotated version of an arbitrarily fixed $\mathcal{R}f(\mathbf{h}_0, \circ)$, i.e.

$$\mathcal{R}f(\mathbf{h}, \mathbf{r}) = \mathcal{R}f(\boldsymbol{g}\mathbf{h}, \boldsymbol{g}_0\boldsymbol{g}\boldsymbol{g}_0^{-1}\mathbf{r}). \tag{48}$$

for all $\boldsymbol{g} \in \mathbf{SO}(3)$. Thus $\mathcal{R}f(\mathbf{h}_0, \mathbf{r})$ for an arbitrarily fixed $\mathbf{h}_0$ is sufficient to determine f. Analogously, $\mathcal{R}f(\mathbf{h}, \mathbf{r}_0)$ for an arbitrarily fixed $\mathbf{r}_0$ is sufficient, too.

Inversion: Special cases (8)

An orientation probability density function f is called surface texture if there exists a specific orientation $\boldsymbol{g}_0 \in \mathbf{SO}(3)$ such that f is rotationally symmetric with respect to the two–dimensional set of modes $\boldsymbol{g}_0^{\perp} = \{\boldsymbol{g} \in \mathbf{SO}(3) \,|\, \omega(\boldsymbol{g}, \boldsymbol{g}_0^{-1}) = \pi\}$, i.e. $f(\boldsymbol{g})$ depends only on the orientation distance

$$\text{dist}\,(\boldsymbol{g}, \boldsymbol{g}_0^{\perp}) = \pi - \omega(\boldsymbol{g}\boldsymbol{g}_0^{-1})$$

Since the distances dist $(\boldsymbol{g}, \boldsymbol{g}_0)$ and dist $(\boldsymbol{g}, \boldsymbol{g}_0^{\perp})$ sum to π, $\mathcal{R}f(\mathbf{h}_0, \circ)$ is sufficient to recover f.

Numerical Inversion

Ill–posedness (1)

A system of linear equations $A\mathbf{x} = \mathbf{y}$ is called ill-posed if largely different vectors $\mathbf{x}$ result in very similar vectors $\mathbf{y}$, i.e. if small changes in the right–hand side $\mathbf{y}$ imply large changes in the "solution" $\mathbf{x}$.

Ill–posedness (2)

A system of linear equations with the Hilbert matrix H_n defined by its elements $h_{ij} = \frac{1}{i+j-1}$, $i, j = 1, \ldots, n$, is a well known example of a notoriously ill-conditioned problem. The matrix is symmetric and positive definit, thus non-singular, but badly conditioned, even for small values of n, and with rapidly growing condition number for increasing n.

If the right hand side of

$$H_n\mathbf{x} = \mathbf{b}$$

is specified by $b_i = \sum_{j=1}^{n} h_{ij}$ the unique solution obviously is $\mathbf{x} = \mathbf{1}$, but because the H_n are poorly conditioned, care must be exercised when the system of linear equations is solved numerically.

Ill–posedness (3) – Hilbert matrix

Hilbert, 1894

$$\begin{pmatrix} 1 & 1/2 & 1/3 & \dots & 1/n \\ 1/2 & 1/3 & 1/4 & \dots & 1/(n+1) \\ \vdots & & \ddots & & \vdots \\ 1/n & 1/(n+1) & \dots & & 1/(2n-1) \end{pmatrix} \begin{pmatrix} x_1 \\ x_2 \\ \vdots \\ x_n \end{pmatrix} = \begin{pmatrix} \sum_{j=1}^{n} 1/j \\ \sum_{j=1}^{n} 1/(j+1) \\ \vdots \\ \sum_{j=1}^{n} 1/(j+n-1) \end{pmatrix}$$

The condition number of H_n is

n	1	2	3	4	5	6
cond(H_n)	1.93×10^1	5.24×10^2	1.55×10^4	4.77×10^5	1.50×10^7	4.75×10^8

Numerical Inversion of the Spherical Radon transform

Methods of numerical inversion are provided by applying

- Harmonic Method/s
- Component Fit Method/s
- Discrete Method/s
- Approximation with Zonal Functions
- Optimum Splines – kriging
- Spherical Wavelets
- ...

Concise Survey of Numerical Methods (1)

Harmonic Method/s. The harmonic method dating back to (Bunge, 1965; Roe, 1965) applies the Fourier slice theorem. It considers **h** rather as a parameter than a variable, and subsequently $P_{\mathbf{h}}(\mathbf{r}) \equiv P(\mathbf{h}, \mathbf{r})$ as a function defined on $\mathbb{S}^2$. Fixing a maximum series expansion degree L appropriately chosen according to the data supply, it (i) approximates the harmonic coefficients $F_\ell^m(\mathbf{h}_i)$, $\ell = 0, \dots, L$, $m = -\ell, \dots, \ell$, of $P_{\mathbf{h}_i}$, $i = 1, \dots, N$, by solving the least squares problem

$$\sum_{j=1}^{N_i} \left| \sum_{\ell=0}^{L} \sum_{m=-\ell}^{\ell} F_\ell^m(\mathbf{h}_i) \mathcal{Y}_\ell^m(\mathbf{r}_{ij}) - \iota_{ij} \right|^2 \to \min$$

and (ii) determines the even harmonic coefficients $(C_\ell^{m,n})$, $\ell = 0, 2, \dots, L$, $m, n = -\ell, \dots, \ell$ of f as solution of the least squares problem

$$\sum_{i=1}^{N} \left| \sum_{n=-\ell}^{\ell} C_\ell^{m,n} \mathcal{Y}_\ell^n(\mathbf{h}_i) - F_\ell^m(\mathbf{h}_i) \right|^2 \to \min .$$

Concise Survey of Numerical Methods (2)

The method cannot consider the required non–negativity of f in a constructive way. With L depending on the data supply, it does not apply to sharp textures.

Concise Survey of Numerical Methods (3)

Algebraic Method/s.

Common to all versions of the algebraic method is the partition of the manifold $\mathbb{S}^3$ or $\mathbf{SO}(3)$, respectively, into boxes. Then it determines an orientation density function as solution of a constrained least squares problem in terms of linear combinations of indicator functions with respect to the boxes.

If the data are irregularly distributed featuring a varying spatial resolution according to local refinement of the spatial data configuration the method tends to lack numerical stability and suffers from largely increasing numerical complexity.

Concise Survey of Numerical Methods (4)

In mathematical tomography fast and stable methods are known for the inversion of the common Radon transform in $\mathbb{R}^3$, in particular the filtered back projection method (cf. Louis, 1999) and the Fourier method (cf. Kunis and Potts, 2003). In the following discussion we distinguish algorithms based on numerical integration or on a least squares approach.

Concise Survey of Numerical Methods (5)

Inversion by Numerical Integration.

Filtered back projection is a method based on numerical integration. Let $\widetilde{\mathcal{R}}$ be the adjoint operator of $\mathcal{R}$ with respect to $\mathrm{L}^2(\mathbf{SO}(3)$ and $\phi_{\boldsymbol{g}\boldsymbol{g}} \in \mathrm{L}^2(\mathbf{SO}(3))$ a kernel spatially localized around $\boldsymbol{g}\boldsymbol{g} \in \mathbf{SO}(3)$ such that a function $\psi_{\boldsymbol{g}\boldsymbol{g}} \in \mathrm{L}^2(\mathbb{S}^2 \times \mathbb{S}^2)$ exists with $\widetilde{\mathcal{R}}\psi_{\boldsymbol{g}\boldsymbol{g}} = \phi_{\boldsymbol{g}\boldsymbol{g}}$. Then

$$\langle f, \phi_{\boldsymbol{g}\boldsymbol{g}} \rangle_{\mathbf{SO}(3)} = \left\langle f, \widetilde{\mathcal{R}}\psi_{\boldsymbol{g}\boldsymbol{g}} \right\rangle_{\mathbf{SO}(3)} = \langle \mathcal{R}f, \psi_{\boldsymbol{g}\boldsymbol{g}} \rangle_{\mathbb{S}^2 \times \mathbb{S}^2} . \qquad (49)$$

Then f is approximated in $\boldsymbol{g}\boldsymbol{g}$ by numerical integration of $\langle \mathcal{R}f, \psi_{\boldsymbol{g}\boldsymbol{g}} \rangle_{\mathbb{S}^2 \times \mathbb{S}^2}$ using the data ι_{ij}, $i = 1, \ldots, N$, $j = 1, \ldots, N_i$. This approach analogously applies to the determination of the (even) coefficients of f with respect to harmonics $D_\ell^{m,n}$ or a wavelet basis ϕ_ℓ^n.

Concise Survey of Numerical Methods (6)

This approach can successfully be used if the data are rather uniformly distributed in the domain of definition. In our case of clustered data they do not apply. Moreover, they cannot constructively consider the required non–negativity.

Concise Survey of Numerical Methods (7)

Inversion by Least Squares.

Least squares approaches assume a subspace $\mathcal{W} \subset \mathrm{L}^2(\mathbf{SO}(3))$ for which the minimization problem

$$J(f) = \sum_{i=1}^{N} \sum_{j=1}^{N_i} |\mathcal{X} f(\mathbf{h}_i, \mathbf{r}_{ij}) - \iota_{ij}|^2 \to \min \qquad (50)$$

is well posed. Depending on the choice of the subspace they lead to different algorithms as following.

Concise Survey of Numerical Methods (8)

Spline Interpolation.

If $\mathcal{W} = \mathcal{H}(A_\ell, \mathbf{SO}(3))$ is assumed to be a reproducing kernel Hilbert space, then the solution of Eq. (50) is given by solving a system of linear equations (Boogaart et al., 2005). There, first numerical results including error bounds were presented.

Again, the major disadvantage is that the required non–negativity cannot directly be incorporated into the algorithm. If the function f is strongly unimodal, the errors tend to be large.

Concise Survey of Numerical Methods (9)

Kriging of Linear Functionals.

It has been shown (cf. Wahba, 1990) that ordinary kriging and spline interpolation are equivalent. Thus, spline interpolation can be interpreted in terms of stoachastics. Given a data set, a reproducing kernel Hilbert space $\mathcal{W}$ can be determined such that the interpolating spline represents the unbiased solution with minimum estimation variance. As usually, the kriging variance can be interpreted as a measure of goodness.

Concise Survey of Numerical Methods (10)

Generalized Harmonic Method.

Let $\mathcal{W}$ be the space of band–limited functions defined on $\mathbf{SO}(3)$ of degree L. Then Eq. (50) can be rewritten as the quadratic minimization problem

$$J(f) = \|Ac - P\|_2^2 \to \min \qquad (51)$$

where c denotes the vector of Fourier coefficients of f up to degree L, and where A denotes the matrix which is defined such that Ac yields the values of the Radon transform for $(\mathbf{h}_i, \mathbf{r}_{ij})$.

Concise Survey of Numerical Methods (11)

If $(\mathbf{g}_k)_{k=1}^M$ is a set of approximately uniformly distributed points of $\mathbf{SO}(3)$, and B a matrix such that $(Bc)_k = f(\mathbf{g}_k)$, then the constraint $f \geq 0$ can be approximated by $Bc \geq 0$. To accomplish satisfying results the size of the matrix B must be of the same order as the size of A. For high resolution texture analysis with about $100,000$ degrees of freedom, the resulting problem is numerically prohibitive.

Concise Survey of Numerical Methods (12)

Generalized Algebraic Method.

Let $(\mathbf{g}_k)_{k=1}^M$ be a set of approximately uniformly distributed points of $\mathbf{SO}(3)$ and ϕ a radially symmetric kernel defined on $\mathbf{SO}(3)$. Then we define the subspace $\mathcal{W}$ as the set of all linear combinations of translates of ϕ into the points $\mathbf{g}_k$. Setting $f = \sum_{k=1}^M c_k \phi(\mathbf{g}_k \cdot)$ and defining the matrix A such that for an arbitrary vector of coefficients $c \in \mathbb{R}^k$ the vector Ac gives the values of the Radon transform of f for $(\mathbf{h}_i, \mathbf{r}_{ij})$. Then Eq. (50) can again be rewritten as a quadratic minimization problem

$$J(f) = \|Ac - P\|_2^2 \to \min \tag{52}$$

Concise Survey of Numerical Methods (13)

Compared with the generalized harmonic method the required non–negativity can be approximated by the simpler constraints $c \geq 0$. If a solution with non–negative coefficients exists, then the method converges to it. For the resulting quadratic minimization problem with bound constraints exist largely efficient algorithms. There common base is the implementation of a fast matrix–vector multiplication Ac. It can be achieved by realizing this matrix–vector multiplication by a twofold application of the spherical Fourier transform.

Additional Modeling Assumptions for Pole Figure Inversion (1)

A natural modeling assumption to compensate for the lack of information is

$$f(\mathbf{g}) \geq 0$$

Despite its apparent simplicity, this constraint is often hard to realize for many algorithms.

This difficulty may be avoided by explicitly prescribing the form of the ODF, e.g. as superposition of zonal ansatz–functions.

Additional Modeling Assumptions for Pole Figure Inversion (2)

Other additional modeling assumptions may address the smoothness of the function to be reconstructed. The objectives may be to minimize the norm or to maximize the entropy of the solution to be favoured.

The advantage of the entropy criterion is that it guarantees non–negativity without additional efforts.

Zonal Ansatz–Functions

Examples of zonal ansatz–functions are spherical kernels as the (i) spherical Brownian, (ii) spherical de la Vallée Poussin, (iii) spherical Cauchy, (iv) von Mises-Fisher probability density function for $\mathbb{S}^3$

$$\text{(i)} \quad \chi_\rho(t) = \frac{1}{4\pi}\sum_{\ell=0}^{\infty}(2\ell+1)\,\exp[-\ell(\ell+1)\rho]\,P_\ell(t) = b(t;\rho)$$

$$\text{(ii)} \quad \chi_\rho(t) = \frac{1}{4\pi}\sum_{\ell=0}^{\infty}(2\ell+1)\,\frac{\mathcal{I}_\ell(\rho)-\mathcal{I}_{\ell+1}(\rho)}{2B(\frac{3}{2},\rho+\frac{1}{2})}\,P_\ell(t) = \frac{1}{B(1,\rho+1)}\cos^{2\rho}(t) = v_n(t)$$

$$\text{(iii)} \quad \chi_\rho(t) = \frac{1}{4\pi}\sum_{\ell=0}^{\infty}(2\ell+1)\,\rho^{2\ell}\,P_\ell(t) = \frac{1}{4\pi}\frac{1-\rho^2}{(1+\rho^2-2\rho\cos t)^{3/2}} = p_\rho(t)$$

$$\text{(iv)} \quad \chi_\rho(t) = \frac{1}{4\pi}\sum_{\ell=0}^{\infty}(2\ell+1)\frac{\mathcal{I}_{\ell+1/2}(\rho)}{\mathcal{I}_{1/2}(\rho)}P_\ell(t) = \frac{\rho}{4\pi\sinh\rho}\exp(\rho t) = m(t;\rho)$$

$$\text{(v)} \quad \chi_\rho(t) = \frac{1}{4\pi}\sum_{\ell=0}^{\infty}(2\ell+1)\,\frac{\mathcal{I}_\ell(\rho)-\mathcal{I}_{\ell+1}(\rho)}{\mathcal{I}_0(\rho)-\mathcal{I}_1(\rho)}\,P_\ell(t) = \frac{1}{4\pi\sinh\rho}I_0(\frac{\rho}{2}(1+t))\exp(\frac{\rho}{2}(t-1)) = (\mathcal{R}M)(t;$$

leading to the spherical singular integrals of (i) Gauss-Weierstrass, (ii) de la Vallée Poussin, (iii) Abel–Poisson, (iv) von Mises–Fisher.

All of them may be used as their spherical Radon transforms are known.

Discrete Algebraic Method/s to Resolve the Inversion Problem

Simultaneous Series Expansion into Indicators (1)

Let the orientation density function $f(\boldsymbol{g})$ be normalized such that

$$\frac{1}{\mathrm{vol}(\mathbb{G})}\int_{\mathbb{G}} f(\boldsymbol{g})d\boldsymbol{g} = 1$$

Let $\mathcal{Z}(\mathbb{G}) = (G_n)_{n=1,\ldots,N}$ be a partition of $\mathbb{G}$; then we set

$$f(\boldsymbol{g}) = \sum_{n=1}^{N} x_n \mathbb{1}_{G_n}(\boldsymbol{g})$$

$$x_n = \frac{1}{\mathrm{vol}(G_n)}\int_{G_n} f(\boldsymbol{g})d\boldsymbol{g}, \quad n = 1,\ldots,N$$

Then

$$\sum_{n=1}^{N}\frac{\mathrm{vol}(G_n)}{\mathrm{vol}(\mathbb{G})}x_n = \frac{1}{\mathrm{vol}(\mathbb{G})}\sum_{n=1}^{N}\int_{G_n} f(\boldsymbol{g})d\boldsymbol{g} = 1$$

Simultaneous Series Expansion into Indicators (2)

Analogously, the pole density function $P(\mathbf{h},\mathbf{r})$ defined by

$$P(\mathbf{h},\mathbf{r}) = \frac{1}{2\pi}\int_{G^{\pm}(\mathbf{h},\mathbf{r})} f(\boldsymbol{g})d\boldsymbol{g}$$

with the path of integration

$$G^{\pm}(\mathbf{h},\mathbf{r}) = \{\boldsymbol{g}\in\mathbf{SO}(3)\,|\,\boldsymbol{g}(\pm\mathbf{h})=\mathbf{r}\}$$

normalized such that

$$\frac{1}{\text{area}(S^2)}\int_{S^2} P(\mathbf{h},\mathbf{r})ds(\mathbf{r}) = 1$$

Simultaneous Series Expansion into Indicators (3)

Let $\mathcal{Z}(S^2) = (Z_p)_{p=1,\ldots,P}$ be a partition of S^2; then we set

$$\begin{aligned} P(\mathbf{h},\mathbf{r}) &= \sum_{p=1}^{P} y_p(\mathbf{h})\mathbb{1}_{Z_p}(\mathbf{r}) \\ y_p(\mathbf{h}) &= \frac{1}{\text{area}(Z_p)}\int_{Z_p} P(\mathbf{h},\mathbf{r})ds(\mathbf{r}),\quad p=1,\ldots,P \end{aligned}$$

Then

$$\sum_{p=1}^{P}\frac{\text{area}(Z_p)}{\text{area}(S^2)}\,y_p(\mathbf{h}) = \frac{1}{\text{area}(S^2)}\sum_{p=1}^{P}\int_{Z_p} P(\mathbf{h},\mathbf{r})ds(\mathbf{r}) = 1$$

Simultaneous Series Expansion into Indicators (4)

$$\begin{aligned} y_p(\mathbf{h}) &= \frac{1}{\text{area}(Z_p)}\int_{Z_p} P(\mathbf{h},\mathbf{r})ds(\mathbf{r}) \\ &= \frac{1}{2\pi\text{area}(Z_p)}\int_{Z_p}\int_{G^{\pm}(\mathbf{h},\mathbf{r})}\sum_{n=1}^{N} x_n\mathbb{1}_{G_n}(\boldsymbol{g})d\boldsymbol{g}ds(\mathbf{r}) \\ &= \frac{1}{2\pi\text{area}(Z_p)}\sum_{n=1}^{N} x_n\int_{Z_p}\int_{G^{\pm}(\mathbf{h},\mathbf{r})\cap G_n}\mathbb{1}_{G_n}(\boldsymbol{g})d\boldsymbol{g}ds(\mathbf{r}) \\ &= \sum_{n=1}^{N}\frac{\text{vol}(G_n\cap T_p(\mathbf{h}))}{\text{vol}(T_p(\mathbf{h}))}\,x_n \\ &= \sum_{n=1}^{N}\text{prob}(G_n|\,T_p(\mathbf{h}))\,x_n \\ &= \sum_{n=1}^{N}\pi_{pn}(\mathbf{h})\,x_n \qquad (53) \end{aligned}$$

Simultaneous Series Expansion into Indicators (5)

... and also

$$\begin{aligned} y_p(\mathbf{h}) &= \frac{1}{2\pi\,\text{area}(Z_p)}\sum_{n=1}^{N}\text{vol}(G_n\cap T_p(\mathbf{h}))\,x_n \\ &= \frac{1}{2\pi\,\text{area}(Z_p)}\sum_{n=1}^{N}\frac{\text{vol}(G_n\cap T_p(\mathbf{h}))}{\text{vol}(G_n)}\,x_n\,\text{vol}(G_n) \\ &= \frac{1}{2\pi\,\text{area}(Z_p)}\sum_{n=1}^{N}\pi'_{pn}(\mathbf{h})\,x_n\,\text{vol}(G_n) \qquad (54) \end{aligned}$$

where

$$\begin{aligned} T_p(\mathbf{h}) &= \bigcup_{\mathbf{r}\in Z_p} G^{\pm}(\mathbf{h},\mathbf{r}) = \{\boldsymbol{g}\in G|\boldsymbol{g}(\pm\mathbf{h})\in Z_p\} \\ \text{vol}(T_p(\mathbf{h})) &= 2\pi\,\text{area}(Z_p) \\ \pi'_{pn}(\mathbf{h}) &= \frac{\text{vol}(G_n\cap T_p(\mathbf{h}))}{\text{vol}(G_n)} = \text{prob}(T_p(\mathbf{h})|G_n) \end{aligned}$$

Simultaneous Series Expansion into Indicators (6)

... and

$$\begin{aligned}\frac{\pi'_{pn}(\mathbf{h})\,\mathrm{vol}(G_n)}{2\pi\ \mathrm{area}(Z_p)} &= \frac{\mathrm{vol}(G_n \cap T_p(\mathbf{h}))}{2\pi\ \mathrm{area}(Z_p)} \\ &= \frac{\mathrm{vol}(G_n \cap T_p(\mathbf{h}))}{\mathrm{vol}(T_p(\mathbf{h})}) \\ &= \mathrm{prob}(G_n|T_p(\mathbf{h})) = \pi_{pn}(\mathbf{h})\end{aligned}$$

Then

$$\sum_{p=1}^{P} \pi'_{pn}(\mathbf{h}) = 1 \qquad \sum_{n=1}^{N} \pi'_{pn}(\mathbf{h}) = ?$$

and

$$\sum_{n=1}^{N} \pi_{pn}(\mathbf{h}) = 1 \qquad \sum_{p=1}^{P} \pi_{pn}(\mathbf{h}) = ?$$

Notational Alternatives (7)

Notationally closer to probability and statistics, it would be much nicer to define

$$\begin{aligned}\int_G f(\boldsymbol{g})d\boldsymbol{g} &= 1 \\ x_n &= \int_{G_n} f(\boldsymbol{g})d\boldsymbol{g} = \mathrm{prob}(\boldsymbol{g} \in G_n), \quad n = 1, \ldots, N \\ f(\boldsymbol{g}) &= \sum_{n=1}^{N} \frac{x_n}{\mathrm{vol}(G_n)} \mathbb{1}_{G_n}(\boldsymbol{g})\end{aligned}$$

and analogously

$$\begin{aligned}\int_{S^2} P(\mathbf{h},\mathbf{r})ds(\mathbf{r}) &= 1 \\ y_p(\mathbf{h}) &= \int_{Z_p} P(\mathbf{h},\mathbf{r})ds(\mathbf{r}) = \mathrm{prob}(\boldsymbol{g}\mathbf{h} \in Z_p), \quad p = 1, \ldots, P \\ P(\mathbf{h},\mathbf{r}) &= \sum_{p=1}^{P} \frac{y_p(\mathbf{h})}{\mathrm{area}(Z_p)} \mathbb{1}_{Z_p}(\mathbf{r})\end{aligned}$$

Notational Alternatives (8)

and see immediately

$$\begin{aligned}y_p(\mathbf{h}) &= \frac{1}{2\pi}\int_{Z_p}\int_{G^{\pm}(\mathbf{h},\mathbf{r})} f(\boldsymbol{g})d\boldsymbol{g} \\ &= \frac{1}{2\pi}\sum_{n=1}^{N} \frac{\mathrm{vol}(G_n \cap T_p(\mathbf{h}))}{\mathrm{vol}(G_n)}\, x_n \\ &= \frac{1}{2\pi}\sum_{n=1}^{N} \frac{\mathrm{vol}(G_n \cap T_p(\mathbf{h}))}{\mathrm{vol}(T_p(\mathbf{h}))} \frac{\mathrm{vol}(T_p(\mathbf{h}))}{\mathrm{vol}(G_n)}\, x_n\end{aligned}$$

which is

$$\mathrm{prob}(\boldsymbol{g}\mathbf{h} \in Z_p) = \frac{1}{2\pi}\sum_{n=1}^{N} \mathrm{prob}(T_p(\mathbf{h})|G_n)\mathrm{prob}(\boldsymbol{g} \in G_n), \quad p = 1, \ldots, P$$

However, the notation adopted here is closer to texture analysis and the numerical realization, as $\mathrm{prob}(G_n|T_p(\mathbf{h}))$ is faster to calculate than $\mathrm{prob}(T_p(\mathbf{h})|G_n)$.

Maximum Entropy Solution (1)

Eq. (54) is the formula of total probability

$$\begin{aligned}y_p(\mathbf{h})\ \mathrm{area}(Z_p) &= \frac{1}{2\pi}\sum_{n=1}^{N} \mathrm{prob}(T_p(\mathbf{h})|G_n)\ x_n\ \mathrm{vol}(G_n) \\ \mathrm{prob}(\boldsymbol{g}\mathbf{h} \in Z_p)\ \mathrm{area}(S^2) &= \frac{1}{2\pi}\sum_{n=1}^{N} \mathrm{prob}(T_p(\mathbf{h})|G_n)\ \mathrm{prob}(\boldsymbol{g} \in G_n)\ \mathrm{vol}(G)\end{aligned}$$

Maximum Entropy Solution (2)

In practical applications, usually an number of pole density functions corresponding to different crystal forms $\mathbf{h}_j, j = 1, \ldots, J$, are sampled, resulting in a set of linear systems

$$\pi(\mathbf{h}_j)\mathbf{x} = \mathbf{y}(\mathbf{h}_j) \;\; j = 1, \ldots, J$$

Due to the rank–deficiency of each π–matrix, an additional modeling assumption is required to achieve uniqueness. The modeling assumption is provided by the entropy

$$S(\mathbf{x}) = -\sum_{n=1}^{N} x_n \ln x_n$$

Maximum Entropy Solution (3)

Thus, the favoured solution is

$\text{argmax}_{\mathbf{x}\in\mathbb{R}^N} S(\mathbf{x})$ subject to $\pi(\mathbf{h}_j)\mathbf{x} = \mathbf{y}(\mathbf{h}_j), \;\; j = 1, \ldots, J, \;\; \text{and} \;\; x_n \geq 0$

or equivalently

$$\text{argmin}_{\mathbf{x}\in\mathbb{R}^N} -S(\mathbf{x}) \;\text{s.t.}\; \pi(\mathbf{h}_j)\mathbf{x} = \mathbf{y}(\mathbf{h}_j), \;\; j = 1, \ldots, J, \;\; \text{and} \;\; x_n \geq 0 \tag{55}$$

where $\pi(\mathbf{h}_j)$ is a $P \times N$ matrix, $\mathbf{x} \in \mathbb{R}^N$, and $\mathbf{y}(\mathbf{h}_j) \in \mathbb{R}^P, j = 1, \ldots, J$.

Maximum Entropy Solution (4)

The Langrangian of (55) is

$$L(\mathbf{x}, \lambda) = S(\mathbf{x}) + \sum_{j=1}^{J} \lambda_j^t [\pi(\mathbf{h}_j)\mathbf{x} - \mathbf{y}(\mathbf{h}_j)]$$

where $\lambda_j \in \mathbb{R}^P$ are the dual vectors of Lagrange multipliers.

Accordingly, the dual function is defined as

$$g(\lambda) = \min_{\mathbf{x}\in\mathbb{R}_+^N} L(\mathbf{x}, \lambda) \tag{56}$$

Maximum Entropy Solution (5)

A necessary condition for minimization of (56) is $\nabla_{\mathbf{x}} L(\mathbf{x}, \lambda) = 0$ which yields

$$\nabla S(\mathbf{x}) = -\sum_{j=1}^{J} \pi^t(\mathbf{h}_j)\lambda_j$$

which are the Kuhn–Tucker conditions. An iterative primal–dual algorithm for solving (55) may be derived by iterating both primal $\{\mathbf{x}^k\}_{k=0}^{\infty}$ and dual $\{\lambda_j^k\}_{k=0}^{\infty}$ vectors such that

$$\nabla S(\mathbf{x}^k) = -\sum_{j=1}^{J} \pi^t(\mathbf{h}_j)\lambda_j^k$$

To do so the corrections of the dual vectors have to be prescribed.

Maximum Entropy Solution (6)

The Kuhn–Tucker conditions for (55) become

$$x_n = \exp\Big\{\Big(\sum_{j=1}^{J}\pi^t(\mathbf{h}_j)\lambda_j\Big)_n - 1\Big\},\quad n=1,\ldots,N \qquad (57)$$

with

$$\Big(\sum_{j=1}^{J}\pi^t(\mathbf{h}_j)\lambda_j\Big)_n = \sum_{j=1}^{J}\sum_{p=1}^{P}\pi_{pn}(\mathbf{h}_j)\lambda_{jp},\quad n=1,\ldots,N \qquad (58)$$

Eqs. (57), (58) imply

$$x_n = \exp(-1)\exp\Big\{\sum_{j=1}^{J}\sum_{p=1}^{P}\pi_{pn}(\mathbf{h}_j)\lambda_{jp}\Big\},\quad n=1,\ldots,N$$

Maximum Entropy Solution (7)

and hence

$$\begin{aligned} f(\boldsymbol{g}) &= \sum_{n=1}^{N}\exp(-1)\exp\Big\{\sum_{j=1}^{J}\sum_{p=1}^{P}\pi_{pn}(\mathbf{h}_j)\lambda_{jp}\Big\}\mathbb{1}_{G_n}(\boldsymbol{g}) \\ &= \exp(-1)\exp\Big\{\sum_{j=1}^{J}\sum_{p=1}^{P}\sum_{n=1}^{N}\pi_{pn}(\mathbf{h}_j)\mathbb{1}_{G_n}(\boldsymbol{g})\lambda_{jp}\Big\} \\ &= \exp(-1)\exp\Big\{\sum_{j=1}^{J}\sum_{p=1}^{P}T_{pj}(\boldsymbol{g})\lambda_{jp}\Big\} \qquad (59) \end{aligned}$$

with

$$T_{pj}(\boldsymbol{g}) = \sum_{n=1}^{N}\pi_{pn}(\mathbf{h}_j)\mathbb{1}_{G_n}(\boldsymbol{g})$$

Maximum Entropy Solution (8)

Since

$$\text{prob}(\boldsymbol{g}\in G_n) = \frac{\text{vol}(G_n)}{\text{vol}(G)}x_n$$

it is obvious

$$\begin{aligned} \text{E}(T_{pj}(\boldsymbol{g})) &= \sum_{n=1}^{N}\pi_{pn}(\mathbf{h}_j)\text{prob}(\boldsymbol{g}\in G_n) \\ &= \sum_{n=1}^{N}\pi_{pn}(\mathbf{h}_j)x_n = y_p(\mathbf{h}_j),\quad p=1,\ldots,P,\quad j=1,\ldots,J \qquad (60) \end{aligned}$$

Thus, the favoured solution is the exponential distribution of form (59) with maximum entropy subject to fixed expectation (60) of their minimally sufficient statistics $T_{pj}(\boldsymbol{g})$. The maximum likelihood estimates of the parameters λ_{jp} always satisfy (60).

Maximum Entropy Solution (9)

An algorithm prescribing the dual vectors of the form

$$\lambda_j^{k+1} = \lambda_j^k + \rho_k\gamma^k,\quad j=1,\ldots,J,\quad k=0,1,2,\ldots$$

where ρ_k is a relaxation parameter. By defining

$$x_n^k = \exp\Big\{\Big(\sum_{j=1}^{J}\pi^t(\mathbf{h}_j)\lambda_j^k\Big)_n - 1\Big\}$$

the corresponding primal iteration scheme becomes

$$x_n^{k+1} = x_n^k\exp\Big\{\rho_k\Big(\sum_{j=1}^{J}\pi^t(\mathbf{h}_j)\gamma_j^k\Big)_n\Big\},\quad n=1,\ldots,N,\quad k=0,1,2,\ldots$$

As starting vector $\mathbf{x}_n^0 = \frac{1}{N}$ is taken.

Maximum Entropy Solution (10)

If only one component of λ_j^k is changed in every step k (Gauss–Seidel type scheme), then the primal iteration becomes

$$x_n^{k+1} = x_n^k \exp\Big\{\rho_k \sum_{j=1}^{J} \pi_{pn}(\mathbf{h}_j)\gamma_{jp}^k\Big\}, \quad n = 1,\ldots,N, \quad p = k \pmod P + 1$$

Let $\pi_p^t(\mathbf{h}_j)$ denote the p–th row of the matrix $\pi(\mathbf{h}_j)$. As the entries $\pi_{pn}(\mathbf{h}_j) \geq 0$, the choice

$$\gamma_{jp}^k = \ln \frac{y_p(\mathbf{h}_j)}{\pi_p^t(\mathbf{h}_j)\mathbf{x}^k}, \quad j = 1,\ldots,J, \quad p = k \pmod P + 1 \qquad (61)$$

is preferred over

$$\gamma_{jp}^k = y_p(\mathbf{h}_j) - \pi_p^t(\mathbf{h}_j)\mathbf{x}^k, \quad j = 1,\ldots,J, \quad p = k \pmod P + 1$$

and the primal iteration scheme eventually reads

$$x_n^{k+1} = x_n^k \Big(\frac{y_p(\mathbf{h}_j)}{\pi_p^t(\mathbf{h}_j)\mathbf{x}^k}\Big)^{\rho_k \pi_{pn}(\mathbf{h}_j)}, \quad n = 1,\ldots,N, \quad p = k \pmod P + 1$$

which corresponds to single–step notation.

Maximum Entropy Solution (11)

If all components of the dual iterate λ_j^k are changed in every step (Jacobi type scheme), then (61) turns into

$$\gamma_{jp}^k = \ln \frac{y_p(\mathbf{h}_j)}{\pi_p^t(\mathbf{h}_j)\mathbf{x}^k}, \quad j = 1,\ldots,J, \quad p = 1,\ldots,P$$

and the primal iteration scheme reads

$$\begin{aligned} x_n^{k+1} &= x_n^k \exp\Big\{\rho_k \Big(\sum_{j=1}^{J} \pi^t(\mathbf{h}_j)\gamma_j^k\Big)_n\Big\} \\ &= x_n^k \prod_{j=1}^{J}\prod_{p=1}^{P} \Big(\frac{y_p(\mathbf{h}_j)}{\pi_p^t(\mathbf{h}_j)\mathbf{x}^k}\Big)^{\rho_k \pi_{pn}(\mathbf{h}_j)}, \quad n = 1,\ldots,N \end{aligned}$$

which corresponds to block–iterative notation.

Maximum Entropy Solution (12)

One of the conditions of convergence is $0 \leq \pi_{pn}(\mathbf{h}_j) \leq 1$.

If $0 \leq \pi_{pn}(\mathbf{h}_j) \leq \frac{1}{b(\mathbf{h}_j)} < 1$ a scaling of $\pi_{pn}(\mathbf{h}_j)$ with $b(\mathbf{h}_j)$ leads to

$$x_n^{k+1} = x_n^k \prod_{j=1}^{J}\prod_{p=1}^{P} \Big(\frac{y_p(\mathbf{h}_j)}{\pi_p^t(\mathbf{h}_j)\mathbf{x}^k}\Big)^{\rho_k \min_j(b(\mathbf{h}_j))\, \pi_{pn}(\mathbf{h}_j)}, \quad n = 1,\ldots,N$$

The end

Thank you for your attention!

helmut.schaeben@geo.tu-freiberg.de

The end

"The (Gödel's incompleteness) theorem assures that mathematics is inexhaustible. Our experience assures us that mathematics is inexhaustibly interesting", Arthur Sard, A View of Mathematics

References

References (1)

Bernstein, S., Schaeben, H., 2005, A one-dimensional Radon transform on $SO(3)$ and its application to texture goniometry: Mathematical Methods in the Applied Sciences, in print

Bernstein, S., Hielscher, R., Schaeben, H., 2005, The generalized spherical Radon transform and its application in texture analysis: submitted

Boogaart, K.G.v.d., Hielscher, R., Prestin, J., Schaeben, H., 2005, Application of the radial basis function method to texture analysis: Journal of Computational and Applied Mathematics, in print

Bunge, H.J., 1969, Mathematische Methoden der Texturanalyse: Akademie Verlag, Berlin

References (2)

Bunge, H.J., 1982, Texture Analysis in Materials Science: Butterworths, London

Cerejeiras, P., Schaeben, H., Sommen, F., 2002, The spherical X-ray transform: in Sommen, F., Sprößig, W., (eds.), Clifford Analysis in Application, Mathematical Methods in the Applied Sciences 25, 1493 – 1507

Esling, C., Muller, J., Bunge, H.J., 1982, An integral formula for the even part of the texture function or "the apparition of the f_Π and f_Ω ghost distributions: J. Physique 43, 189 – 195

Funk, P., 1913, Über Flächen mit lauter geschlossenen geodätischen Linien: Math. Ann. 74, 278 – 300.

References (3)

Funk, P., 1916, Über eine geometrische Anwendung der Abel'schen Integralgleichung: Math. Ann. 77, 129 – 135.

Helgason, S., 1984, Groups and Geometric Analysis: Academic Press

Helgason, S., 1994, Geometric Analysis on Symmetric Spaces: Mathematical Surveys and Monographs 39, American Mathematical Society

Helgason, S., 1999, The Radon Transform, 2nd edition: Birkhäuser

Louis, A.K., 1996, Approximate inverse for linear and some nonlinear problems: Inverse Problems 12, 175 – 190

References (4)

Louis, A.K., 1999, A unified approach to regularization methods for linear ill–posed problems: Inverse Problems 15, 489 – 498

Matthies, S., 1979, On the reproducibility of the orientation distribution function of texture samples from pole figures (ghost phenomena): phys.stat.sol.(b) 92, K135 – K138

Matthies, S., 1982, Aktuelle Probleme der quantitativen Texturanalyse: ZfK–480, Zentralinsitut für Kernforschung Rossendorf

Matthies, S., Vinel, G.W., Helming, K., 1987, Standard Distributions in Texture Analysis: Akademie Verlag Berlin

References (5)

Matthies, S., Helming, K., Steinkopff, T. and Kunze, K., 1988, Standard distributions for the case of fibre textures: phys. stat. sol. (b) 150, K1 – K5

Muller, J., Esling, C., Bunge, H.J., 1981, An inversoin formula expressing the texture function in terms of angular distribution functions: J. Physique 42, 161 – 165

Müller, C., 1998, Analysis of Spherical Symmetries in Euclidean Spaces: Springer

Nikolayev, D.I., Schaeben, H., 1999, Characteristics of the ultrahyperbolic differential equation governing pole density functions: Inverse Problems 15, 1603 – 1619

References (6)

Radon, J., 1917, Über die Bestimmung von Funktionen durch ihre Integralwerte längs gewisser Mannigfaltigkeiten: Berichte über die Verhandlungen der Königlich Sächsischen Gesellschaft der Wissenschaften zu Leipzig, Math.-Phys. Klasse 69, 262 – 277

Ramm, A.G., Katsevich, A.I., 1996, The Radon Transform and Local Tomography: CRC Press, Boca Raton

Schaeben, H., Boogaart, K.G.v.d., 2003, Spherical harmonics in texture analysis: Tectonophysics 370, 253-268

Wahba, G., 1990, Spline models for observational data, CBMS-NFS Regional Conference Series in Applied Mathematics 59, SIAM, Philadelphia

Mathematics of Tetxure Analysis

On the rôle of the Darboux differential equation

Radon Transform for $\mathbf{SO}(3)$

Let $f : \mathbf{SO}(3) \mapsto [0, \infty)$ be a probability density function of a random rotation $\boldsymbol{g} \in \mathbf{SO}(3)$.

For any given direction $\mathbf{h} \in \mathbb{S}^2$ the probability density function of coincidence of the random direction $\boldsymbol{g}\mathbf{h} \in \mathbb{S}^2$ with a given direction $\mathbf{r} \in \mathbb{S}^2$ is provided by the 1d totally geodesic Radon transform

$$\mathcal{R}f(\mathbf{h}, \mathbf{r}) = \frac{1}{2\pi} \int_{G(\mathbf{h},\mathbf{r})} f(\boldsymbol{g}) d\boldsymbol{g} \tag{62}$$

with fibres

$$G(\mathbf{h}, \mathbf{r}) = \{\boldsymbol{g} \in \mathbf{SO}(3) \,|\, \boldsymbol{g}\mathbf{h} = \mathbf{r}\}$$

The Radon transform is a function on $\mathbb{S}^2 \times \mathbb{S}^2$, where a pair $(\mathbf{h}, \mathbf{r}) \in \mathbb{S}^2 \times \mathbb{S}^2$ refers to a 1d geodesic ("great circle") of $\mathbf{SO}(3)$.

Darboux Differential Equation

$\mathcal{R}f(\mathbf{h}, \mathbf{r})$ satisfies the differential equation

$$(\Delta_{\mathbf{h}} - \Delta_{\mathbf{r}})\, \mathcal{R}f(\mathbf{h}, \mathbf{r}) = 0 \tag{63}$$

where $\Delta_{\mathbf{h}}$ stands for the Laplace–Beltrami operator with respect to the spherical coordinates of $\mathbf{h}$.

General Solution of Darboux Differential Equation

The general solution of the Darboux differential equation is in terms of spherical harmonics

$$\mathcal{R}f(\mathbf{h}, \mathbf{r}) = \sum_{\ell=0}^{\infty} \sum_{m=-\ell}^{\ell} \sum_{n=-\ell}^{\ell} C_\ell^{mn}\, Y_\ell^m(\mathbf{h})\, Y_\ell^n(\mathbf{r}) \tag{64}$$

and in terms of characteristics

$$\mathcal{R}f(\mathbf{h}, \mathbf{r}) = \sum_{\ell} \sum_{k} u_\ell(\boldsymbol{g}_k \mathbf{h} \cdot \mathbf{r}) \tag{65}$$

where $\boldsymbol{g}_k \in \mathbf{SO}(3)$ are arbitrary orientations and $u_\ell \in C^2(\mathbb{R}^1)$ are some appropriately chosen real twice differentiable functions (Nikolayev and Schaeben, 1999), in particular u_ℓ are radially symmetric with respect to $\boldsymbol{g}_k\mathbf{h}$ or $\boldsymbol{g}_k^{-1}\mathbf{r}$, $k = 1, \ldots, K$, respectively.

While the spherical harmonics refer to localization in **frequency** domain, radial basis functions refer to localization in **spatial** domain.

Localization in Frequency or Spatial Domain (1)

The relationship between localization in spatial or frequency domain can actually be expressed in terms of an "uncertainty" resembling Schroedinger's well known uncertainty relation (cf. Freeden et al., 1998).

frequency domain:

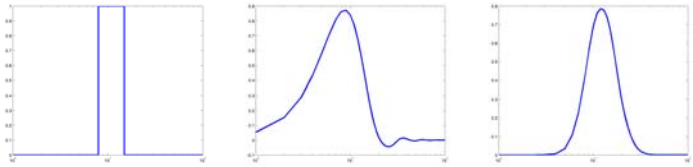

spatial domain:

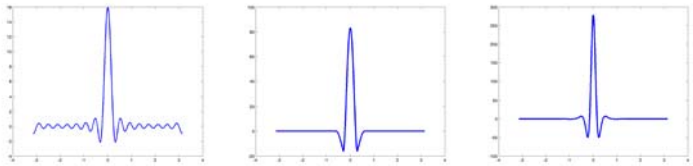

Figure: Examples of Radially Symmetric Wavelets on the Sphere.

Localization in Frequency or Spatial Domain (2)

As a compromise we may favour functions which are well localized in both domains, more specifically in functions which are radially symmetric (in spatial domain) and with Fourier coefficients which vanish smoothly and sufficiently fast.

This concept can be mathematically formalized in terms of Sobolev spaces.

Hielscher, R., 2007, The inversion of the Radon transform on the rotational group and its application to texture analysis: PhD thesis, Freiberg

Boogaart, K.G.v.d., Hielscher, R., Prestin, J., Schaeben, H., 2007, Kernel-based methods for inversion of the Radon transform on SO(3) and their applications to texture analysis: Journal of Computational and Applied Mathematics 199, 122-140

Localization in Frequency or Spatial Domain (3)

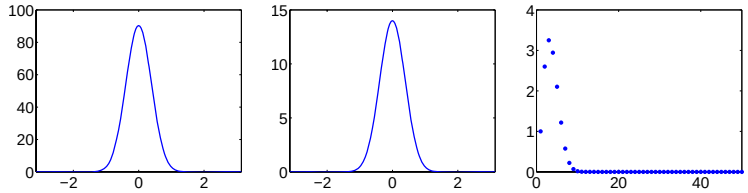

Figure: The de la Vallée Poussin kernel for $\kappa = 13$ (left) and its Radon transform (middle) on the spatial domain, and their spectral representation on the frequency domain (right).

Localization in Frequency or Spatial Domain (4)

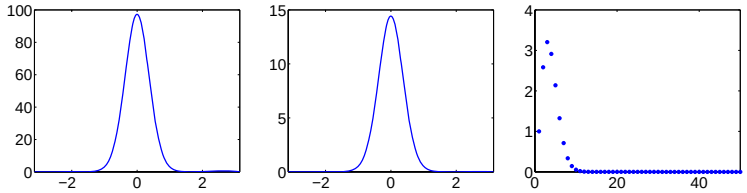

Figure: The von Mises–Fisher kernel for $\kappa = 7.5$ (left) and its Radon transform (middle) on the spatial domain, and their spectral representation on the frequency domain (right).

Resolution of the Inversion Problem

Then the non–linear problem to be solved reads

$$\tilde{\mathbf{c}} = \operatorname{argmin} \sum_{i=1}^{I} \sum_{j_i=1}^{J_i} \| \sum_{m=1}^{M} a(\mathbf{h}_i)\, c_m\, \mathcal{R}\psi_\kappa(\boldsymbol{g}_m \mathbf{h}_i, \mathbf{r}_{j_i}) + b(\mathbf{h}_i, \mathbf{r}_{j_i}) - \iota_{ij_i} \|^2 + \lambda \| \sum_{m=1}^{M} c_m\, \psi_\kappa(\circ \boldsymbol{g}_m^{-1}) \|^2_{\mathcal{H}(\mathbf{SO}(3)}\ , \tag{66}$$

where λ is the parameter of regularization weighting the penalty term.

Conclusions

The Darboux differential equation is instrumental to understand the inversion problem of texture analysis.

With the notion of Sobolev spaces it characterizes the range of the Radon transform and thus of the orientation–to–pole density operator.

Its general solution suggest two ways to tackle the inversion problem numerically - or a compromise of the two:
Radially symmetric basis functions approximated with truncated harmonic series expansions.

Mathematical Texture Analysis

Problems, Exercises, Home Work

Home Work – Problem 1

What are the angle and axis of the rotation represented by the quaternion

$$q(t) = q_1 \cos t + q_2 \sin t, \quad t \in [0, 2\pi)$$

with

$$q_1 = \frac{1 - rh}{\|1 - rh\|} \text{ and } q_2 = \frac{h + r}{\|h + r\|}$$

for arbitrary $(\mathbf{h}, \mathbf{r}) \in \mathbb{S}^2 \times \mathbb{S}^2$ with $\mathbf{r} \neq \pm\mathbf{h}$.

Home Work – Problem 2

Given four mutually orthogonal quaternions $q_i \in \mathbb{S}^3$, $i = 1, 2, 3, 4$.

1. Prove that the two circles $C(q_1, q_2)$ and $C(q_3, q_4)$ are orthogonal.
2. If $C(q_1, q_2)$ represents $G(\mathbf{h}, \mathbf{r})$, what does $C(q_3, q_4)$ represent? Proof!
3. If $C(q_1, q_2)$ represents $G(\mathbf{h}, \mathbf{r})$, what is the quaternion representation of $G(\mathbf{r}, \mathbf{h})$? Proof!

Home Work – Problem 3

We have for all $\gamma \in [0, 2\pi)$

$$\boldsymbol{g}(\alpha, \beta, \gamma)\, \mathbf{c}_{K_C} = \boldsymbol{g}(\alpha, \beta, \gamma) \begin{pmatrix} 0 \\ 0 \\ 1 \end{pmatrix}_{K_C} = \begin{pmatrix} \cos\alpha \sin\beta \\ \sin\alpha \sin\beta \\ \cos\beta \end{pmatrix}_{K_S} =: \mathbf{r}_{K_S} \ .$$

Proof that the projection of $\mathbf{z}_{K_S}$ onto the tangential plane at $\mathbf{r}$

$$(\mathbf{z}_{K_S})_T(\mathbf{r}) \ = \ \frac{\mathbf{z}_{K_S} - (\mathbf{z}_{K_S} \cdot \mathbf{r})\, \mathbf{r}}{\|\mathbf{z}_{K_S} - (\mathbf{z}_{K_S} \cdot \mathbf{r})\, \mathbf{r}\|}$$

and the projection of $\boldsymbol{g}\mathbf{a}_{K_C}$ onto the tangential plane at $\mathbf{r}$

$$(\boldsymbol{g}\mathbf{a}_{K_C})_T(\mathbf{r}) \ = \ \boldsymbol{g}\,\mathbf{a}_{K_C} - (\mathbf{a}_{K_C} \cdot \mathbf{c}_{K_C})\, \mathbf{r} = \boldsymbol{g}\,\mathbf{a}_{K_C}$$

enclose the angle $\pi - \gamma$ to be interpreted as the angle ω between the orthogonal projection of $\boldsymbol{g}\,\mathbf{a}_{K_C}$, being counterclockwise rotated by γ about $\mathbf{r}$, and the orthogonally projected $\mathbf{z}_{K_S}$ when $(\boldsymbol{g}\mathbf{a}_{K_C})_T(\mathbf{r}), (\mathbf{z}_{K_S})_T(\mathbf{r})$, and $\mathbf{r}$ are thought of as a right-handed system.

Home Work – Problem 4

Let

$$U_\epsilon(\boldsymbol{g}_0) := \{\boldsymbol{g} \in \mathbf{SO}(3) \,|\, \angle(\boldsymbol{g}_0, \boldsymbol{g}) < \epsilon\},$$

Show that

$$V_\epsilon(\boldsymbol{g}_0) := \{(\mathbf{h}, \mathbf{r}) \in \mathbb{S}^2 \times \mathbb{S}^2 \,|\, \angle(\boldsymbol{g}_0\mathbf{h}, \mathbf{r}) < \epsilon\},$$

and

$$W_\epsilon(\boldsymbol{g}_0) := \{(\mathbf{h}, \mathbf{r}) \in \mathbb{S}^2 \times \mathbb{S}^2 \mid \exists\, \boldsymbol{g} \in U_\epsilon(\boldsymbol{g}_0) \text{ such that } \boldsymbol{g}\mathbf{h} = \mathbf{r}\}$$

are equivalent.

Home Work – Problem 5

1. If $f : \mathbf{SO}(3) \to \mathbb{R}$ is central with respect to a given $\boldsymbol{g}_0 \in \mathbf{SO}(3)$, i.e. it degenerates to a function $f_m : [0, \pi] \to \mathbb{R}$ according to
$$f(\boldsymbol{g}; \boldsymbol{g}_0) = f_a(\omega(\boldsymbol{g}\boldsymbol{g}_0^{-1}))$$
its Radon transform $\mathcal{R}f$ simplifies analogously. Proof its explicit form.
2. Is the inverse of the above statement also true? Proof!

Home Work – Problem 6

Let $f : \mathbf{SO}(3) \to \mathbb{R}$ represent a fibre texture, i.e. for a given pair $(\mathbf{h}_0, \mathbf{r}_0) \in \mathbb{S}^2 \times \mathbb{S}^2$ it is

$$f(\boldsymbol{g}; (\mathbf{h}_0, \mathbf{r}_0)) = f_c(\boldsymbol{g}\mathbf{h}_0 \cdot \mathbf{r}_0)$$

How does this assumption simplify the general inverse problem to determine a function from its Radon transform?

Home Work – Problem 7

1. Give an elementary proof that the Radon transform satisfies the Darboux differential equation (hint: substitution of variables or harmonic series expansion).
2. The Radon transform satisfies the Darboux differential equation. Does the generalized Radon transform satisfy any differential equation?